THE PREPARATION AND CATALYTIC ACTIVITY OF IRON OXIDE SILICA NANOFIBERS FOR THE FENTON DEGRADATION OF METHYLENE BLUE.

Dissertation submitted in fulfilment of the requirements for

the degree of

MAGISTER TECHNOLOGIAE: CHEMISTRY

in the

FACULTY OF APPLIED AND COMPUTER SCIENCES

DEPARTMENT OF CHEMISTRY

PHINDILE MTHOMBO

Student Number: 212124439

SUPERVISOR: PROF. MJ MOLOTO

CO-SUPERVISOR: DR. EL VILJOEN

VAAL UNIVERSITY OF TECHNOLOGY

Academic year 2020

DECLARATION

I, Mthombo Phindile (212124439): Magister of Technologiae: Chemistry in the Department of Chemistry, Faculty of Applied and Computer Sciences.

Miss P. Mthombo	……	…….
Candidate	Signature	Date
Prof M.J Moloto	…….	……..
Supervisor	Signature	Date
Dr E.L Viljoen	…….	…….
Co-Supervisor	Signature	Date

DEDICATION

This dissertation is dedicated to the Almighty God, my mom, Ms Bonisiwe Thabitha Mthombo and my siblings (Salvador, Thandi and Promise Mthombo).

ACKNOWLEDGMENTS

Firstly I thank God for the gift of life, I thank Him for His Mercy, Grace and His everlasting love. To God be the glory forever and ever, Amen!

I would like to extend my gratitude to my supervisor Prof M.J Moloto for giving me tremendous support throughout this work and for the motivations that kept me moving even when it felt impossible to carry on. Thanks for your support, patience and guidance thought-out this research, I would also like to extend my gratitude to my co-supervisor Dr E.L Viljoen for always been available for consultation, your door was always open and thanks for giving me amazing support. My sincere gratitude goes to my family, my mother Bonisiwe Thabitha Mthombo, and siblings (Salvador, Thandi and Promise Mthombo) for their support, unconditional love and their prayers. I thank them for their encouragement and understanding. I am grateful for the faith you had in me and for always being my pillar of strength.

I would like to thanks my friends (Abel Mayanga, Tsakani Mathebula, Tercia Ngobeni, Zondi Nate and Busisiwe Mabaso). I am very grateful for all the support you've shown and the encouraging speeches you gave me. I will also like to thank my colleagues (Oyandi, Lebogang, Matlhatse, Wanda, Mpho, Zoleka, Nare, Abera, Nkuli, Theo, Sanni, Teboho and Mpumi for their input and comments they played a vital role.

My deepest thanks to the Vaal University of Technology for allowing me to use their facilities and for the tutoring opportunity. Special thanks to the Nanotechnology Catalysis Adsorption and Phytochemicals (NCAP) group for their constructive criticism, guidance and support throughout this period of study.

Lastly, I would also like to thank the National Research Funding (NRF) and Sasol for funding.

CONFERENCES

1. 3rd interdisciplinary Research and postgraduate Conference (Oral presentation). The preparation of iron oxide silica nanofibers using electrospinning. Held on the 17th and 18th October 2018 Quest Conference.

2. ANSO-MMU-SAJ OREC International Conference (Oral presentation). The preparation and catalytic activity of iron-oxide silica nanofibers for the Fenton degradation of Methylene Blue. Held from 4th to 6th September 2019, at the Maasai Mara University main campus, Narok- Kenya.

3. NANOAFRICA 2020 Conference, (Poster presentation), fabrication of silica Nanofibers incorporated with Iron oxide using a different route and for its catalytic activity for the Fenton degradation of methylene blue. Held on the of April at Kempton Park, Johannesburg

MANUSCRIPTS UNDER PREPARATION:

1. Mthombo P, Moloto MJ, Viljoen EL, Synthetic approaches to silica fibres supported on iron oxide nanoparticles, to be submitted to the materials science journal
2. Mthombo P, Moloto MJ, Viljoen EL, Fenton degradation of methylene blue using impregnation formulated silica/iron oxide nanofibers, to be submitted to materials and catalysis journal

DISSERTATION OUTLINE:

This dissertation is divided into 4 chapters. The outline of the chapters is as follows.

Chapter 1: Background and Literature review

This chapter gives the background which is the general information related to the topic and the literature review that explain more detailed information based on Nanotechnology, Electrospinning of metal-based silica nanofibers, Wastewater treatment of dyes and degradation methods of methylene blue. It also highlights the problem statement, aim and objectives of this research

Chapter 2: Research methodology.

In this chapter, the materials and methodology procedure are described in detail. These include the chemicals used, methods of synthesis of the iron-oxide silica nanofibers using three different routes, electrospinning and their catalytic application of the Fenton degradation of methylene blue. It also includes their characterization techniques.

Chapter 3: Results and discussion.

In this chapter, the results obtained from the characterization technique and application in chapter 2 are fully interpreted in detail.

Chapter 4: Conclusions and recommendations

This chapter gives the overall conclusions and recommendations about the study.

LIST OF ABBREVIATIONS

°C	Degrees Celsius
AOP	Advanced oxidation process
dH_2O	Deionised water
DMF	N,N – dimethyl sulfoxide
FTIR	Fourier transform infrared spectroscopy
KV	kilovolts
k	rate constant
MB	Methylene blue
ml	Millilitres
mPa	milipascal
NP's	Nanoparticles
NF's	Nanofibres
PAN	Poly acrylonitrile
PEO	poly ethylene oxide
PL	Photoluminescence
PVA	Poly vinyl alcohol
R^2	linear regression coefficient
SEM	Scanning electron microscope
TEM	Transmission electron microscope
TEOS	Tetraethyl-orthosilicate
TGA	Thermogravimetry analysis
UV-VIS	ultraviolet-visible spectroscopy
WHO	World health organisation
XRD	X-ray powder diffraction

ABSTRACT

Several industries utilize species of synthetic dyes that are found in their wastewater, which is passed out in the environment. Methylene blue is one of the organic dyes that causes water pollution. It causes damage to the aquatic eco-system and health problems to human beings. It is non-biodegradable due to its chemical nature. Advanced oxidation processes (AOP's) have been developed for the degradation of these dyes, however, some of these methods are limited due to their high cost and low efficiency. Among these methods, Fenton catalysis has been proven to be an effective method due to its low cost, high efficiency, and re-usability. Iron oxide nanoparticles have been mainly used in Fenton process however they are also limitated due to the forming of secondary pollutants, due to catalysts recovery difficulties, hence they require supporting materials.

In this work, iron oxide-based catalyst supported on silica nanofibers were fabricated via electrospinning of silica sol incorporated with iron oxide, using three different routes, (a) Method 1 - wetness incipient impregnation, (b) Method 2 - direct addition of iron precursor to the silica sol and (c) Method 3 - incorporation of iron oxide nanoparticles into silica sol. The effect of iron oxide concentration loadings (1 wt%, 2 wt% and 5 wt %) was studied. Increase in iron content resulted in agglomeration of nanoparticles as embedded in the fibers as evident from their SEM images in method 3.1. The SEM results showed diameters from method 1, 2 and 3 ranging from the distribution ranges of 276 – 288 nm, 243 – 265 nm and 188 nm, respectively. EDS showed the presences of Si, P, Fe, O and P. XRD showed a crystalline phase of magnetite (9 nm) and goethite (32 nm) method 1 and 3, with vibrational modes at 3300 cm^{-1}, 1100 cm^{-1}, 950 cm^{-1} and 580 cm^{-1} ascribed to O-H, Si-O-Si, Si-O and Fe-O on the FTIR spectra, it showed both the presence of silica and iron oxide.

The degradation of methylene blue was monitored by UV-Vis spectroscopy, the Fenton catalytic activity of the iron-oxide supported on silica nanofibers showed higher catalytic activity compared to the unsupported iron-oxide nanoparticles. The catalyst prepared by wetness incipient impregnation (method 1) had a degradation efficiency of 69.1%, the direct addition of iron precursor to the silica sol (method 2) had 75.2% and incorporation of iron oxide nanoparticles magnetite and goethite with the silica sol had 53.7% and 34.7%, respectively. The catalyst prepared by the direct addition of iron precursor in the sol (method 2) showed a high catalytic activity compared to the other catalyst prepared by other methods. Unsupported Iron oxide nanoparticles had a higher degree of leaching of 1.28 ppm magnetite, and 1.68 ppm

goethite, compared to the supported iron oxide in method 1 and method 3. The catalyst incorporated with goethite showed a high degree of leaching, 3.95 ppm and 1.33 ppm. The catalyst with high catalytic activity showed a lower degree of leaching with 0.05 ppm.

TABLE OF CONTENTS

LIST OF TABLES

LIST OF TABLES

CHAPTER 1

1. BACKGROUND AND LITERATURE REVIEW

Nanostructured materials are described as materials with particle size ranging between 1-100 nm (Xu et al., 2012). These materials are extensively studied due to their unique chemical and physical properties compared to their bulk materials. Iron oxide nanoparticles are amongst the most widely studied metal oxides, it's known to be one of the most stable metal oxides (Wang et al., 2014), inexpensive (Campos et al., 2015) and they are found in abundance (Coelho et al., 2014). Iron oxide nanoparticles are mostly used in various fields of chemistry (Ali et al., 2016), physics (Lodhia et al., 2009) and biotechnology (Ge et al ., 2009) and they have a a wide range of application in water treatment (Wang et al., 2018), separations (Thomas et al., 2020), sensors (Lui et al., 2009), nonreactors (Santra et al., 2000) and in optical devices, due to their remarkable properties (Wang et al., 2000) such as their optical (Hernandez et al., 2020), electrical and magnetic properties (Panta and Bergmann, 2015), hence over the years they have attracted attention in adsorption, coagulation, filtration and optical devices (Carraro et al., 2014). They also have been demonstrated to have high catalytic activity in the remediation of organic dyes (Rasheed and Meera., 2016). However, the catalytic activity is affected by their ability to form large sludge in homogeneous catalytic applications (Shin et al 2008). Thus, their applications on large scales is limited (Yang et al., 2019). Several studies have shown that these drawbacks can be minimized by the introduction of supporting materials such as clay (Cacciotti et al., 2019), silica (Kosa et al., 2016), alumina (Mosallanejad et al.,2018, Arsalanfar et al., 2014), zeolites (Papa et al., 2018) and carbon (Popov et al., 2017). Although in recent years there are studies of silica nanofibers as supporting material for catalyst (Mishra et al., 2012).

Nanofibers have unique mechanical and thermal properties, hence they became important in a wide range of applications (Lubasova and Netravali, 2020). Therefore, the synthesis of silica-based fibers ranging from nanometer to micrometer fibres has been reported by various research groups. Several methods have been reported for the synthesis of nanofibers (Huang et al., 2003) . Nanofibers can be fabricated by the conventional methods which are known as non-electrospinning techniques and electrospinning technique.

1.1. Non- electrospinning methods

The non-electrospinning methods such as self-assembly, centrifugal jet, solution bow spinning, phase separation and freeze-drying are applied in various fields, however they are found to have some disadvantages (Gugulothi et al., 2019). The phase separation method occurs due to physical incompatibility in a solution. The solvent is extracted from the solution and the remaining phase still have to undergo four basic stages that include polymer dissolution, gelation, extraction and freezing (Misra et al., 2007), while the self-assembly is a bottom-up nanomaterial synthesis method. In this method, molecules arrange themselves into a pattern of structure though hydrogen forces and electrostatic reaction. The small molecules come together based on intermolecular forces hence leading to long chains (Kajbafvala et al., 2013). These methods have disadvantages of non-continuous fibers, limited to certain polymers, complex, non-uniform, low productivity and take longer to fabricate fibers. However, electrospinning is a simple advantageous method (Kumar et al., 2017).

1.2.Electrospinning and silica nanofibers.

Electrospinning methods are one of the unique and versatile methods that can produce nanofibers in various shapes and sizes (Stepanyan et al., 2014), it can produce stable and uniform nanofibers (Mochane et al., 2019). It consists of three basic components, the high voltage power supply, syringe, and ground collector (Figure 1) (Long et al., 2019). The high voltage supply induces the electrostatic force that charges the polymer solution in the syringe fed through a capillary connection (Chen et al., 2017). The induced positively charged jet is therefore ejected and deposited to the ground collector (Shi et al., 2015). The advantages of electrospinning is its design set up that make it possible for the parameters optimization (Gee et al., 2018).

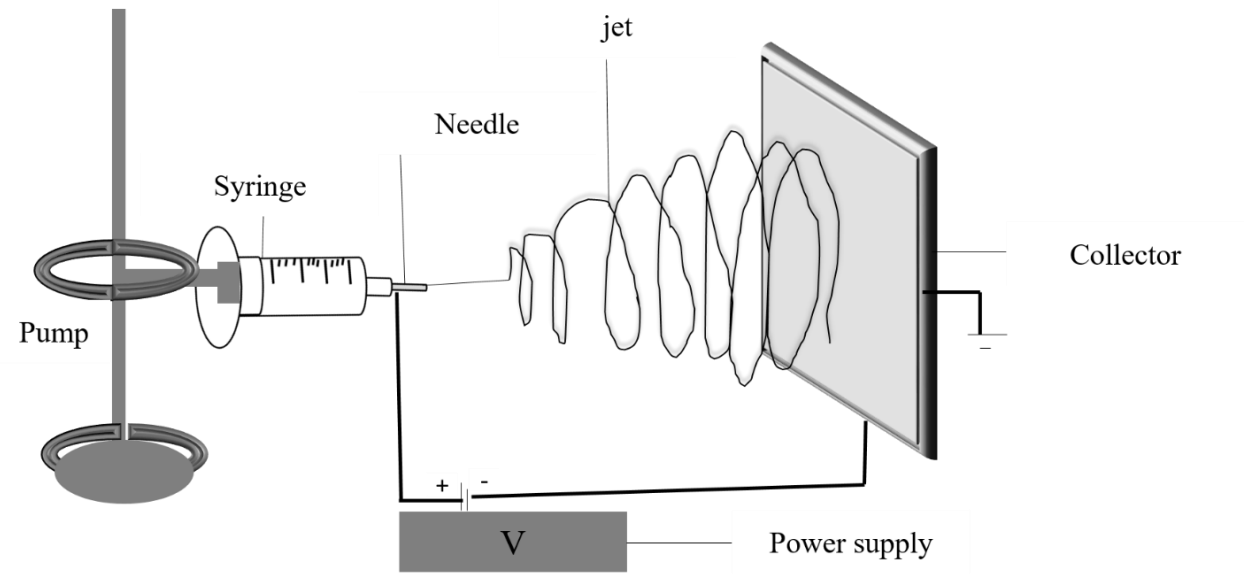

Figure 1: Typical example of electrospinning set-up.

1.2.1. Optimization of parameters

During electrospinning, some parameters play an important role and they need to be taken into consideration (Leach et al., 2011), These parameters can be divided into three groups: processing conditions (distance between the capillarity and the ground collector, applied voltage, needle diameter, volume feed rate,) ambient conditions including (the flow rate at which the solution is released) and intrinsic properties of the solution (the viscosity of the solution, polymer concentration, molecular weight of the polymer, electrical conductivity, elasticity, and surface tension) (Fridrikh et al., 2003), Varying these parameters makes it possible to get different sizes and shapes (Chen et al., 2009). Hence electrospinning can enhance the properties of the nanofibers making them more suitable as supporting material. Optimization could lead to the production of longer and continuous fibers with a desirable diameter (Chen et al., 2019).

Geltmeyer et al.,(2013) conducted a study where they used the sol-gel method for the optimisation of sol viscosities for the stability of electrospinning of silica nanofibers. They showed that the sol-gel solutions, with a viscosity ranging between 120 and 200 mPa.s, are electrospinable forming uniform bead-less nanofibers as compared to solutions of viscosity lower or higher than 120 and 200 mPa.s forming unstable nanofibers with a larger diameter. They also reported that electrospinning with a dilute sol was also possible, but electrospinning of the fresh sols was more stable. They succeeded in illustrating the importance of viscosity

and the degree of crosslinking of the sols for the stable electrospinning of silica nanofibers. Viscosity affects the formation of fibers, studies have confirmed that at very low viscosities only fibers beads can be formed, while at higher viscosities the ejection of polymer solution becomes poor, therefore it's important to get the optimum viscosity (Veleirinho et al., 2007)

The increase in voltage can lead to an increase or a decrease in fibres diameter due to stretching of polymeric droplets and evaporation of solvents from the solution, Choi et al.(2003) also reported a study for the fabrication of nanofibers using the sol-gel and electrospinning methods. The silica sol-gel was prepared at room temperature using tetraethyl orthosilicate (TEOS), deionised water, ethanol, and hydrochloric acid (HCl) (TEOS: Ethanol: Water: HCl) (1:2:2:0.01). During the electrospinning, the voltage was varied from 10 kV to 16 kV at 10 cm. It was observed that the electrospun silica nanofibers obtained at 10 kV were thicker than those obtained at 12 kV. A decrease in diameter was also observed as the applied voltage was further increased ranging from 200 - 600 nm this suggested that an increase in voltage results in an increase in fibre diameter.

Shah et al. (2012) prepared silica nanofibres using the sol-gel method by the addition of tetraethyl orthosilicate (TEOS): phosphoric acid (H_3PO_4): water (H_2O) in the ratio of (1: 0.01:11). Polyvinyl alcohol was added as a polymer precursor. The mixture was then electrospun and during the electrospinning, the applied voltage ranged from 15-20 kV at a distance of 6 cm. After the nanofibers were obtained, the effect of calcination at different temperature was studied. The obtained results showed a crystalline phase on the XRD pattern. The increase in calcination temperatures influenced the morphology of the nanofibres. Nanofibers obtained at high calcination temperatures had a rougher surface and smaller diameter than those calcined at lower temperatures. Those calcined at lower temperatures were more stable, with a diameter ranging from 200-300 nm. This route might open new doors for producing pure nanofibers of inorganic materials with porous surfaces. Figure 2 shows the surface of the nanofiber after calcination, the surface becomes rougher and porous increasing the surface area.. All these parameters are significant including the type of materials use and the polymers.

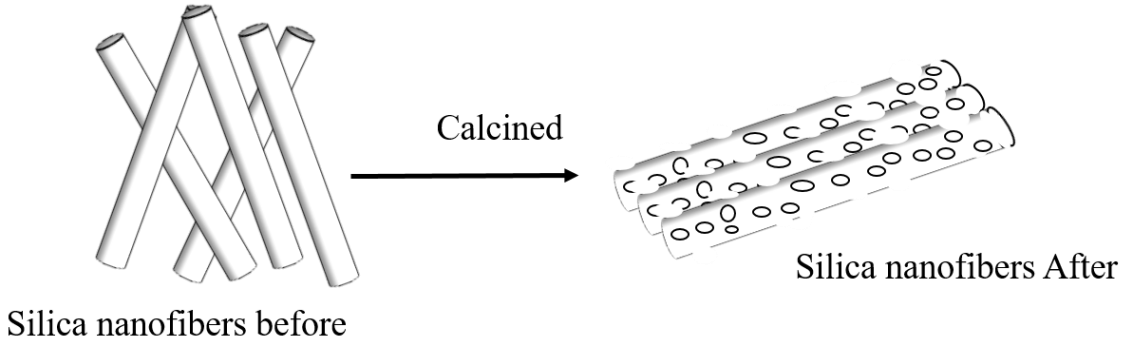

Figure 2: Silica nanofibers before and after calcination.

1.3. Silica and Polymers composite

Electrospinning of silica-based materials can be challenging and results in poor mechanical strength and stability however, electrospinning of silica materials can be electrospun in two ways. The first method being the direct spinning of sol-gel solutions containing alkoxide precursors and, secondly by the addition of carrying polymers such as PVA (Shao et al., 2001), poly (ethylene) oxide (PEO) (Fouda et al., 2013) and polyacrylonitrile (PAN) (H, Wang et al., 2018). Electrospinning inorganic matrices such as silica can be challenging, while silica nanofibres prepared from a solution containing the carrying polymers are more easily adjusted (Veleirinho et al., 2007), producing nanofibres that are controllable and uniform in size (Toskas et al. 2013). There are unique properties exhibited by polymer/silica nanofibers and they have gained more attention in different industries, mainly in wastewater treatment (Geltmeyer et al., 2013, Shah et al., 2012)

1.4. Iron oxide supported on silica nanofibers

The use of nanofibers incorporated with nanoparticles of smaller diameters are interesting materials in the heterogeneous catalysis because of their remarkable characteristics, including high pore volume, tunable and uniform pore size and high surface area, however, the catalytic uses of pure silica are limited (Coelho et al., 2014). Materials with such remarkable properties attract various fields of applications mainly wastewater treatment. Therefore, silica nanofibers incorporated with metal oxide nanoparticles or metal oxides are promising to have good catalytic activities (Shi et al., 2015). To improve catalytic activity, impregnation of metal oxides such as Al_2O_3, TiO_3, Fe_2O_3 into silica nanofibers (Malara et al., 2019), as supporting structures, have been applied. Amongst these transitional metals, iron is good when supported on silica (see chapter 1 section 1). However, the chemistry between the support and the supporting materials are of great interest to minimize the leaching and to get effective results

on the application of the materials. There are several methods in which iron oxide can be introduced into the silica nanofibers such as ancient wetness impregnation, direct addition of metal oxide precursor in the spinning solution and direct incorporation with nanoparticles and impregnation of nanofibers nanoparticles, however, there is not much available literature that compares these methods, and it is not known which method gives the highest catalytic activity and how is their leaching degree.

Bowker et al. (2007) highlighted that it is evident the preparation methods of catalyst are a curious factor in determining the efficiency of the materials. Incipient wetness impregnation involves the support material with metal salts. During this process the metal salts aqueous solution is introduced into the pores of the surface of the support with a little volume of liquid used. This process requires a high temperature for conversion (Cheng et al., 2002). The direct syntheses with metal salts method, during this method the support and the catalyst are prepared simultaneously. The metal salts are directly added during the support preparation process. Finally, in the incorporation of nanoparticle method, the nanoparticles are integrated into support before it solidifies (Shinjinaetal et al., 2017).

1.5. Wastewater pollution

Wastewater has been highlighted as one of the major problems that have been faced globally, due to the high rate of water pollution (Njeruh et al., 2010). Some of these pollutants are generated from textile, paper and other industries. Among these pollutants, 10 to 25 per cent are industrial colouring dyes released during the dye processes and 2 to 20 per cent are released directly as aqueous waste in different fields of the environment (Suteu et al., 2015). These dyes have a nitrogen-nitrogen double bond (N=N) and are found to be environmentally unfriendly and toxic to living organisms (Wang et al., 2017). With respect to organic dyes, it can be highlighted that colouring dyes have a high volume to change the environment due to their strong colours and visual pollutants, which primarily affect the photosynthesis process and can cause harm to the living organisms (Nogueira et al., 2014). They become a serious health hazard to living organisms and species that live in water, due to their poisonousness and persistence after being cast out to the environment or rivers (Njeruh, 2010).

1.6. Methylene blue

Methylene blue is among these organic dyes, it is one of the dyes that are non-biodegradable due to its chemical nature, with chemical formula $C_{16}H_{18}C_lN_3S$ (Salman 2016), the molecular

weight of 373.90 g/mol and maximum adsorption wavelength of 660 nm (Koch, 2013). It is a cationic dye and a synthetic substance that does not occur naturally (States, 2008) and is synthesised commercially by oxidation of N, N-dimethyl-phenyl diamine with sodium dichromate ($Na_2Cr_2O_7$) in the presence of sodium thiosulfate ($Na_2S_2O_3$), followed by further oxidation in the presence of N,N-dimethylaniline (Koch, 2013). Figure 3 shows a typical example of the methylene blue and its aromatic structure and which brought serious eco-environmental problems. It is a heteropoly aromatic structure that can cause damage to plants and animals that live in water, as well as human health, it has negative impacts on both the environment and living organisms (Ramakrishna et al., 2006). If inhaled, it can lead to shornesst breath and, if digested, it leads to nausea, diarrhoea, vomiting (Khadaie et al., 2012), pains, mental disturbance, pain micturition and biennia syndrome (Zarubica, 2016, Bhatia et al., 2017, Chequer et al., 2017). It is very difficult to biodegrade due to its complex aromatic structure (Kim et a*l.*, 2013), chemical nature and molecular size (Wallace et al., 2001). Therefore, the degradation of methylene dye in wastewater is of great interest and has been extensively studied due to the high rate of water pollution and it is a problem commonly faced globally, as well as its increase on a daily basis (Cotto-Maldonado et al., 2017).

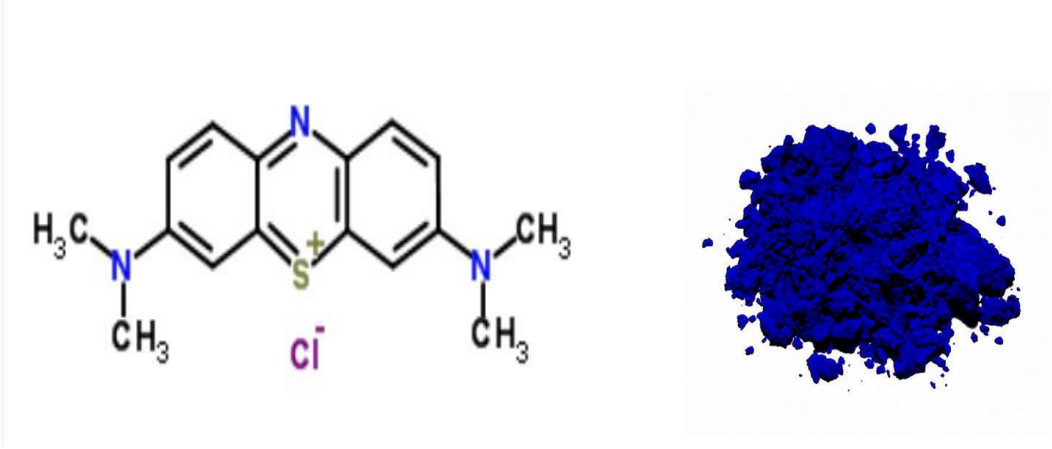

Figure 3: Powder and structural formula of methylene blue.

1.7. Conventional methods

In recent years, conventional chemical, physical, and biological treatment (Ong et al., 2011) such as adsorption, coagulation (Yu-li et al., 2006), filtration, sedimentation and advanced oxidation methods (Chen et al., 2016) have been used for the removal of dyes in wastewater (Chen et al., 2016) (Zarubica, 2016). However, there are limitations in most of the methods due to their low effectiveness and expevsive (Yu-li et al., 2006; Nie et al., 2013).

1.7.1. Biological process and Adsorption process

The are many studies conducted on the removal of dyes in wastewater, biological methods is one of the methods used, it is cheap and easy to use however they are limited because they cannot readily degrade the dyes due to their chemical nature, complex structure and molecular weight, they result in sludge (Yu-li et al., 2006). Wang et al., 2016 reported a two-phase process in developing biological methods for decolouration of dyes, the first process is an anaebolic method followed by an anaerobic process. During the dye degradation, the metaboliess formed as a dye reduction can further be catabolized either by these process. The intermediates products synthesized during dye decolouration can also be reduced by other enzymes such as a hydroxylase and oxygenase that are also produced by bacterias. Muda et al., 2013 reported a similar process of the degradation of dyes that requires multiple processes.

Adsorption is one of the methods mostly applied to the removal of organic pollutants (Ahamend et al., 2018). In adsorption processes an adsorbent with high porosity material that are used to adsorb the pollutants. When a solution containing absorbable solute comes into contact with a solid that has a high porous surface structure, the are intermolecular forces that taks place because some of the solute molecules from the solution can be deposited to the solid surface (Rashed, 2013). Adsorption based techniques are non-denaturing, highly selective, energy-efficient, and relatively inexpensive because of convenience, ease of operation and simplicity of design.

Among these methods, catalysis has been demonstrated to be an effective method due to its high effectiveness, its re-usability, affordability, and it can be scaled up in a way to obtain a profitable treatment of quite a different pollutant concentration (Lueta et al., 2017). Catalysis and catalysts play a major role in today's technology and it is an important material used for the chemicals and materials manufacturing and pollutant controlling systems (Heveling, 2012). However, the use of catalysts the iron-based heterogeneous Fenton and metal oxide supported on silica nanofibers has gained considerable research attention due to its high rate of dye removal and its wide pH (Jung et al., 2009). Therefore, advanced oxidation processes like Fenton oxidation, photo-catalysis oxidation and ozone oxidation, have been highly considered due to their ability to remove the textile dye in wastewater(Wang et al., 2017).

1.8. Fenton Process

The discovery of the Fenton process was in the 19th century by a scientist called H.J Fenton. This discovery was observed when the oxidation reaction of tartaric acid and dihydroxy maleic

acid by hydrogen peroxide in the presence of ferrous iron was used. This reaction begins by the separation of the oxidising agent (H_2O_2) which is an extremely reactive species, with the high oxidative potential of 2.80 volts (Neyens & Baeyens, 2003), these radicals have an ability to attack specific compounds. Hence, recently the Fenton reaction is mainly used for wastewater treatment due to its ability to oxidising organic materials into inorganic compounds such as water and carbon dioxide in mild conditions (Nogueira et al. 2014). Fenton reactions are one of the advanced oxidation processes (AOP) used for treating wastewater; it uses hydrogen peroxide in the presence of ferrous iron as a catalyst, these are mainly responsible for oxidising the organic pollutants in wastewater, therefore, degrading them completely to inorganic materials (Nogueira et al., 2014). The following equations 1 to 7 show the steps in the mechanisms of the formation of radicals in the Fenton process. The reaction consists of the following seven elementary reactions (Wang et al., 2014).

The formation of hydroxyl radicals:

$$Fe^{2+} + H_2O_2 \rightarrow \quad Fe^{3+} + \bullet OH + OH^- \qquad \text{eq. 1}$$

$$\bullet OH + Fe^{2+} \rightarrow \quad Fe^{3+} + OH^- \qquad \text{eq. 2}$$

$$Fe^{3+} + H_2O_2 \rightarrow \quad Fe - OOH3^+ + H^+ \qquad \text{eq. 3}$$

$$Fe - OOH^{3+} \rightarrow \quad \bullet HO_2 + Fe^{2+} \qquad \text{eq. 4}$$

$$Fe^{2+} + \bullet HO_2 \rightarrow \quad Fe^{3+} + OH_2^- \qquad \text{eq. 5}$$

$$Fe^{2+} + \bullet HO_2 \rightarrow \quad Fe^{2+} + O_2 + H^+ \qquad \text{eq. 6}$$

$$\bullet OH + H_2O_2 \rightarrow \quad H_2O + HO_2 \qquad \text{eq. 7}$$

In generating the high content chemical oxidant of hydroxyl (·OH) and per hydroxyl radicals (·OOH) oxidised organic species present in the wastewater into harmless, stable and inorganic water (Nogueira *et al.*, 2014). Figure 4 shows the colour change of the methylene blue before the degradation and after the degradation, the water changed from deep blue to colorless. Figure 5 shows a possible degradation mechanism of methylene blue by Fenton reaction (Wang J. et al. 2014). Ideally the methylene blue needs to be fully mineralized to carbon dioxide and water since the intermediates like phenol is also harmful to the environment.

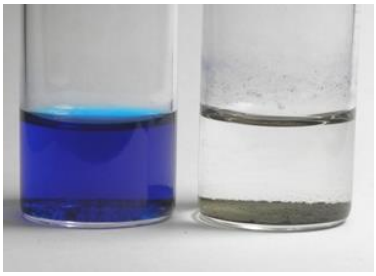

Figure 4: Methylene blue solutions before degradation and after degradation (Nogueira *et al.*, 2014).

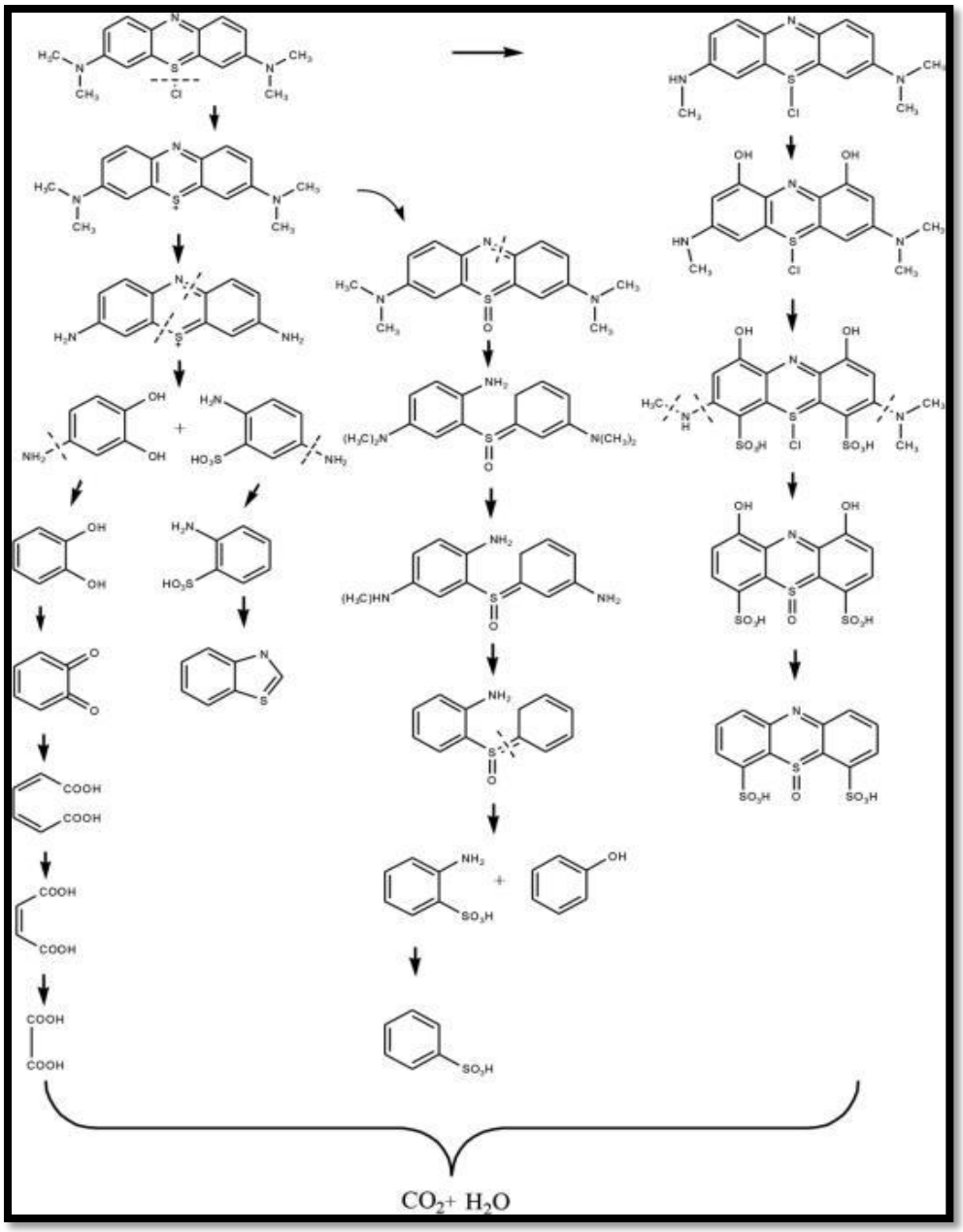

Figure 5: Degradation mechanism of methylene blue by Fenton reaction. (Wang J. at al.,2014).

Therefore, introducing nanostructured materials with good catalytic activity properties in Fenton processes such as nanofibers will enhance the catalytic activity for the removal of dyes. Nanofibers exhibit good properties, with small diameters and a porous surface. These membranes possess excellent permeable properties and are favoured in environmental remediation areas. The nanoparticles supported on polymers; silicates and metal oxide substrates have gained interest because of their stability, reusability and good catalytic properties (Patel et al., 2007). Wang et al. (2017) studied the efficiency of bimetallic compound nanoparticle for the degradation of methylene blue using the Fenton reaction. The Fe/Cu bimetallic nanoparticles were supported on carbon nanofibers and were prepared by electrospinning. The prepared catalysts (Fe/Cu/CNF) were used for the Fenton catalytic performance for the degradation of azo dye and acid orange. Therefore, the results obtained showed that the catalyst possesses porous structures with a high specific surface area and a matrix of carbon nanofibers. The catalytic activity resulted in up to 97.7 per cent by (Fe-Cu/CNF) and this technology has gained attention in the Fenton chemistry.

Nie et al. (2013) conducted a study for the synthesis of polyacrylamide/copper sulphide composite nanofibers and recyclability of the catalyst for the removal of dyes. The nanofibers were prepared by a hydrothermal method and the electrospinning technique with a voltage of 18 kV at 20 cm. The synthesised nanofibers showed high removal efficiency for the degradation of methylene blue in the presence of hydrogen peroxide and the catalyst was recovered. It was concluded the material is perfect for recyclability for Fenton reaction, therefore, metal oxide oxides and metal sulphide supported on nanofibers promises to be a good technology in water purification.

Wang et al. (2017) also conducted a study for the fabrication of flexible self-standing Cu-Al_2O_3 fibrous membrane via the electrospinning technique for Fenton catalysis of bisphenol degradation. The effect of calcination temperature, pH and the concentration of the metal precursor on the fibres and average diameter was investigated. The fibres decreased with an increase in the metal precursor concentration and a slight decrease with increase in calcination temperatures (600, 700, 800 $^{\circ}$C). It was observed that the fibres calcined at 600 $^{\circ}$C could be bent and remain cohesive without any cracks, showing that the membranes have excellent flexibility.

This study is based on the preparation and catalytic activity of the iron oxide supported on polymer-silica nanofibers for the degradation of methylene blue using the Fenton reaction. The silica nanofibres will be synthesised by the electrospinning technique and blended with iron oxide nanoparticles (1 wt%, 2.5 wt% and 5 wt%) or impregnated with iron solution. Thus, the resultant iron oxide-silica nanofibers will be used with hydrogen peroxide in Fenton oxidation methods for the removal of methylene blue in the water.

1.9. Problem statement

Water pollution is a global problem, of which organic dyes such as methylene blue constitute major pollutants in water. These dyes result in substantial losses to the economy, damage to the aquatic ecosystem, are harmful to all living organisms and they are non-biodegradable. Due to the complexity of economic need to use dyes and demand for clean water, methods for the degradation of these dyes are pivotal. Thus, the Fenton reaction with the iron oxide-silica nanofibers catalyst is one of the methods that can be used for the removal of these dyes and a catalyst with improved activity and stability needs to be developed.

1.10. AIM AND OBJECTIVES

The main aim of the study is to prepare silica nanofibers with embedded iron oxide nanoparticles using three different routes for their Fenton reaction in the degradation of methylene blue.

In summary, this study focuses on the following aim and objectives:

1.10.1. Aim

- To investigate the catalytic activity of the iron oxide-silica nanofibres using the Fenton reaction for the degradation of methylene blue.

1.10.2. Objectives

- To prepare silica nanofibers using electrospinning technique and optimize the voltage (20, 25 and 30 kV).
- To characterize the synthesized silica nanofibers using SEM, FTIR and XRD.
- To impregnate the fabricated silica nanofibers with iron nitrate (1 wt%, 2 wt% and 5 wt%) using incipient wetness impregnation.
- To fabricate iron oxide silica nanofibers using direct addition of iron nitrate (1 wt%, 2 wt% and 5 wt%) in the spinning solution by electrospinning technique.
- To prepare iron oxide nanoparticles using co-precipitation and precipitation methods.
- To characterize the synthesized iron oxide nanoparticles using, TEM, XRD, UV-Vis, PL, FTIR and Raman spectroscopy.
- To fabricate silica nanofibers incorporated with iron oxide nanoparticles (1 wt%, 2 wt% and 5 wt%) by electrospinning technique.
- To calcine the fabricated iron oxide silica nanofibers at 400 °C.
- To characterize the synthesized iron oxide silica nanofibers using, SEM, XRD, and FTIR spectroscopy.
- To evaluate the effect of Fenton degradation of methylene blue using the prepared iron oxide silica nanofibers in method 1, method 2 and method 3.
- To conduct the leaching test for the prepared iron oxide silica nanofibers catalysts in method 1, method 2 and method 3.

CHAPTER 2

2. RESEARCH METHODOLOGY

2.1. Chemical reagents

Tetraethyl orthosilicate (TEOS, 98%) reagent grade, poly (vinyl alcohol) (PVA 98 000 MW), phosphoric acid (H_3PO_4, 98.9%), iron (III) nitrate nonahydrate ($Fe(NO_3)_3•9H_2O$, 98%), hydrogen peroxide (H_2O_2, 32%), methanol (CH_3OH, 99%), sodium hydroxide (NaOH, 98.9%), isopropanol alcohol (C_3H_7OH, 99.7%), ethanol (C_2H_5OH, 99,7%), aluminium foil, methylene blue (MB)($C_{16}H_{18}ClN_3S$, 98%), iron(II)chloride tetrahydrate ($FeCl_2·4H_2O$, 99.0%), iron(II)chloride hexahydrate ($FeCl_3·6H_2O$, 99.99%) and tetraethylammonium (TEA)(C_8H_2lNO, 25%) were purchased at sigma Aldrich (south Africa). All chemicals were used as purchased, without any further modification.

2.2. Experimental (Preparation of Iron oxide silica nanofibers using different routes).

Scheme 3.1 shows the steps involved in the preparation of iron oxide silica nanofibers using three different methods. Method 1: the preparation of iron oxide silica nanofibers by incipient wetness impregnation of iron nitrate into the silica nanofibers on this method pure silica nanofibers were firstly prepared by sol-gel method and electrospinning. During the electrospinning, the voltage was varied to obtain an optimum. The fabricated fibres were impregnated by iron nitrate solution at different concentrations and calcined.

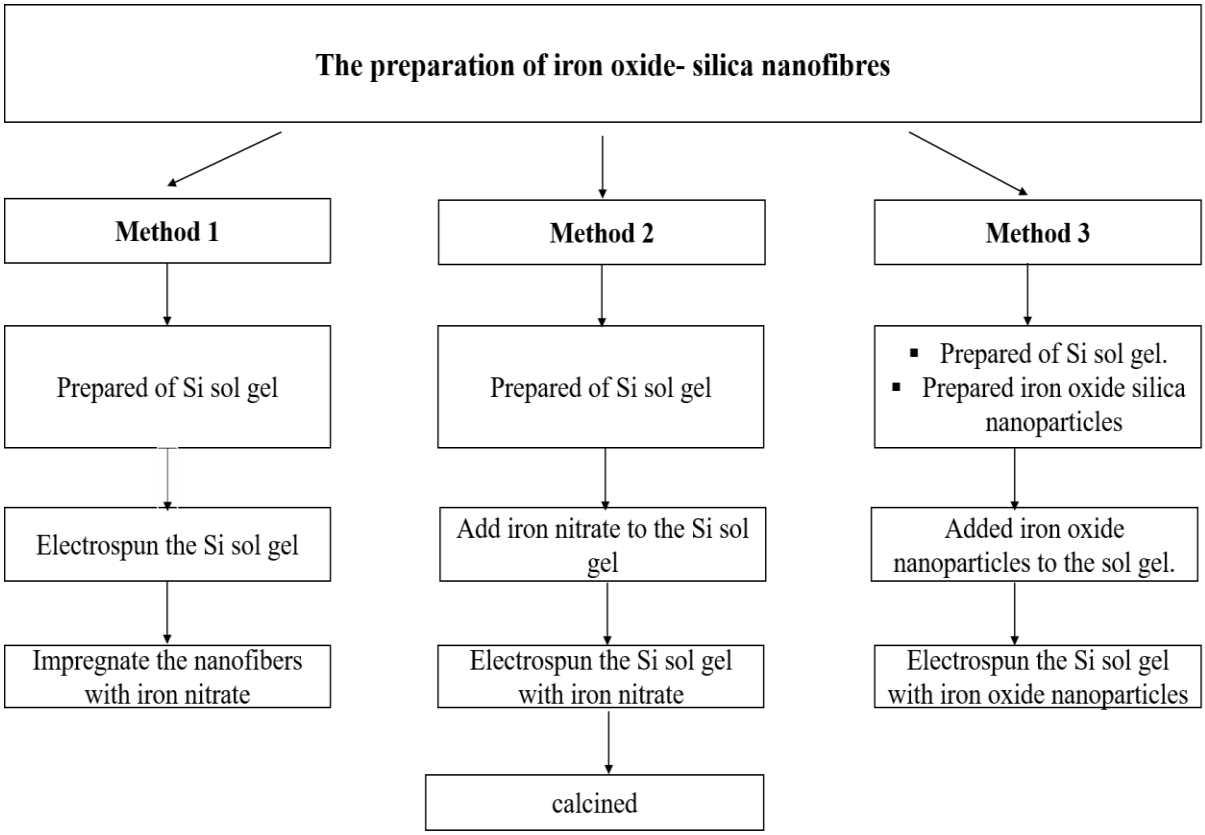

Scheme 1: Flow diagram to represent the methods used in preparing nanofibers.

2.2.1. The preparation of iron oxide silica nanofibers using incipient wetness impregnation (Method 1).

The method was adopted from (Shao et al., 2002) (modified) and further modified. Sol-gel of tetraethyl orthosilicate (TEOS): phosphoric acid (H_3PO_4): deionised water (dH_2O) with a molar composition of 1: 0.01: 10 respectively were prepared by hydrolysis and polycondensation process. A solution of deionised water and phosphoric acid was slowly added to TEOS with vigorous stirring at room temperature, the stirring was continued for 5 hours to obtain a clear colourless solution. While 10 wt.% of polyvinyl alcohol (PVA) solution was prepared by dissolving 10 g of PVA powder in 90 mL of deionised water for 2 hours at 80 °C. An equivalent mass of 10 % polyvinyl alcohol (PVA) was added to silica sol dropwise and stirred for 12 hours at room temperature.

The prepared polymer solution was electrospun. The solution was contained in a syringe connected to the high voltage power supply. The applied voltage was ranging between10, 15 and 20 kV at a distance of 10 cm from between the nozzle tip and ground collector. A jet deposited in an aluminium foil was collected and dried for 12 hours at 70 °C under vacuum to

remove water residues. The prepared silica nanofibers were impregnated with iron nitrate using a spin coater and calcined at 400°C to obtain iron oxide-silica nanofibers.

2.2.2. The preparation of iron oxide silica nanofibers using the direct addition of iron nitrate precursor (Method 2)

A sol-gel of tetraethyl orthosilicate (TEOS): phosphoric acid (H_3PO_4): deionised water (dH_2O) with a molar composition of 1: 0.01: 10 respectively were prepared by hydrolysis and polycondensation process. A solution of deionised water and phosphoric acid was slowly added to TEOS with vigorous stirring at room temperature, the stirring was continued for 5 hours to obtain a clear colourless solution. While 10 wt.% of polyvinyl alcohol (PVA) solution was prepared by dissolving 10 g of PVA powder in 90 mL of deionised water for 2 hours at 80 °C. An equivalent mass of 10 % polyvinyl alcohol (PVA) was added to silica sol dropwise followed by the addition of iron nitrate precursor (1 wt%, 2 wt% and 5 wt %). The solution was further stirred at room temperature for 12 hours to form a homogenous mixture.

The prepared polymer solution was electrospun. The solution was contained in a syringe connected to the high voltage power supply. The applied voltage was ranging between 10, 15 and 20 kV with a distance of 10 cm from between the nozzle tip and ground collector. A jet deposited in an aluminium foil was collected and dried for 12 hours at 70 °C under vacuum to remove water residues. The prepared silica nanofibers were impregnated with iron nitrate using a spin coater and calcined at 400 °C to obtain iron oxide-silica nanofibers.

2.2.3. Preparation of silica nanofibers incorporated with iron oxide nanoparticles (magnetite). (Method 3)

This method was adopted from (Fatehi et al., 2017), iron oxide nanoparticle was synthesised by co-precipitation method. The two iron salts, $FeCl_3.6H_2O$ (0.02 mol) and $FeCl_2.4H_2O$ (0.01 mol) were dissolved in 150 mL of de-ionized water and stirred at 70 °C for 2 hours under reflux. Sodium hydroxide (5 M) was added dropwise to obtain a pH of 11 and it was continuously stirred for an hour under nitrogen. The formed precipitate was collected by centrifuge and washed 3 times with hot deionised water and washed once with ethanol to remove the water residue and it was dried at 50 °C for 2 hours.

Sol-gel solution with the molar composition of tetraethyl orthosilicate (TEOS): phosphoric acid (H_3PO_4): deionised water (dH_2O) 1: 0.01: 10 was prepared by hydrolysis and condensation process of the metal alkoxide. The preparation of sol-gel was done by dropwise addition of

aqueous H_3PO_4 to TEOS with vigorous stirring at room temperature. The mixture was reacted for 5 hours at room temperature. An equivalent mass of 10 wt% of PVA solution was added dropwise into the silica gel. The prepared iron oxide nanoparticles (1 wt%, 2 wt% and 5 wt%) were added to the sol and the reaction continued to stir for 12 hours. The obtained fibres were calcined at 400 °C.

The prepared polymer solution was electrospun as follows; the solution was contained in a syringe connected to the high voltage power supply. The applied voltage was varied from 10, 15 and 20 kV with a distance of 10 cm from between the nozzle tip and ground collector. A jet deposited in an aluminium foil was collected and dried for 12 hours at 70 °C under vacuum to remove water residues. The prepared silica nanofibers were impregnated with iron nitrate using a spin coater and calcined at 400 °C to obtain iron oxide-silica nanofibers.

2.2.4. Preparation silica nanofibers incorporated with iron oxide nanoparticles.

Iron oxide nanoparticles were prepared by the addition of 43,69 mL tetraethylammonium hydroxide (TEA) to 100 mL volumetric flask and filled up to the mark with distilled water. The solution was transferred to three-neck round bottom flask and was stirred in a magnetic stirrer until it reaches 85 $^{\circ}$C. The solution of iron nitrate ($Fe(NO_3)_3 . H_2O$) (0.02 mol) dissolved in 10 mL of deionised water and was added to the solution. Followed by the addition of 0.9102 mL of hydrogen peroxide (H_2O_2). The reaction was allowed to stir for 1 hour 30 minutes, then cooled down to room temperature. The solution was centrifuged with 50 mL of methanol to collect the precipitate and was washed with 0.1 M of hydrochloric acid (HCl) two times to remove the unreacted species, three-time with deionised water. It was washed with the methanol to remove the traces of water and dried overnight at room temperature.

Sol-gel solution with a molar composition of tetraethyl orthosilicate (TEOS): phosphoric acid (H_3PO_4): deionised water (dH_2O) 1: 0.01: 10 was prepared by hydrolysis and condensation process of the metal alkoxide. The preparation of sol-gel was done by dropwise addition of aqueous H_3PO_4 to TEOS with vigorous stirring at room temperature. The mixture was reacted for 5 hours at room temperature. An equivalent mass of 10 wt% of PVA solution was added dropwise into the silica gel. The prepared iron oxide nanoparticle (1 wt.%, 2 wt.% and 5 wt.%) were added to the sol and the reaction continued to stir for 12 hours. The obtained fibres were calcined at 400 °C.

The prepared polymer solution was electrospun. The solution was contained in a syringe connected to the high voltage power supply. The applied voltage was ranging between 10, 15 and 20 kV with a distance of 10 cm from between the nozzle tip and ground collector. A jet deposited in an aluminium foil was collected and dried for 12 hours at 70 °C under vacuum to remove water residues. The prepared silica nanofibers were impregnated with iron nitrate using a spin coater and calcined at 400 °C to obtain iron oxide-silica nanofibers.

2.3. Fenton degradation of Methylene blue.

The prepared catalyst (0.005 g) was placed in 500 mL beaker and 50mL deionised water was added, followed by the addition of 10 mL of 1000 ppm of methylene blue. The mixture was covered with aluminium foil to avoid photodegradation. Another 20 mL of deionised water was added and stir at 500 rpm using a magnetic stirrer for 1 hour at 50 °C to ensure the adsorption-desorption equilibrium. A volume of 20 mL of H_2O_2 (30%) was added to start the reaction for the breaking down of methylene blue. 1 mL of the solution was sampled at At time intervals of 0, 5, 10, 20, 30, 40, 50 and 60 minutes into 100 mL volumetric flask and 1 mL of isopropanol was added to quench the reaction. The solution was diluted to the mark with deionized water and analysed using the UV-vis spectrophotometer. The catalyst was recovered from the reaction by centrifuging.

2.4. Leaching tests

A mass of 0.005 g of the catalyst was placed in 500 mL beaker and 50mL deionised water was added, followed by the addition of 10 mL of 1000 ppm of methylene blue. The mixture was covered with aluminium foil to avoid photodegradation. Another 20 mL of deionised water was added and stir at 500 rpm using a magnetic stirrer for 1 hour at 50 °C to ensure the adsorption-desorption equilibrium. 20 mL of H_2O_2 (30 %) was added to start the reaction for the breaking down of methylene blue. Approximately 1 mL of the solution was sampled at 60 minutes into 100 mL volumetric flask and 1 mL of isopropanol was added to quench the reaction. The solution was diluted to the mark with deionized water and analysed using the atomic Adsorption spectrophotometry (AAS).

2.5. Characterization techniques.

These characterization instruments were used to investigate the chemical and physical properties of the prepared materials. Characterizations were done internally and also send to external facilities.

The chemical composition and functional groups of iron oxide nanoparticles and iron oxide-silica nanofibers were determined using Perkin-Elmer 400 IR Spectrometer, universal ATR with diamond detector a wavenumber range from 400-4000 cm^{-1}. The optical properties of the iron oxide nanoparticles were studied using UV-Vis spectrophotometer analysis, performed with a double beam spectrometer-Perkin Elmer Lambda 25 UV/Vis with a tungsten and deuterium lamp. The spectra were collected from 180-1100 nm using a bandwidth of 1 nm with a fixed slit. The quantitative studies for dye degradation were carried out using Thermo Scientific Evolution 220 UV-Vis spectrophotometer single beam. Photoluminescence analysis was performed at room temperature using Jasco spectrofluorometer FP-8600 equipped with XE lamp, 150 W, with bandwidth excitation slit 5 nm and the emission ranging from 200-1010 nm. The crystallinity and phase of the materials were investigated by X-ray diffraction patterns were recorded using the Shimadzu-XRD 700, X-ray diffractometer with Cu Ka radiation (λ-1.154056 A˚). A scan speed of 1˚/minute, current 30 mA and voltage of 40 kV. A secondary monochromated Co K α radiation (I =1, 7902 Å) was used, the measurements were taken at high angle 2θ in a range of 5˚-90˚ with a scan speed of 0.1˚ 2θ s^{-1}. The crystalline sizes were estimated by Debye-Scherer equation and the d spacing were determined using Bragg's law. The size and shape of the nanoparticles were determined from JEOL JEM-2100 transmission electron microscope operating at accelerating voltage of 200 kV and tungsten wire filament. The silica nanofibers and iron oxide nanofibers images were obtained using an FEI Nova NanoSEM 230 with a field emission gun and Field emission scanning microscopy (FE-SEM) (ZEISS ultra plus, Germany). For leaching studies atomic adsorption spectroscopy was used (AAS), AA-7000 dual atomizer model spectrometer from Shimadzu (Kyoto Japan), with iron cathode lamp operating at a wavelength of 58 nm, with acetylene purged.

CHAPTER 3

3. RESULTS AND DISCUSSION

This chapter covers the discussion of results from three different methods employed during the fabrication of the iron oxide-silica nanofibers in this study. The approaches used include the preparation of iron oxide silica nanofibers by incipient wetness impregnation of iron nitrate into the silica nanofibers (method 1), the preparation of iron oxide-silica nanofibers by direct addition of iron nitrate in the spinning solution (method 2) and the preparation of iron oxide-silica nanofibers by incorporating iron oxide nanoparticles directly on the spinning solution (method 3). Various conditions were set for the preparation of the catalysts such as the effect of loading iron oxide (1 wt.%, 2 wt.% and 5 wt.%) and effect of calcination. While the variation of voltage was done in pure fibres to obtain the optimum voltage. These materials were characterised using instruments in Chapter 3 section 2.5. Fenton degradation was exploited using all the prepared catalysts in method 1, 2 and 3. The preparation of the catalyst can be influenced by the method used and hence the exploration of the three approaches to establish the best method for the formation of the catalyst that will be suitable for the catalytic application. This will depend on the morphology, diameter and the surface to volume ratio that will give high surface area by creating more active sides on the material to provide the best possible conditions for the Fenton catalytic reaction.

3.1. Iron oxide-silica nanofibers prepared using incipient wetness impregnation method (Method 1)

3.1.1. Characterization of pure silica nanofibers using FTIR spectroscopy

The FTIR spectra gives the formation of the functional group present on the silica NF's, with a vibrational mode at the region between 4000 - 500 cm^{-1}. Figure 6 a shows 10 wt.% PVA solution spectra with a broad peak at a region 3300 cm^{-1} which is due to the hydroxyl (O-H) vibration from PVA and another peak was observed at 1640 cm^{-1} assigned to C-C stretching from the aromatic ring. Figure 6 b shows silica sol spectra with a broad peak at 3300 cm^{-1} which is ascribed to the O-H bond from the PVA solution and water used during the preparation of the sol, other prominent peaks were observed the at 2970 cm^{-1}, 1600 cm^{-1}, 1100 cm^{-1}, 970 cm^{-1} and 590 cm^{-1} which are ascribed to C-C, C-H, Si-O-Si and the sinol group (Si-OH)

respectively. The O-H peak appeared to be more pronounced in the PVA spectra, compared to silica sol because the PVA solution was mixed with silica sol hence the peak became less pronounced this might indicate the interaction between the PVA and silica sol. It was observed that when the PVA-silica sol electrospun, the O-H peak intensity gradually decreased due to the solvent evaporation and oxidation condensation reaction took place as shown in Scheme 1 (Sahebi et al., 2015). After thermal treatment, the O-H completely disappeared and a gradual increase in Si-O-Si intensity attributed to complete oxidation condensation of silica hydroxyls to silica and desorption of solvent from the fibre surface.

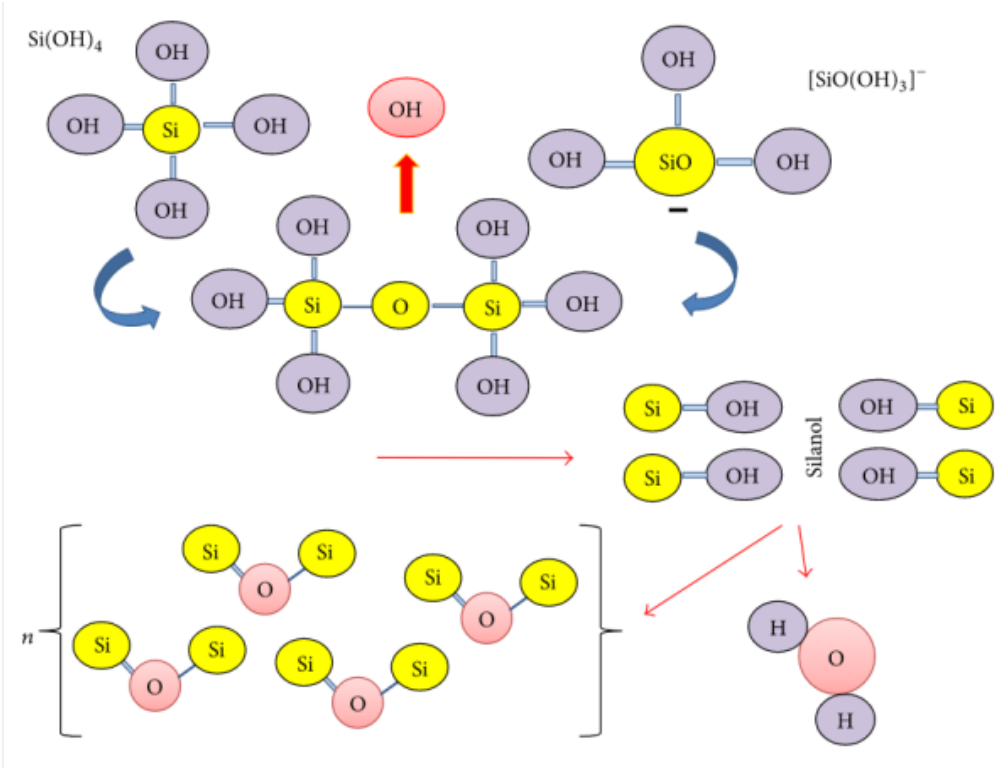

Scheme 2: Oxidation of silica hydroxyls to form silica (Sahebi et al., 2015).

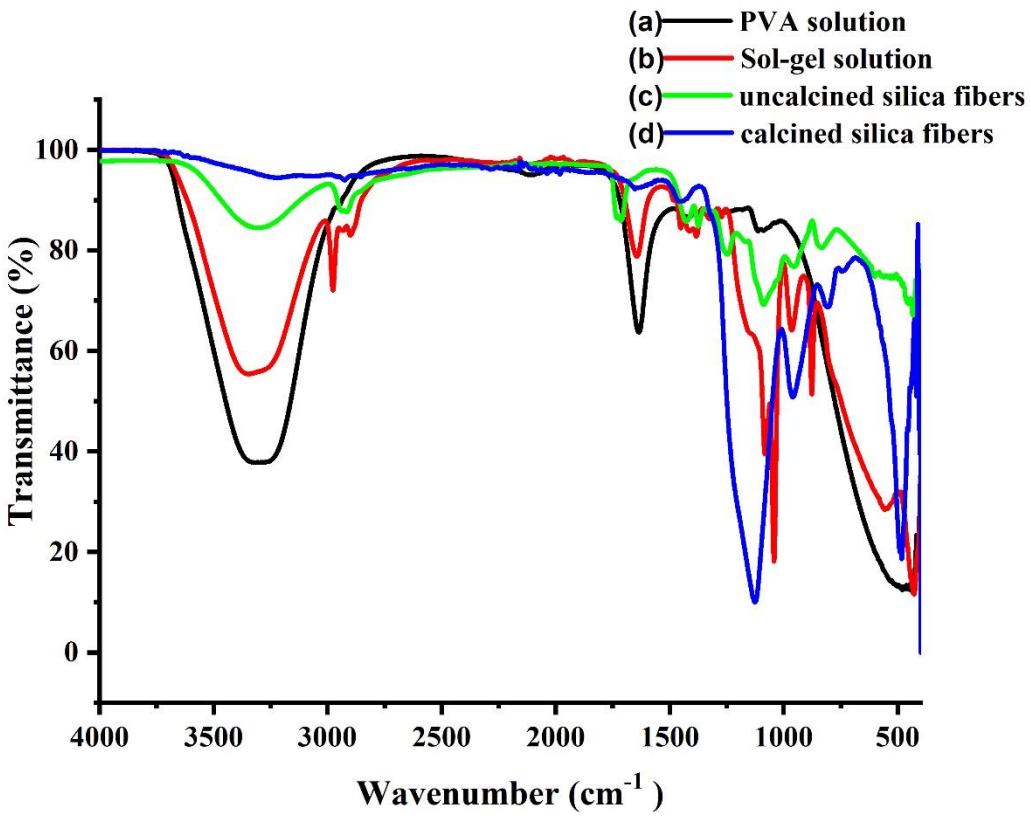

Figure 6: FTIR spectra of (a) PVA, (b) PVA/silica so gel (c) electrospun PVA/silica NF's and (d) calcined silica NF's.

3.1.2. Effect of varying voltage and calcination on pure silica nanofibers.

(a) Effect of voltage variation

The morphology of the electrospun fibres can be influenced by varies parameter such as conductivity, surface tension, viscosity, distance from the tip to the collector, the voltage being among the parameters (Song et al., 2018). The applied electrical field affects the morphology of the fibres (Hobzov et al., 2012). When a strong electrostatic force is applied, charges are generated in the solution, and then the charged solution moves towards the ground collector (Baji et al., 2010). When a charged jet is ejected from the tip at different voltages the fibres formed are in varies shapes and diameter (Wong et al., 2008). Optimising the voltage is a key driver in the design of nanofibers (Zhang et al., 2020) and hence the voltages ranging from 20 to 30 kV were applied and found desirable to produce fibres as compared to electrospraying or forming beads. Figure 7 a, b and c show silica nanofibers electrospun at 20 kV, 25 kV, and 30 kV respectively. When the applied voltage was 20 kV the diameter of the fibre was 341 nm,

while at 25 kV it was 602 nm and at 30 kV it was 349 nm. It was observed that there was an increase in fibres diameter from 20 kV to 25 kV this might be due to the deformation of polymeric droplets (Haider et al., 2018). A decrease in fibres diameter from 25 kV to 30 kV was also observed which attributed to stretching of the polymer. It was observed that at 25 kV was the critical voltage hence a decrease in fibre diameter was observed as the voltage was future increased. A thick fibre mat was obtained at high voltage and the fibres were formed much faster. Therefore, the optimum voltage was found to be 20 kV due to smaller diameter and well-distributed fibres. Applied voltage had effects on both the size and shape of the fibres. Figure 3a and c showed a macaroni like shaped fibres while the fibres are seen in Figure 3b there were wide fibres.

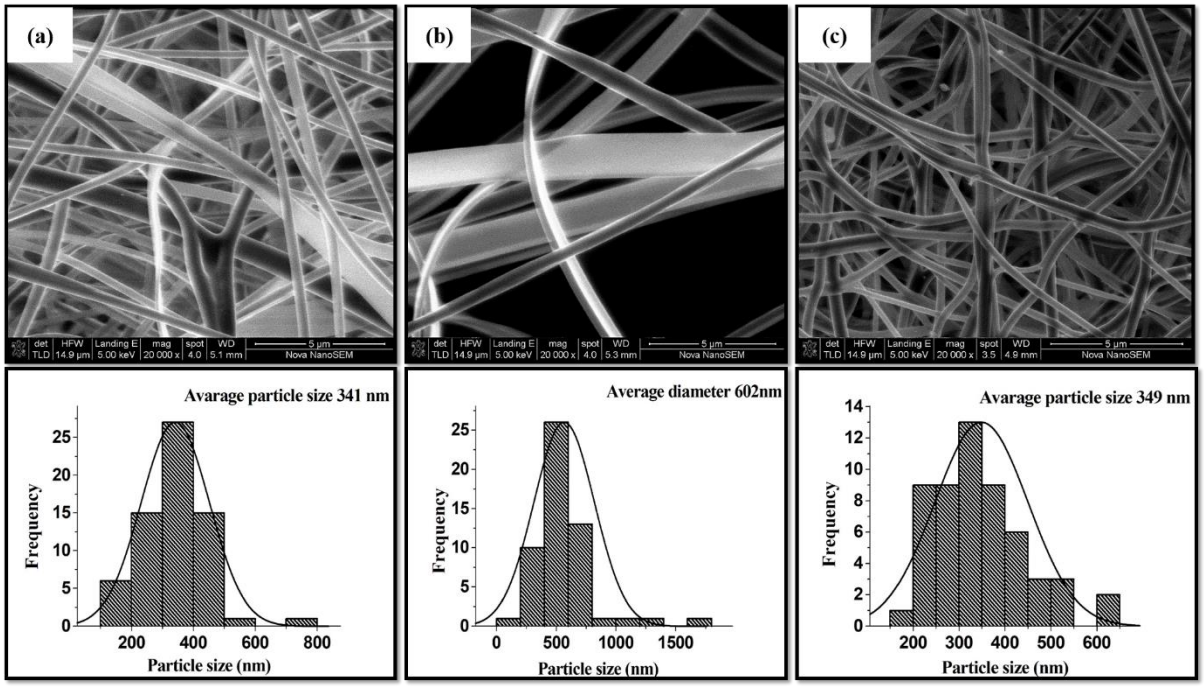

Figure 7: Scanning electron microscopy (SEM) images of iron oxide silica nanofibers electrospun at different voltages (a) 20 kV, (b) 25 kV, and (c) 30 kV and their particle size distribution histogram.

(b) Effect of calcination.

The silica nanofibers were calcined at 400 °C to remove the organic polymer in order to obtain pure silica nanofibers. Figure 8 shows iron oxide silica nanofibers before and after calcination. The calcined fibres prepared at 20, 25 and 30 kV had a smaller average diameter ranging from 276 - 367 nmcompared to the uncalcined iron oxide silica nanofibers which diameter ranging

from 377- 434 nm. The decrease in diameter is attributed to the decomposition of PVA polymer during calcination at 400 °C. The fibre exhibited relative uniform size distribution and well-defined shapes. After calcination, the fibres became smaller as shown in Figure 8 e and g due to thermal treatment that indicates a physical interaction between the organic polymer and the inorganic matrix was present before calcination (Toskas et al., 2011).

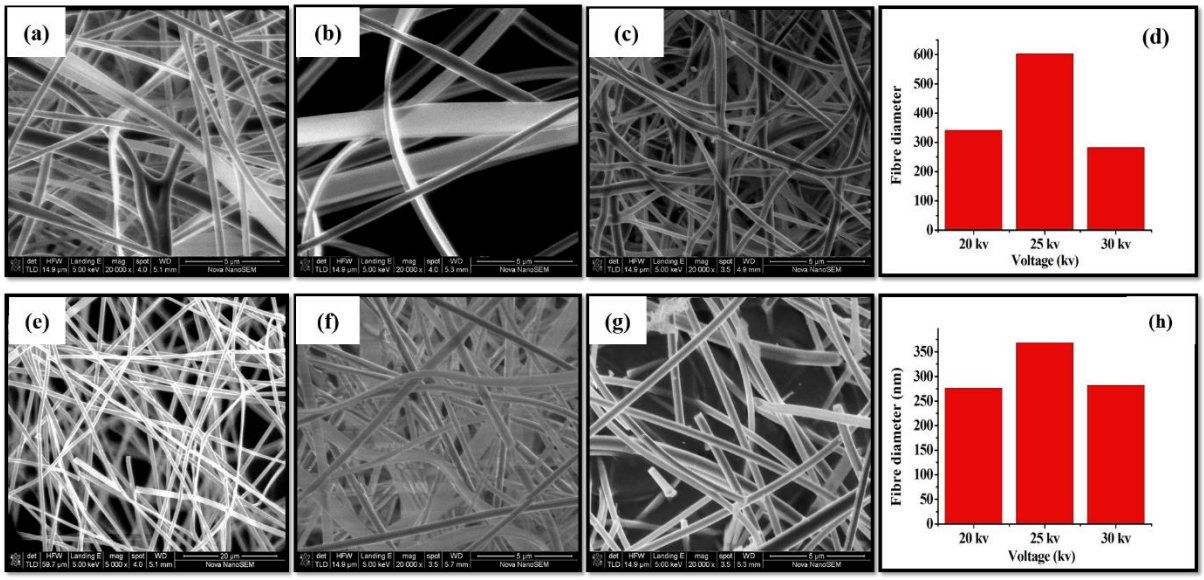

Figure 8: Scanning electron microscopy (SEM) images of silica nanofibers before calcination (a to c) with voltage ranging from 20,25 & 30 kV respectively and after calcination (e to g), and their respective size histograms (d & h). (Calcination temperature is 400 °C).

(c) Fourier transform infrared (FTIR) spectroscopy

The FTIR future confirmed the decomposition of the organic polymer during calcination as observed on the FTIR spectra as shown in Figure 9. The uncalcined silica nanofibers showed a broad peak at 3200 cm^{-1} ascribed to the O-H stretching and other peaks were observed at 1050 cm^{-1} attributed to Si-O-Si, whereas the calcined fibres the O-H peak was no longer visible, indicating the decomposition of PVA on the fibres, that lead to the decrease in fibres diameter as indicated in 3.1.2 b.

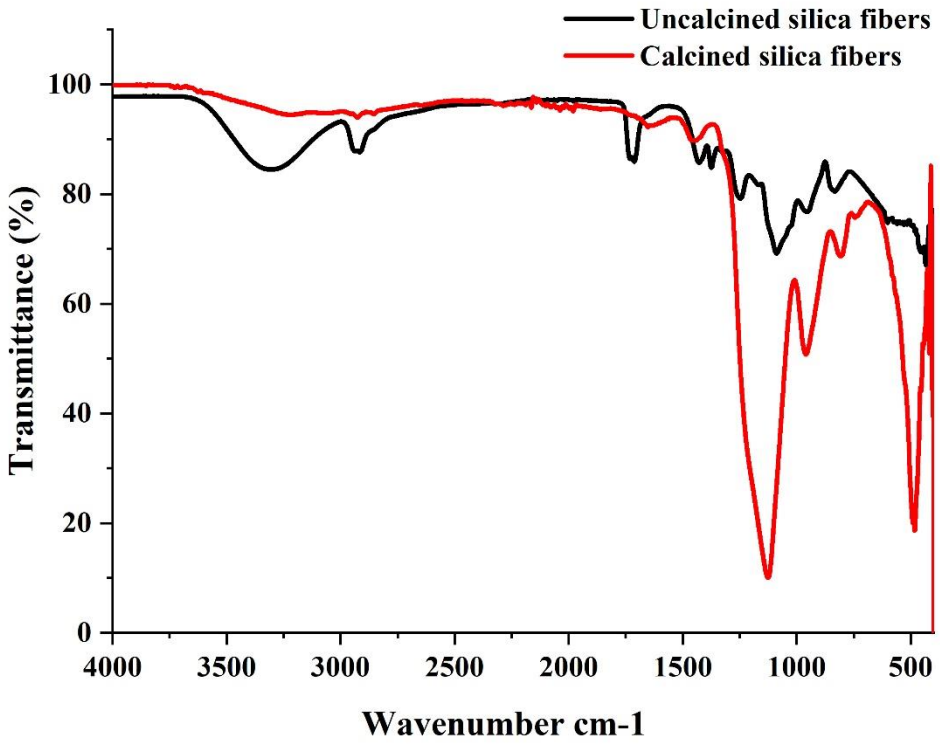

Figure 9: FTIR spectra of iron oxide-silica nanofibers before and after calcination at 400 °C.

3.1.3. Characterization of iron oxide-silica nanofibers using XRD and FTIR spectroscopy.

(a) X-ray diffraction patterns (XRD)

X-ray diffraction Patten (XRD) analysis was performed at room temperature from 0° to 80° to determine the crystalline phase of the silica nanofibers impregnated with 1 wt.%, 2 wt.% and 5 wt.% iron oxide. A broad diffraction peak was observed on the XRD Patten between 20°-30° indicating the amorphous nature of silica nanofibers, no iron oxide diffraction peaks were observed this is attributed to the small crystalline size of the iron oxide, indicating that they are less than 5 nm hence they are lower than the XRD detection limit (Y. Wang et al., 2017). The spectrum of 5 wt.% iron oxide silica nanofibers showed another peak at 35° and 63° attributed to the increase in iron oxide content, this might suggest that the iron oxide is very well dispersed within the support material hence it is amorphous.

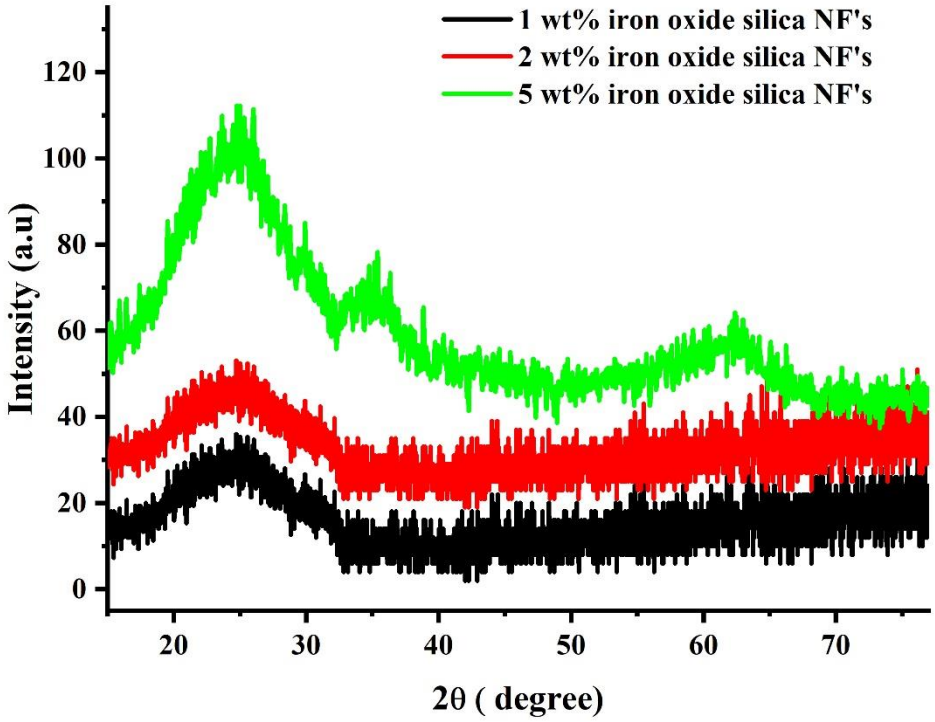

Figure 10: X-ray diffraction pattern of silica nanofibers impregnated 1 wt.%, 2 wt.% and 5 wt.% iron oxide

(b) Fourier transform infrared (FTIR) spectroscopy

Figure 11 presents the FTIR spectra of silica nanofibers with characteristic adsorption band at 1700 cm^{-1}, 1100 cm^{-1} and 870 cm^{-1} attributed to C= C, Si – O – Si and Si-OH. As the iron oxide is introduced a slight shift on the peaks that indicate the interaction between the silica nanofibers and iron oxide. An additional adsorption peak was observed at 520 cm^{-1} characteristics to Fe-O confirming the formation of iron oxide.

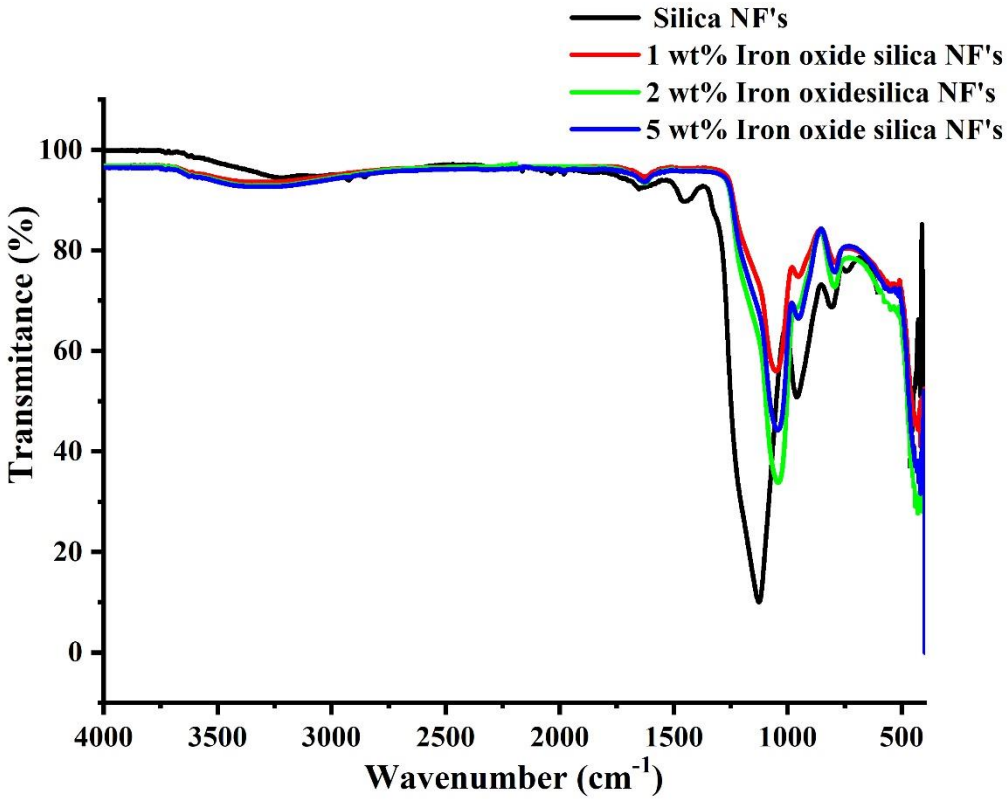

Figure 11: FTIR spectra of silica nanofibers and silica nanofibers impregnated 1 wt.%, 2 wt.% and 5 wt.% iron oxide.

3.1.4. Effect of loading iron oxide and EDS analysis.

(a) Effect of loading iron oxide.

The morphology and the size of the fibres were investigated using the scanning electron microscopy (SEM). The image in Figure 12 a show plain silica nanofibers that appeared to be uniform and continuous with an average diameter of 276 nm. Figure 12 b, c and d showed silica nanofibers impregnated with different loadings of iron oxide. Upon calcination, the impregnated silica nanofibers changed to dark brown indicating the formation of iron oxide similar results were obtained by Patel et al., 2017. A change on the surface of the material was observed after the incipient wetness impregnation the fibres surface slightly changed and layers were forming on the surface attributed to the incorporation of iron oxide, indicating that the iron oxide might be also covering the silica fibre support. The fibres were randomly distributed with an average diameter of 279 nm, 282 nm and 288 nm, it was observed that as the iron loading concentration was increased the fibre diameter also increased. Although the change was not too high from the plain fibres.

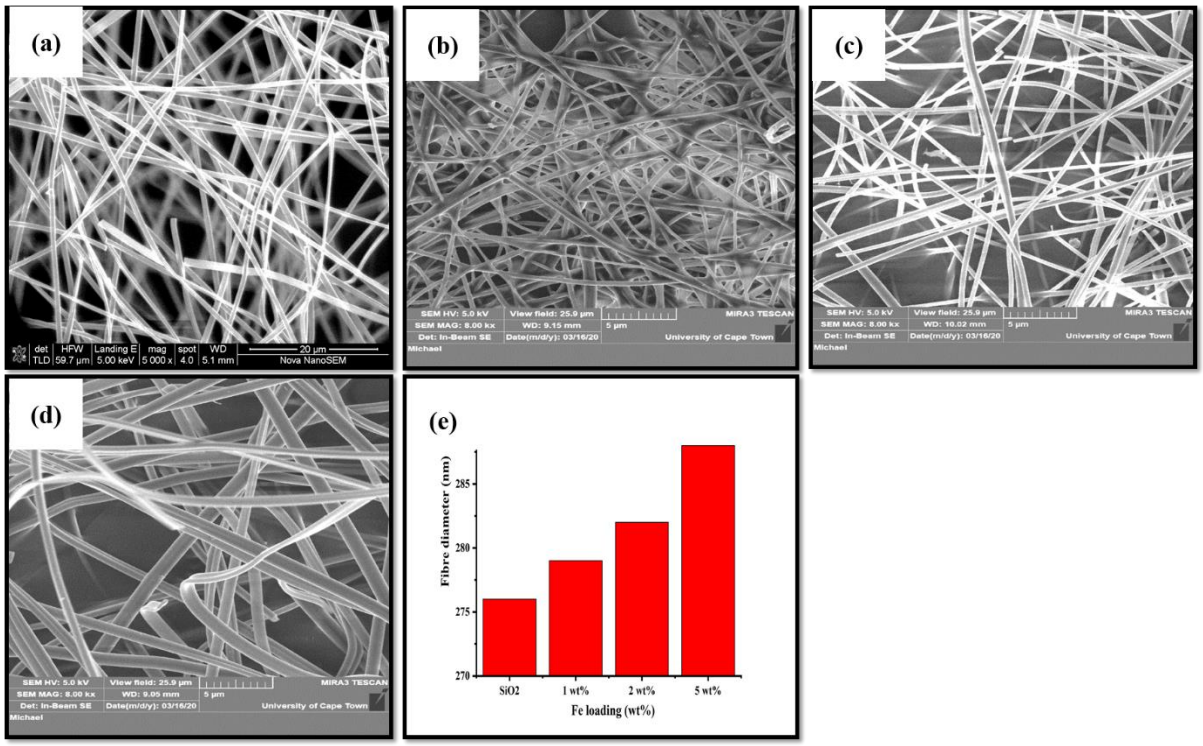

Figure 12: SEM image of (a) silica NF's and (b) 1 wt.%, (c) 2 wt.% and (d) 5 wt.% impregnated iron oxide-silica NF's.

(b) Energy dispersive x-ray spectroscopy (EDS)

The Energy dispersive x-ray spectroscopy (EDS) analysis was used to identify the elemental composition of the obtained material. Figure 13 reveals the presence of C, P, O, Si and Fe and the weight per cent presented in Table 1. The materials contained all the desirable components with smaller traces of phosphorous (P) due to the phosphoric acid used as a catalyst during the preparation of sol-gel. The percentages of iron and oxygen increase with an increase in oxide loading. As observed in table 1 the oxygen of the plain silica nanofibers had a lower oxygen content, however, when the iron oxide was introduced there was an increase in oxygen and the more the iron percentage is increased from 1 wt% to 2 wt% and 5 wt% the oxygen constantly increase primarily due to the oxides attached to the iron metal.

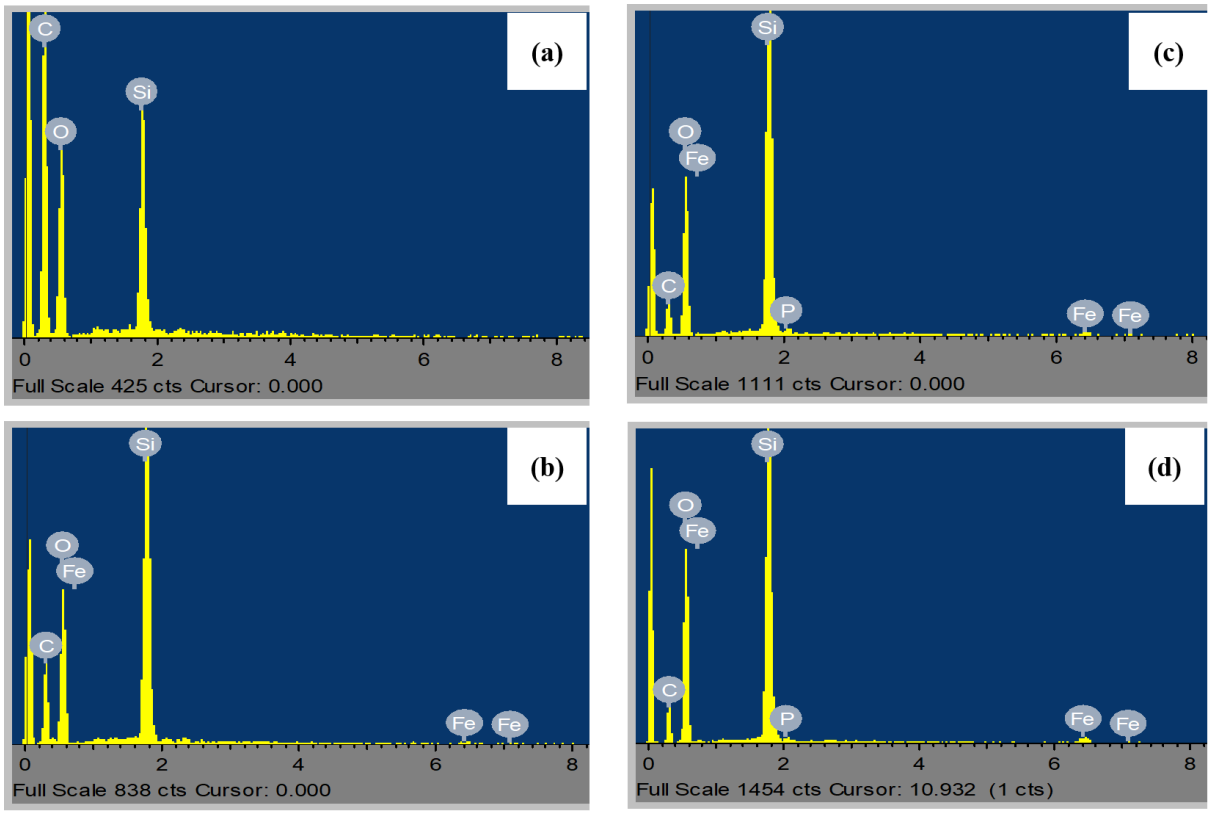

Figure 13: SEM-EDS analysis of silica NF's and (1 wt.%, 2 wt.% and 5 wt.%) impregnated iron.

Table 1: Energy-dispersive X-ray spectroscopy (EDS) Analysis elemental composition silica nanofibers and silica nanofibers impregnated with 1 wt.%, 2 wt.% and 5 wt.% iron oxide

Catalysts	Elements percentage (wt. %)					
	C	O	Si	P	Fe	Total
Silica NF's	8.91	47.10	44.6	0.32	0.00	100
1 wt.% iron oxide silica NF's	7.31	58.28	33,57	0,32	0.52	100
2 wt.% iron oxide silica NF's	6.19	59.33	33.1	0,36	1.02	100
5 wt.% iron oxide silica NF's	4.36	59.12	33,67	0,33	3.52	100

(c) Fenton catalytic activity

The degradation of methylene blue was done in order to determine the catalytic activity by varying different catalysts with different iron oxide percentage loading. The catalysts were first placed in the methylene blue (MB) solution for an hour of adsorption studies then followed by the Fenton degradation process. The Fenton degradation process the catalyst reaction with hydrogen peroxide and that are hydroxyl radicals that are formed. Note that the percentage

removal does not start at zero and this is due to 60 minutes adsorption that took place before catalysis, as described in Chapter 2.3. As shown in Figure 11 adsorption process showed significant removal of MB, about 52.6 % removal was obtained for plain silica NF's within 1 hour. While 20 %, 13.2 % and 7.7 % adsorption removal were obtained for 1wt% iron oxide-silica NF's, 2 wt% iron oxide- silica NF's and 5 wt% iron oxide- silica NF's respectively. Upon addition of hydrogen peroxide (H_2O_2) for Fenton process,the removal efficiency increased by 16.5 %, 25.6 %, 40.2 % and 60.2 % with total removal efficiency of 69.1 %, 45.6 %, 53,2 % and 67.9 % respectively. Silica NF's showed high removal capacity due to its high adsorption capacity on the surface of the material while it had no Fenton catalytic activity effect because there was no radicals' formation. On the other hand, the impregnated material had low adsorption capacity this might be due to the iron sitting on the surface of the fibres resulting to slow adsorption. Although the introduction of iron oxide species on silica nanofibers played a catalytic role. The iron oxide reacts with the hydrogen peroxide producing highly oxidising radicals that subsequently attack the organic species, leading to their degradation, hence increasing the removal efficiency. The more the iron oxide concentration is increased the removal efficiency also increases. It was also observed that time also affects removal efficiency increases, as the time increases the removal efficiency also increase.

During the catalytic activity two stages were observed, the first 30 minutes there was an induction period, due to slow reaction, followed by the oxidation. In the first 30 minutes, the iron ions react with the hydrogen peroxide to generate the hydroxyl radicals that lead to a slow degradation, after 30 minutes the hydroxyl radicals are generated there attracting the organic compounds. Similar results were obtained by Albhisha et al., (2016), where they reported three stages in the photo-Fenton degradation. The first stage was considered as the induction period, the reaction was slow and they suggested that this stage involves the generation of the hydroxyl radicals. In the second stage, there was significant degradation taking place, where the hydroxyl radicals acted as oxidising agents for the degradation of the dye. In the third stage, the reaction rate slowed down and they suggested that it was due to the smaller amount of dye remain hence leading to a slow reaction. While, Xu et al., (2011) suggested that the activation process is due to the surface of iron species and iron dissolution.

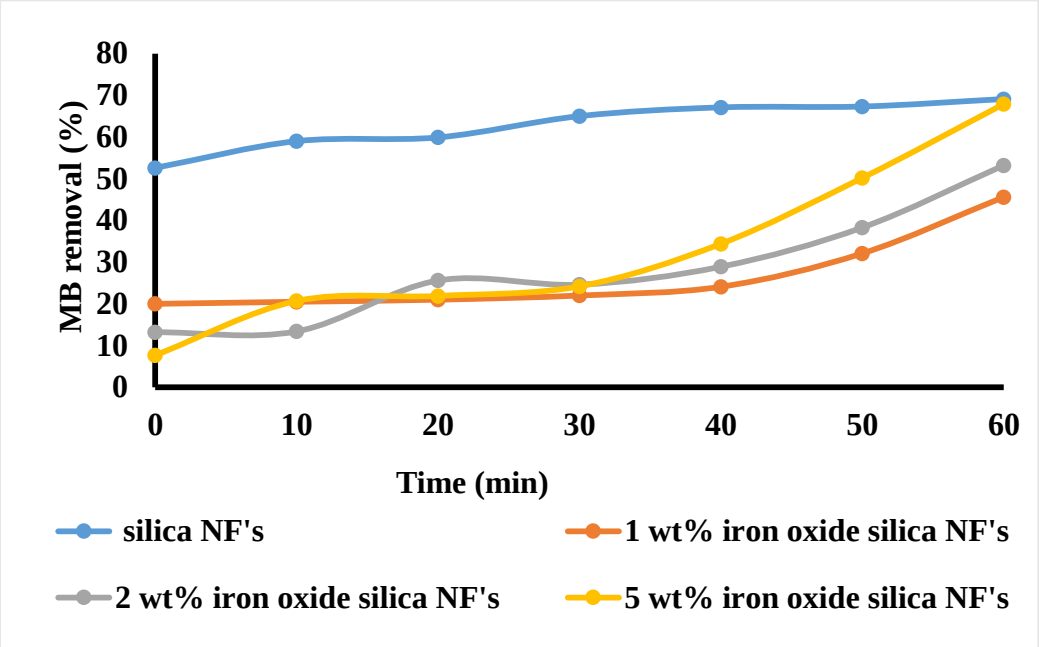

Figure 14: Fenton degradation efficiency of MB using silica nanofibers, 1 wt%, 2 wt% and 5 wt% iron oxide-silica nanofibers catalyst.

(d) Kinetics studies

The kinetic studies for the Fenton process were performed to determine the rate of reaction. The rate can either be described as the pseudo-first-order or pseudo-second-order depending on the best-fitted correlation constant. Pseudo first order and Pseudo second order kinetics were therefore fitted to all data points of the obtained information shown in table 2 represented in (Figure 15 a and b), but low R^2 values were obtained due to an induction period observed during the first 30 minutes of the reaction (see 3.1.4). The results showed that the rate between the pollutant and the catalyst best fitted the Pseudo-first-order due to high correlation coefficient as seen in (Table 2). Table 3 represented in figure 16 a and b showed the correlation after the induction period Xu et al. (2011) showed that when the pH decreases the induction period disappeared (see Figure 16) indicating that the pH plays a role. When the pollutant gets oxidised, the organic acids like oxalic acid and acetic acids form and pH drops, in turn, accelerates the rate of the Fenton reaction. Zhou et al. 2014, studied the course of the induction period. They found out that the calcination temperature played a vital role in the activity, although it needed a long time for the activation. Therefore, it showed that the activation process plays a role.

Table 2: Degradation of MB at different loading of Fe (before the 30 minutes).

Catalysts	Pseudo first order		Pseudo second order	
	k (min^{-1})	**R^2**	**k (ppm^{-1} min^{-1})**	**R^2**
SiO_2 NF's	0.0069	0.9362	0.0002	0.9532
1 wt% iron oxide- SiO_2 NF's	0.0054	0.6834	8×10^{-5}	0.6509
2 wt% iron oxide- SiO_2 NF's	0.0009	0.8750	-0.0001	0.7896
5 wt% iron oxide- SiO_2 NF's	0.0153	0.8279	0.0003	0.7283

Table 3: Degradation of MB at different loading of Fe (after 30 minutes).

Catalysts	Pseudo first order		Pseudo second order	
	k (min^{-1})	**R^2**	**k (ppm^{-1} min^{-1})**	**R^2**
SiO_2 NF's	0.0031	0.8222	0.00004	0.8202
1 wt% iron oxide- SiO_2 NF's	0.0167	0.9647	0.0008	0.9513
2 wt% iron oxide- SiO_2 NF's	0.0207	0.9666	0.0004	0.9462
5 wt% iron oxide- SiO_2 NF's	0.0357	0.9828	0.0008	0.9485

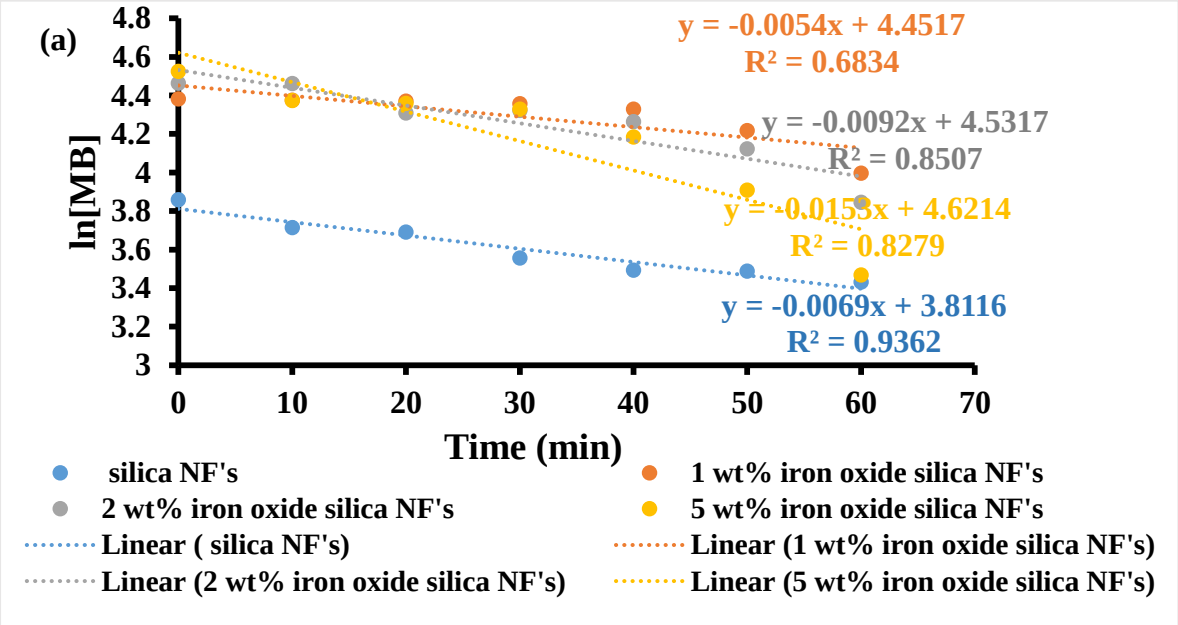

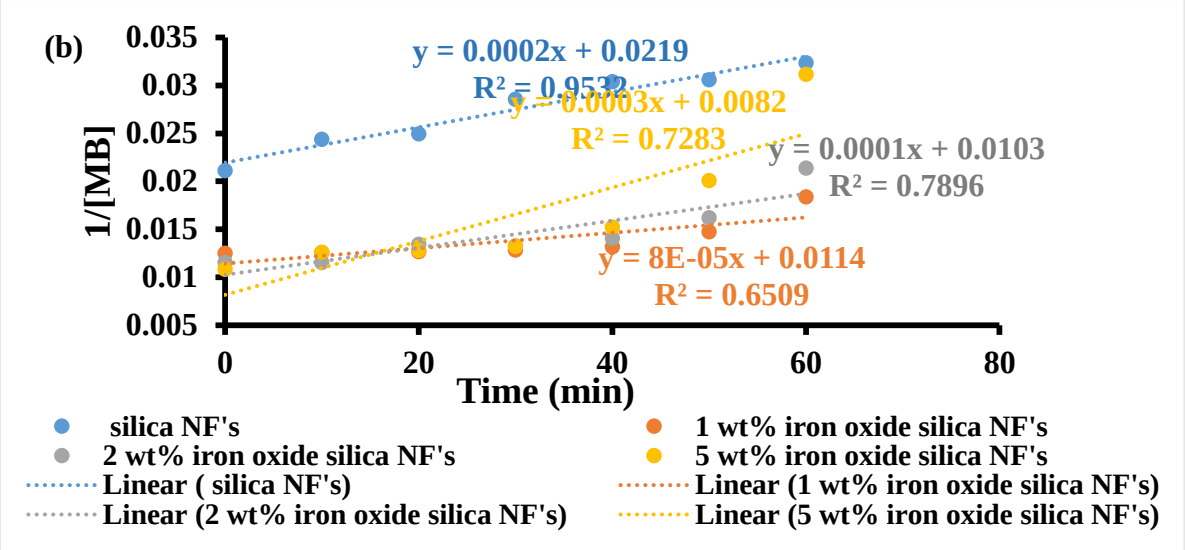

Figure 15: (a) Pseudo first order and (b) pseudo second-order kinetics of silica nanofibers, 1 wt.%, 2 wt.% and 5 wt.% iron oxide-silica nanofibers catalyst all points before and after 30 minutes.

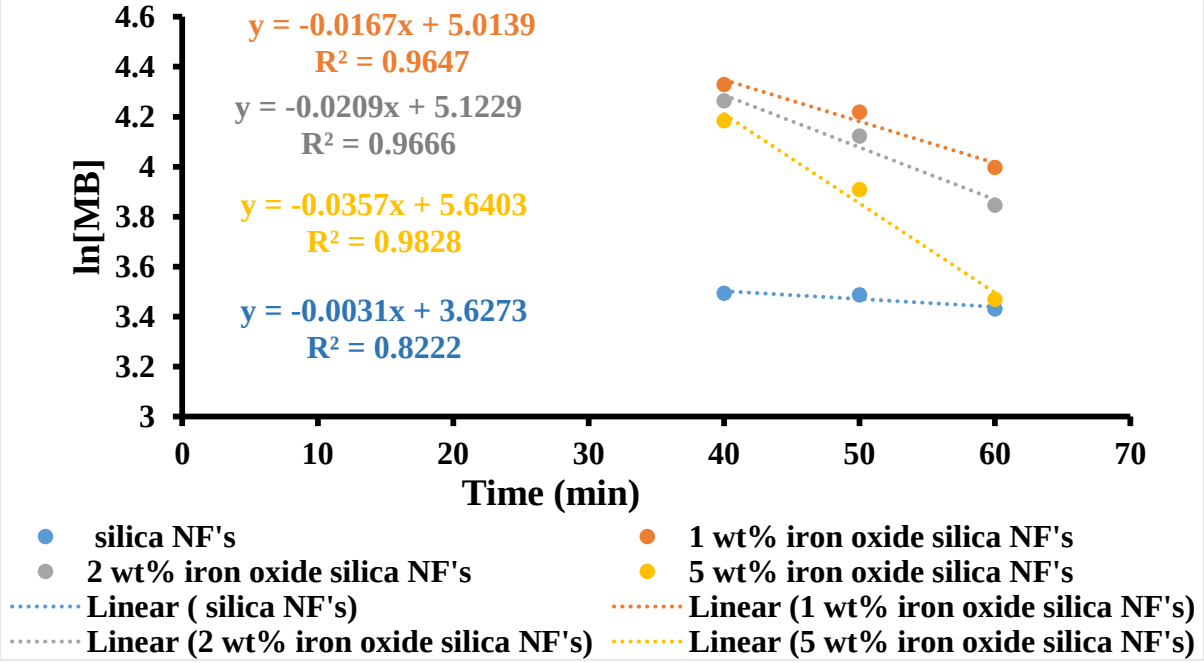

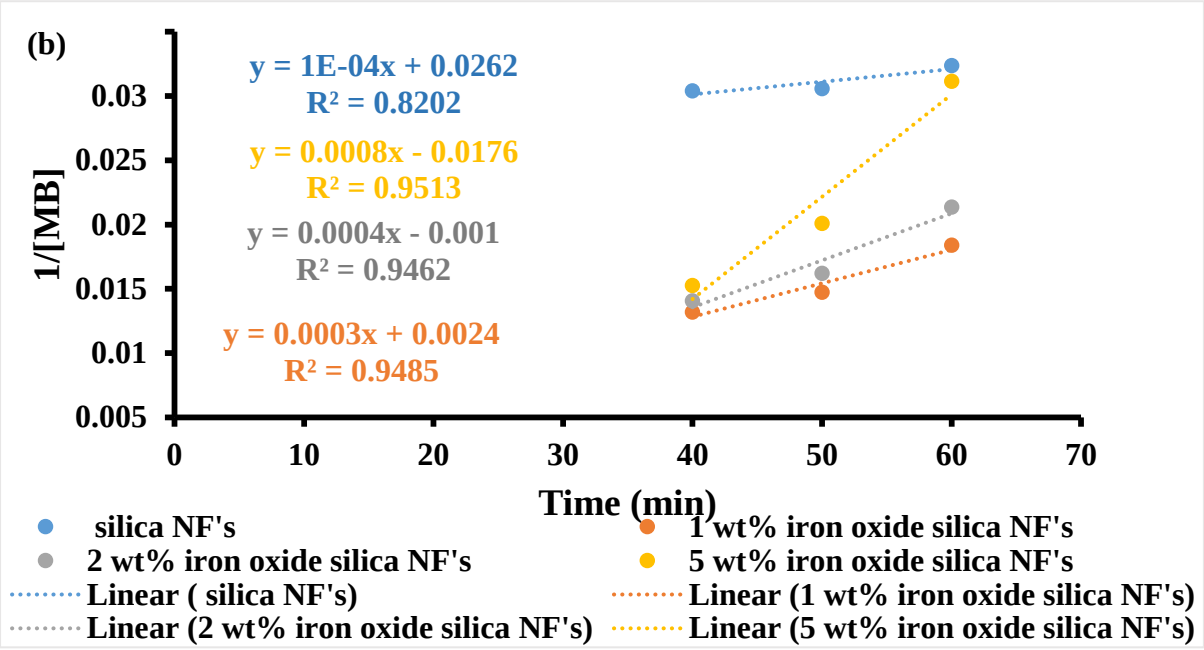

Figure 16: (a) Pseudo first order and (b) pseudo-second-order kinetics of silica nanofibers, 1 wt%, 2 wt% and 5 wt% iron oxide-silica nanofibers catalyst all points after 30 minutes.

3.2. Iron oxide silica nanofibers using the direct addition of iron precursor in the spinning solution. (Method 2)

3.2.1. Characterization of iron oxide-silica nanofibers using XRD

(a) X-ray Diffraction (XRD) analysis

X-ray diffraction pattern provided information about the crystalline phase of the electrospun iron oxide silica nanofibers. Figure 17 a and b shows a diffraction pattern of electrospun 1 wt%, 2 wt% and 5 wt% iron oxide silica nanofibers at 2θ with the scale ranging from 15° to 80^0. An amorphous phase was observed at 2θ = 25° which was due to the silica, which is more visible in Figure 1b. Four diffraction peaks were also observed at the region 38.22°, 44.13°, 64.84° and 77.39° which corresponds to the blank sample holder shown in Figure 17a, this could be due to incomplete coverage of the sample holder by the sample. The spectra showed no visible iron oxide peaks for the percentage loadings of 1 wt%, 2 wt% and 5 wt%, this might be due to small crystalline size or lower concentrations of iron oxide loaded, therefore, it might be below the detection limit of XRD (Maliyekkal et al., 2010). This might also be due to poor coverage of the sample holder by sample the Hence the EDS analysis was done to confirm the presence of iron oxide on the material sees Figure 19.

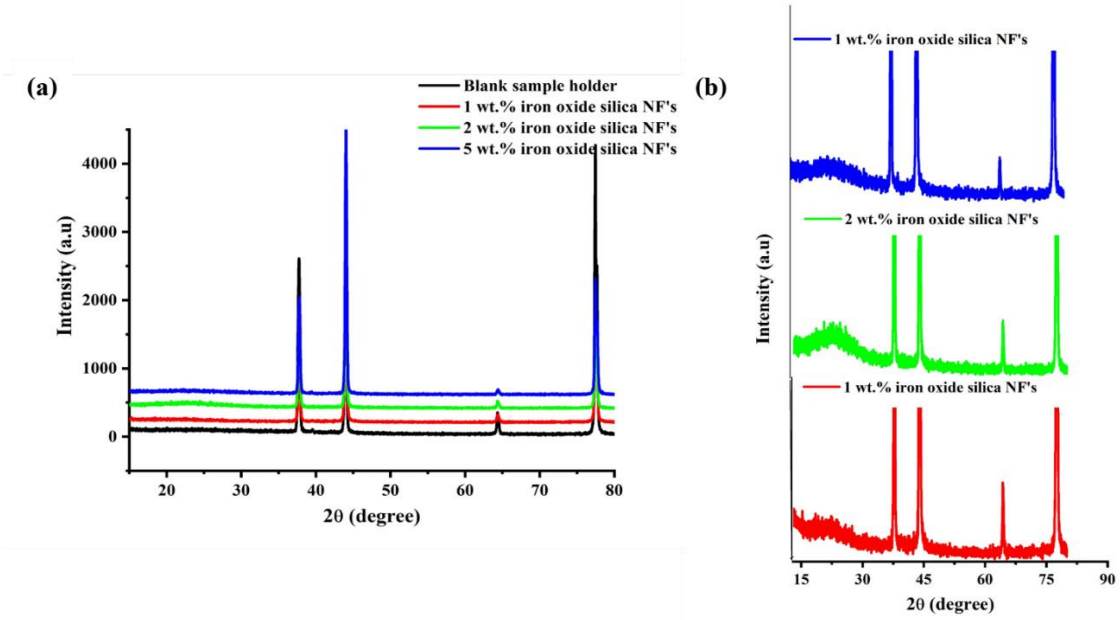

Figure 17: Powder X-ray diffraction (XRD) patterns of (a) blank sample holder, 1 wt%, 2 wt% and 5 wt% iron oxide silica nanofibers, (b) zoom-in spectra of 1 wt%, 2 wt% and 5 wt% iron oxide silica nanofibers.

3.2.2. Effect of loading of iron oxide and EDS analysis

(a) Effect of loading iron oxide

Figure 18 shows the SEM images of the iron oxide silica NF's loaded of 1 wt.%, 2 wt.% and 5 wt.% iron oxide. The loading of iron had an effect on the surface of the fibres, as the iron content was increased the surface becomes rougher with some layers forming. Figure 15 showed beats formation that might be due to the spraying of the jet when the voltage was initially applied. The increase in iron content also has a sight influence on the diameter of the fibre as the iron content increased the fibre diameter increased suggesting that iron influences the thickness of the fibre.

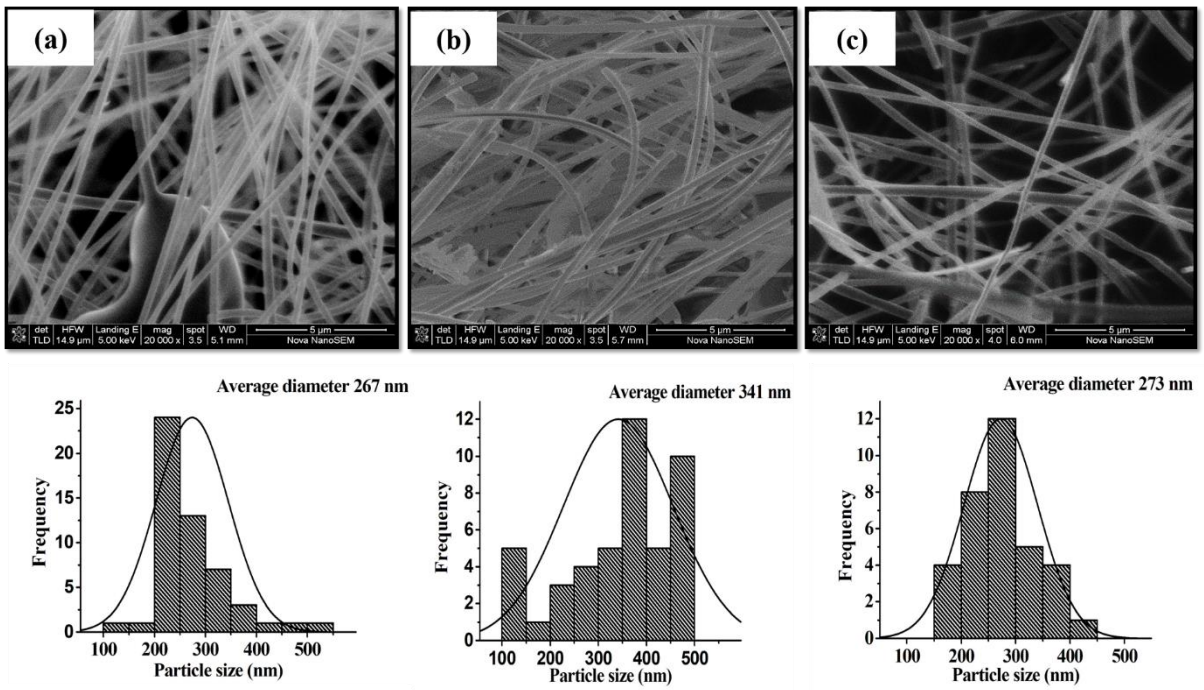

Figure 18: Scanning electron microscopy (SEM) images of silica nanofibers loaded with (a) 1 wt.% (b) 2 wt.% (c) 5 wt.% iron oxide and their distribution graphs.

(b) Energy dispersive x-ray spectroscopy (EDS) Analysis of Iron oxide-silica nanofibers.

The elemental composition was presented by the SEM-EDS analysis that highlighted the presence of C, O, Si, P, and Fe. The presence of Fe and O confirmed the formation of iron oxide. Si attributed to silica, the average atomic percentage formation shown in Figure 19 and Table 4. The results obtained in method 1(Impregnation) Figure 10 and table 1 showed an increase in iron oxide as the iron percentage was increased but compared to this method (direct

addition of iron precursor) all the percentages are approximately around 1 wt%. That results might suggest that the iron oxide doesn't behave the when they are introduced to the silica nanofibers by impregnation and direct addition of iron precursor. The iron oxide introduced by impregnation method is most likely to be sitting on the surface of the silica nanofibers (see 3.1.4 a) hence SEM-EDS detecting most of the material. Whereas on the direct addition method they might be embedded inside the silica nanofibers therefore the SEM-EDS detected only the iron oxide on the surface leading to lower percentages. This played a vital role in the catalytic and adsorption activity (see 3.1.4 c and 3.2.2 c)

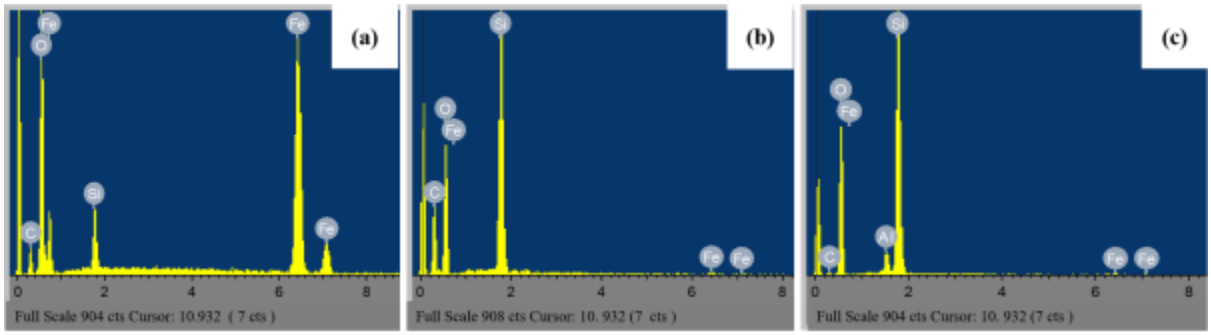

Figure 19: EDS analysis of silica nanofibers loaded with (a) 1 wt.% (b) 2 wt.% (c) 5 wt.% iron oxide.

Table 4: Energy dispersive x-ray spectroscopy (EDS) analysis elemental composition of 1 wt.%, 2 wt.% and 5 wt.% iron oxide silica nanofibers.

Catalysts	Elements percentage (wt. %)						
	C	O	Al	Si	P	Fe	Total
1 wt,% iron oxide silica NF's	25,38	49,37	0,00	27,89	0,37	0,98	100
2 wt.% iron oxide silica NF's	23,27	48,92	0,00	25,84	0,31	1,22	100
5 wt.% iron oxide silica NF's	21,10	52,28	0,34	24,78	0,34	1,16	100

(c) Fenton catalytic activity.

Methylene blue was used to investigate the catalytic activity of 1 wt.% iron oxide- SiO_2 NF's, 2 wt.% iron oxide- SiO_2 NF's and 5 wt.% iron oxide- SiO_2 NF's. 1 wt% iron oxide- SiO_2 NF's showed good adoption properties with a higher removal percentage. Upon addition of hydrogen peroxide (H_2O_2) for Fenton process, the removal efficiency increased by 19.2%, 44.6% and 50.2% for 1 wt.% iron oxide- SiO_2 NF's, 2 wt.% iron oxide- SiO_2 NF's and 5 wt.% iron oxide- SiO_2 NF's respectively. The addition of H_2O_2 in the presences of Fe based catalyst promoted

the formation of hydroxyl radicals, very strong oxidants that react with organic species and mineralise them into less toxic minerals. It was observed that an increase in Fe content leads to an increase in removal capacity. Therefore, the removal of MB was due to both the adsorption process and Fenton catalytic activity. The support adsorbed the MB molecules on the surface of the material, while the OH radical oxidised the MB that leads to higher removal efficiency. Hence 5 wt.% iron oxide- SiO_2 NF's has higher removal due to the synergistic effect of OH radicals and support material.

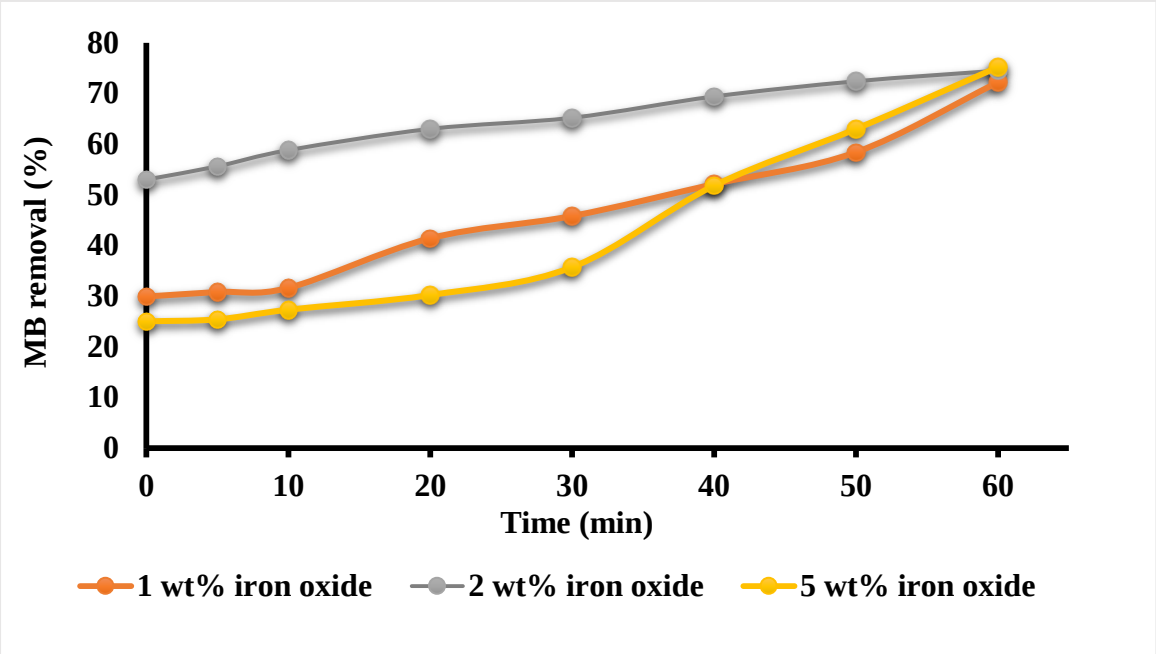

Figure 20: Fenton degradation efficiency of MB using silica nanofibers, 1 wt.%, 2 wt.% and 5 wt.% iron oxide-silica nanofibers catalyst.

During Fenton reaction, the degradation was monitored UV-vis qualitative analysis but it was also observed that as the degradation takes place there was also decolourization taking place, therefore to confirm the physical observations of the intensity of the colour change with time the decolourization of MB was monitored with UV-vis spectrophotometer, spectral analysis, a range of 200 nm-900 nm. MB exhibit character absorption wavelength of 665 nm. Figure 21: showed a rapid decrease in MB absorbance with time upon degradation in presence of 5 wt% iron oxide- SiO_2 NF's catalyst. As the reaction progresses the MB is absorbed in the surface of the catalyst and attacked by the hydroxyl radical oxidants that lead to decolourization. Therefore the Uv-vis confirmed the physical changes with the rapid change in the intensity of the absorbance.

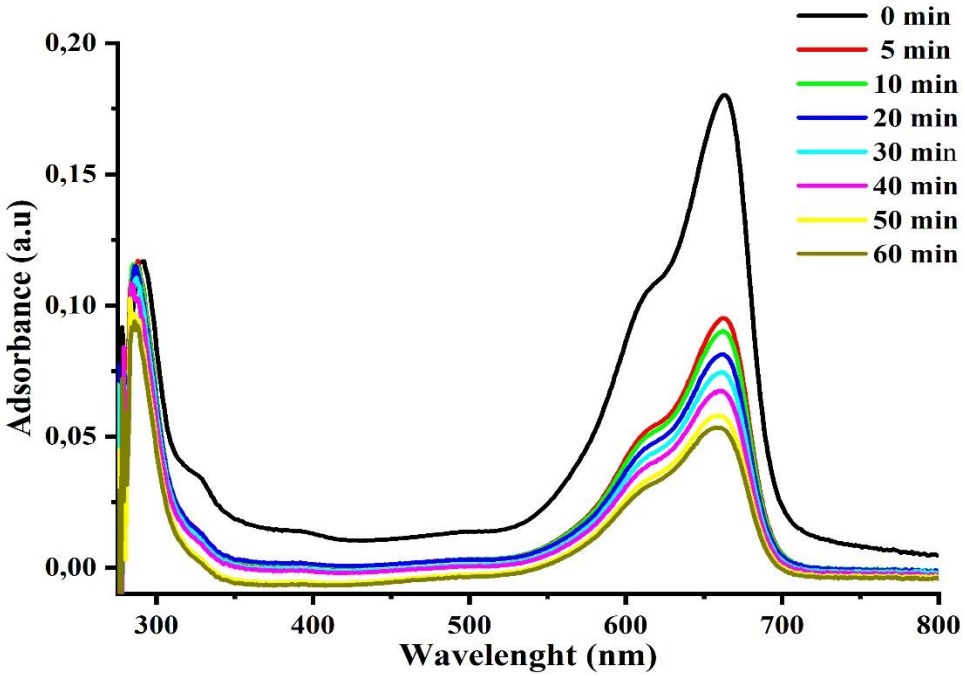

Figure 21: Uv-vis spectroscopy of changes in MB solution during the degradation process by iron oxide-silica nanofibers catalyst.

(d) Kinetics studies

The rate between the catalyst and the pollutant was determined using Pseudo kinetic studies. The calculated pseudo-first-order correlation coefficient of pure silica, 1 wt.%, 2 wt.% and 5 wt.% was 0.9489 min^{-1},0.9952 min^{-1}, 0.8731 min^{-1} and 0.9132 min^{-1} and for Pseudo second-order: 0.9588 $ppm^{-1}min^{-1}$ 0.9936 $ppm^{-1}min$, 0.7863 $ppm^{-1}min$ and 0.82 $ppm^{-1}min$ respectively. 1 wt.% iron oxide- SiO_2 NF's, 2 wt.% iron oxide- SiO_2 NF's and 5 wt.% iron oxide- SiO_2 NF's fit pseudo-first order with higher correlation coefficients and at a faster rate indicating the synergetic effect of composite with high k values of Pseudo first order as shown in Table 5.

Table 5: Pseudo kinetic model of degradation of MB at different loading of Fe.

Catalysts	Pseudo first order		Pseudo second order	
	k (min^{-1})	R^2	k ($ppm^{-1}min^{-1}$)	R^2
1 wt% iron oxide- SiO_2 NF's	0.0102	0.9952	0.0003	0.9936
2 wt% iron oxide- SiO_2 NF's	0.0174	0.8731	0.0002	0.7863
5 wt% iron oxide- SiO_2 NF's	0.0139	0.9933	0.0003	0.82

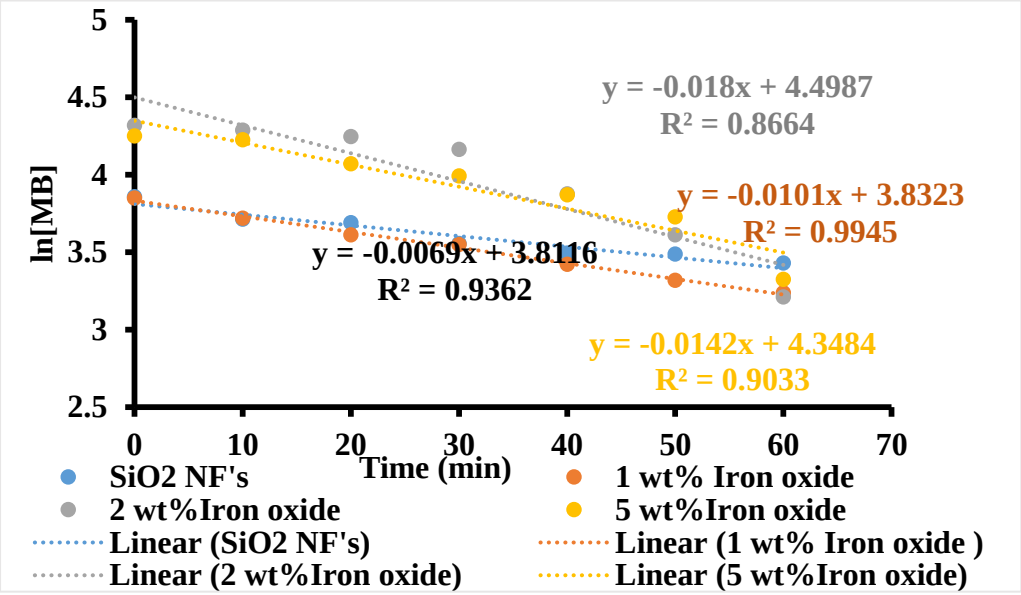

Figure 22: Pseudo first-order kinetics of silica nanofibers, 1 wt%, 2 wt% and 5 wt% iron oxide-silica nanofibers catalyst.

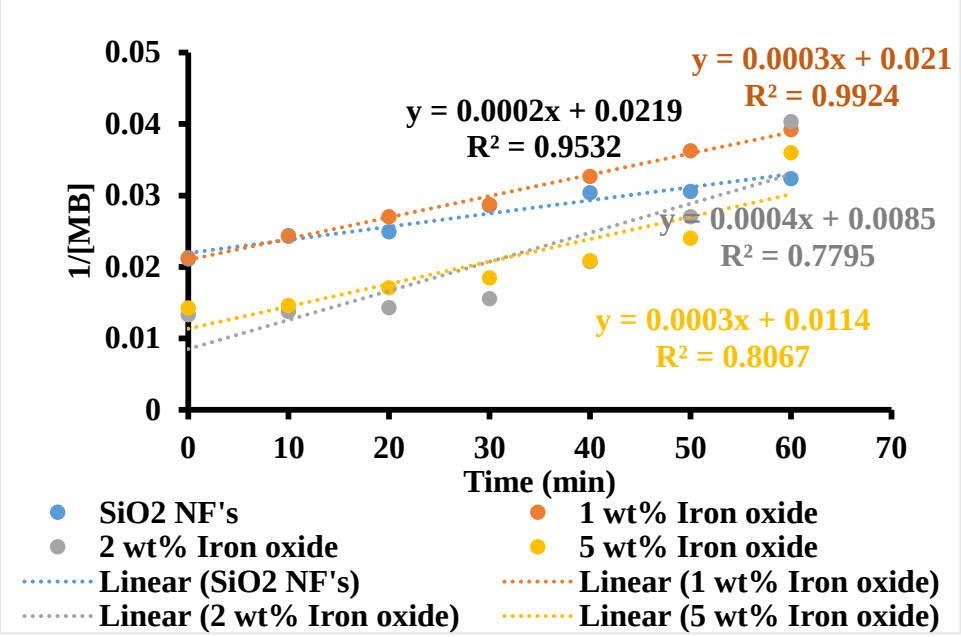

Figure 23: Pseudo second order kinetics of silica nanofibers, 1 wt%, 2 wt% and 5 wt% iron oxide-silica nanofibers catalyst.

3.3. Iron oxide silica nanofibers using direct incorporation of prepared iron oxide nanoparticles (magnetite) (Method 3).

3.3.1. Distribution and characterization of iron oxide nanoparticles (magnetite) and iron oxide-silica nanofibers using FTIR, UV-vis, Tauc plot, PL, XRD, Raman and TEM.

(a) Fourier-transform infrared spectral analysis of iron oxide.

The infrared spectra presented in Figure 24, shows the functional groups present on synthesised iron oxide nanoparticles. A prominent peak was observed at 580 cm^{-1}, assigned to Fe-O stretching which confirm the formation of iron oxide nanoparticles. According to a method adapted from (Fatehi et al., 2017), magnetite was obtained Another peak was observed at 3500 cm^{-1} associated with O-H (hydroxyl group), which is attributed to water molecules adsorbed on the surface of the material.

Figure 24: Fourier transforms infrared FTIR spectrum of iron oxide nanoparticle synthesis by a co-precipitation method.

(b) Optical Properties: Ultraviolet-visible and photoluminescence spectroscopy

Uv-vis and photoluminescence (PL) spectroscopy were used to study the optical properties of the synthesized iron oxide nanoparticles. Absorption spectra were recorded in a range of 200-900 nm at room temperature. Figure 25 shows the Uv-vis spectrum of iron oxide nanoparticles with absorption band edges of 450 nm indicating a decrease in wavelength that showed a blue shift from the bulk material which is ascribed to the quantum size effect thus there was a decrease in particle size. The optical properties of semiconductor nanoparticles are strongly influenced by their crystallite sizes and shapes (Patel et al., 2007).

The optical band gap energy for the synthesized nanoparticles was determined by using the Tauc plot relation and was found to be 3.38 eV. This bandgap energy is greater compared to their bulk material (2.12 eV) (Manikandan et al., 2014). The increase in bandgap energy is attributed to the decrease in particle size as indicated by the Uv-vis absorption wavelength since small particles absorbs at a lower wavelength compare to larger particles. Similar results were obtained by (Peter et.al 2016). The photoluminescence properties were investigated as

shown in Figure 19 below, with an excitation wavelength of 450 nm. Figure 25b, showed sharp emission peaks at a wavelength of 460 nm that indicated a redshift from the absorption band edges and the peak appeared to benarrow signifying that the nanoparticles were monodispersed.

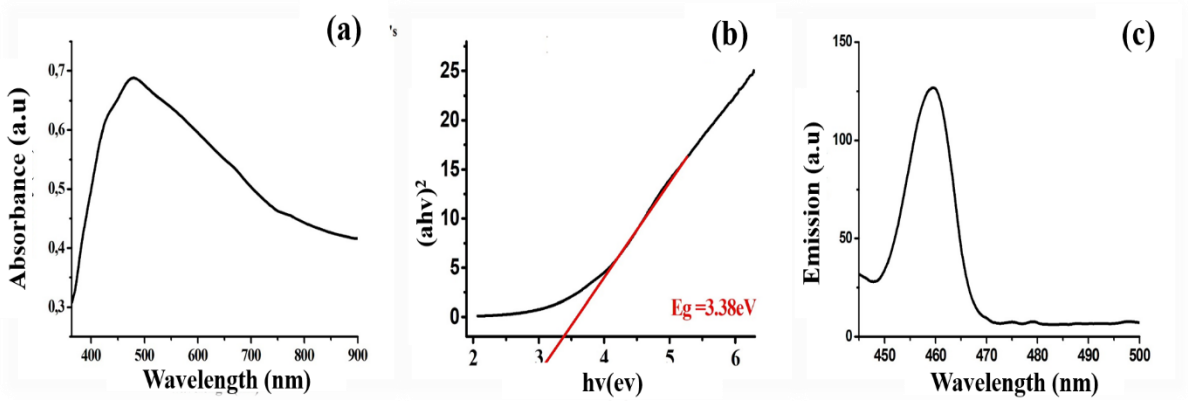

Figure 25: (a) UV-vis spectrum (b) Taut plot (c) photoluminescence spectrum of iron oxide nanoparticle synthesised by a co-precipitation method.

(c) X-ray diffraction pattern (XRD) analysis

Powder X-ray diffraction pattern was used to determine the crystalline phase and the purity of the iron oxide synthesized. Figure 26 showed the relative intensities of the characteristic peak of iron oxide nanoparticles at $2\theta = 18.42^0$, 30.02^0, 35.84^0, 43.17^0, 53.68^0, 56.80^0, 62.51^0 and 74.15^0 corresponding to relative indexes (111), (220), (311), (400), (422), (511), (440) and (533) plane respectively. The obtained results indicated a face centred cubic iron oxide nanoparticles that correspond to the magnetite without any impurities by the database standard (joint committee on Powder diffraction standards, JCPDS file No. 00-019-0629).

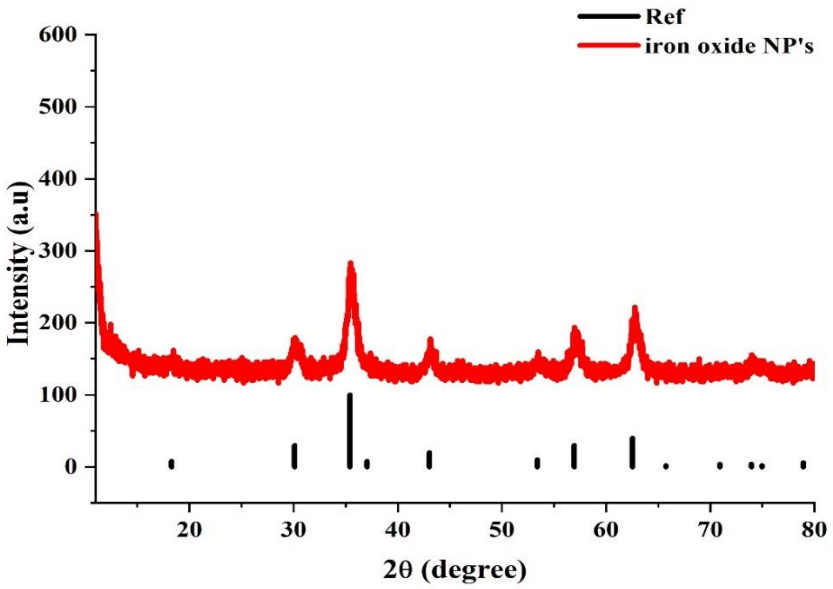

Figure 26: X-ray diffraction Patten of iron oxide nanoparticle synthesised by co-precipitation method.

(d) Raman spectroscopy data analysis.

Raman spectroscopy was used to provide the structural information of the Fe_3O_4 nanoparticles. The spectrum was recorded at a range of 150-1400 cm^{-1}. Figure 27 show strong vibrational modes at 212 cm^{-1}, 269 cm^{-1} and other bands at 383 cm^{-1}, 520 cm^{-1}, 695-954 cm^{-1} ascribed to a $T_{2g}(1)$, Eg, $T_{2g}(2)$, $T_{2g}(3)$ and A_{1g} respectively. The results were in good agreement with the literature. According to literature the vibrational mode for magnetite are observed around 193 (T_{2g} (1)), 306 (Eg), 450 (T_{2g} (2)), 538 (T_{2g} (3)) and 668 cm^{-1} (A_{1g}). Similar results were obtained by Atacan et al., (2017). The A_{1g} bands are relative to the asymmetric stretching of an oxygen atom to metal ions while the presence of vibrational modes (T_{2g} + Eg + A_{1g}) in the spectra is attributed to the cubic inverse-spinel structure of the Fe_3O_4.

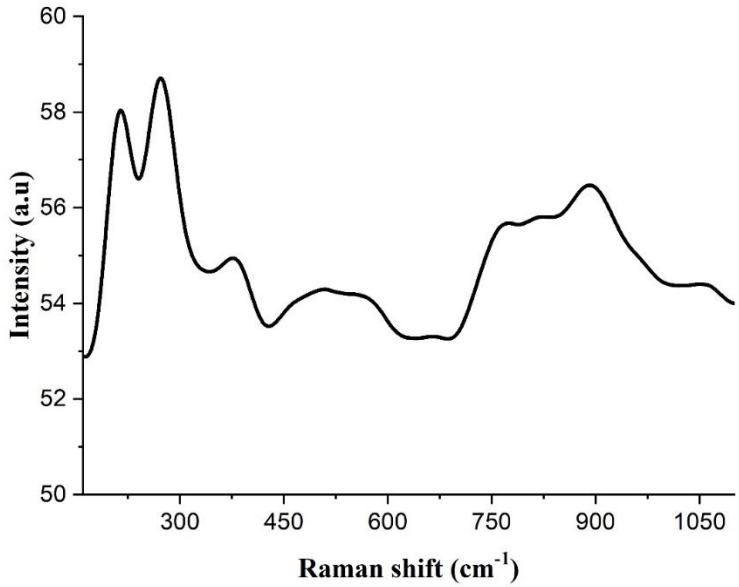

Figure 27: Raman spectra of iron oxide nanoparticle synthesised by a co-precipitation method.

(e) Transmission electron microscope (TEM) analysis

To determine the size and shape of the iron oxide nanoparticles, the transmission electron microscope was used. Figure 28 showed the TEM image and distribution curve of the iron oxide nanoparticles. The particle size distribution of the synthesised material ranged between 2 nm – 30 nm, with an average diameter of 9 nm. The material showed a mixed morphology of spherical and hexagonal shape.

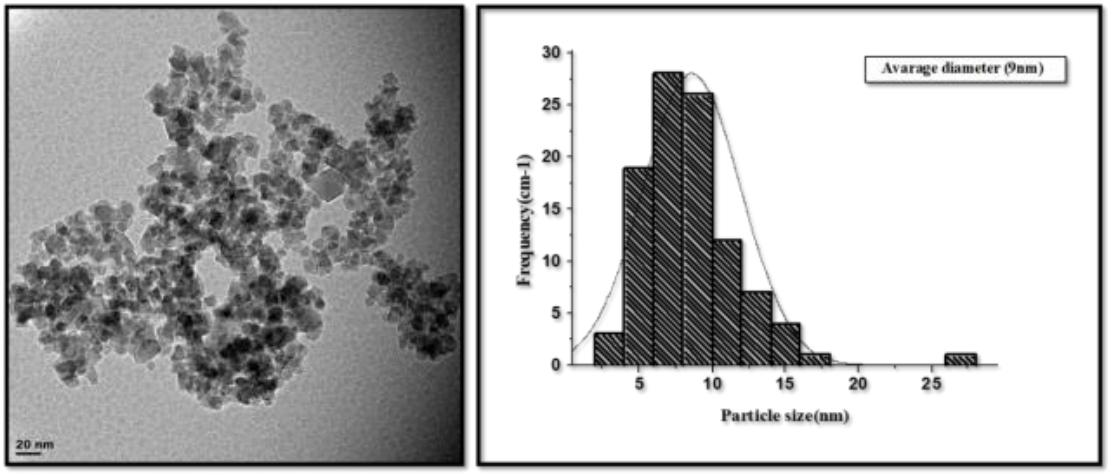

Figure 28: Transmission electron microscope (TEM) of iron nanoparticles synthesized by co-precipitation.

3.3.2. Characterization of iron oxide-silica nanofibers using XRD.

The synthesised iron oxide nanoparticles were incorporated with silica sol to form iron oxide silica nanofibers composite. The powder x-ray diffraction pattern of the iron oxide NP's and iron oxide silica nanofibers represented in Figure 29, which showed diffraction peaks of iron oxide NP's at 2θ = 18.42°, 30.02°, 35.84°, 43.17°, 53.68°, 56.80°, 62.51° and 74.15° corresponding to (111), (220), (311), (400), (422), (511), (440) and (533) plane respectively. Figure 5(b) showed the incorporated iron oxide nanoparticles with silica nanofibers, an amorphous phase diffraction peak was observed at 2θ = 25° ascribed to the nature of silica, which confirms the presence of silica on the material. Two other diffraction peaks were observed at 2θ = 35.84° and 62.51° that are in line with (311) and (440) plane that indicates the presence of iron oxide nanoparticles in the composite. Although not all the magnetite diffraction peaks were visible, this might be due to the diffraction peaks (38.22°, 44.13°, 64.84° and 77.39°) detected from the sample holder which are more intense similar results were obtained in Figure 14. Comparing the results obtained it shows that in all the samples from both method 2 and method 3 the sample coverage was poor because the SEM-EDS showed the presents of both iron and oxygen in both methods. The diffraction peaks from 2θ =18° and 30° were also not visible due to the broad amorphous nature of the silica.

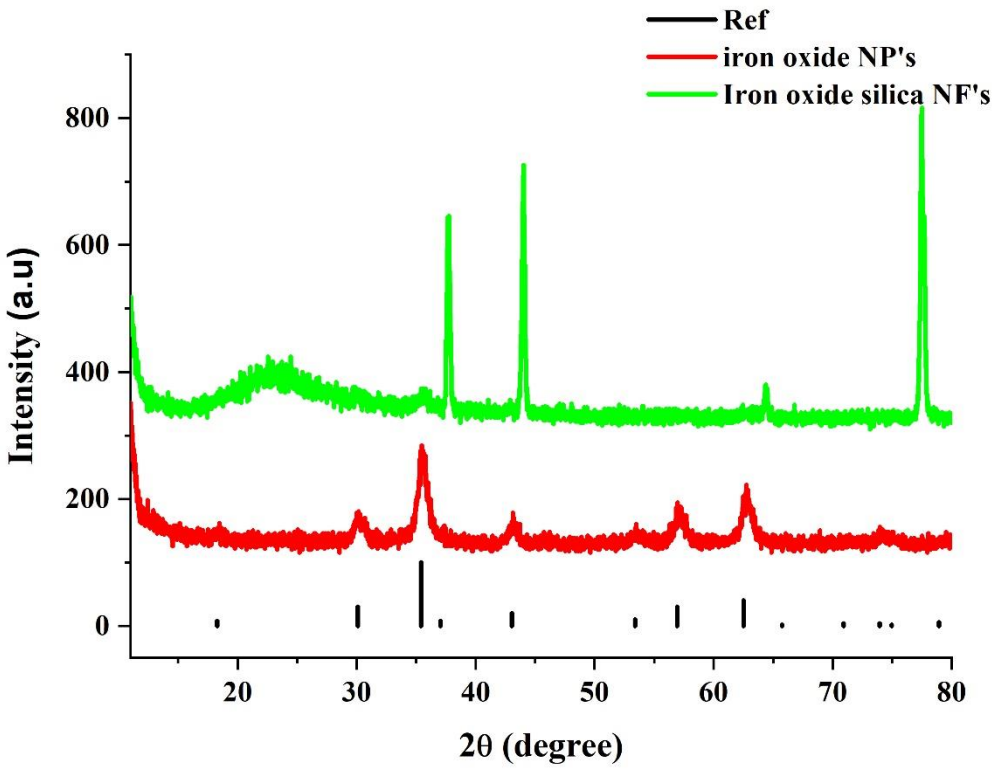

Figure 29: X-ray diffraction Patten of iron oxide and iron oxide -silica nanofibers.

3.3.3. Effect of loading of iron oxide and EDS analysis.

(a) Effect of loading and SEM-EDS analysis.

Figure 30 shows the scanning electron microscope (SEM) of iron oxide nanoparticles incorporated with silica nanofibers. Three-dimensional nanofibers were formed when the silica sol was incorporated with the synthesized iron oxide nanoparticles, the calculated average diameter of the composite was found to be 188 nm. It was observed that on the surface of the fibres there were beats and a layer formed between the fibres which may be the nanoparticle embedded on the fibres or sitting on the surface of the material.

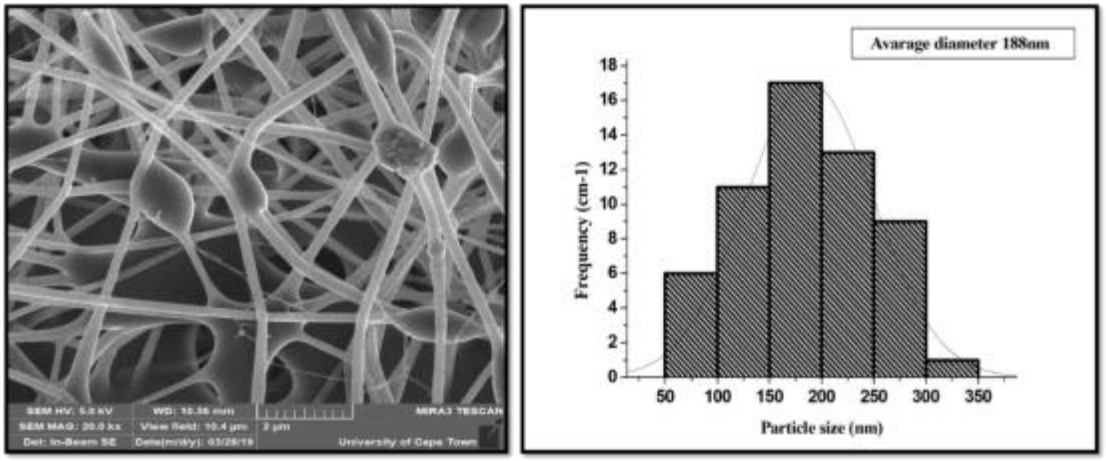

Figure 30: Scanning electron microscope (SEM) of iron oxide silica nanofibers.

When the iron oxide nanoparticles were incorporated into the spinning solution, they were partially dissolved as the nanoparticle percentage was increased to 2 wt.% and 5 wt.%, resulting in the blockage of the solution on the tip of the needle during the electrospinning process, which lead to only 1 wt.% iron oxide silica NF's fabricated. At higher the iron oxide concentration content, the nanoparticles deposited at the centre of the foil, while the PVA/silica gel was deported around the ground collector and with no fibres formation. When the percentage of the iron oxide loaded was increased from 1 wt.% to 2 wt.% and 5 wt.% on the silica sol, the solution becomes more viscous, hence it was very difficult to spin therefore only 1 wt.% was electrospun. SEM-EDS indicated the presence of the nanoparticles embedded on the silica nanofibers as presented in Figure 28 and Table 6.

(b) Energy dispersive x-ray spectroscopy (EDS) Analysis

The energy dispersive x-ray spectrum (SEM-EDS) provided information about an element in the composite. The SEM-EDS spectra in Figure 31 revealed the presences of C, O, Fe, Si and P elements in the composite suggesting that the iron oxide nanoparticle were incorporated into the silica nanofibers. The traces of phosphorous (P) element were due to the phosphoric acid used as a catalyst during the sol-gel preparation. The element percentage is shown in Table 6 below.

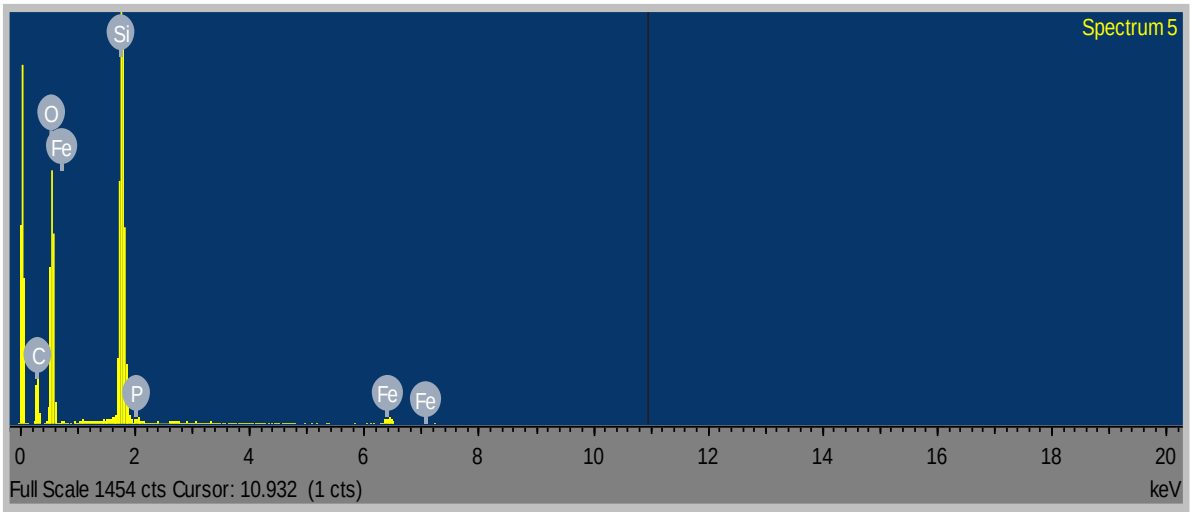

Figure 31: SEM Energy-dispersive X-ray spectroscopy (EDS) of iron oxide silica nanofibers.

Table 6: SEM-EDS atom percentage of the silica nanofibers incorporated with 1 wt.%, 2 wt.% and 5 wt.% iron oxide nanoparticles.

Catalyst	Elements percentage (wt. %)					
	C	O	Si	P	Fe	Total
1 wt.% iron oxide silica NF's	22.84	54.59	19.57	0,29	2.71	100

(c) Fenton catalytic activity studies

Iron oxide nanoparticles and silica nanofibers incorporated with 1 wt.% iron oxide nanoparticles, were used to investigate the Fenton catalytic activity on MB. Iron oxide NP's showed adsorption removal of 30 % with 10 % for 1 wt.% iron oxide silica NF's. The Fenton catalytic process increased removal efficiency by 27, 7% and 37 % respectively. Higher removal was observed on iron oxide nanofibers, indicating that composite improved the removal efficiency this is ascribed to the synergistic effect of silica nanofibers and iron oxide composite. The spinning of 2 wt.% and 5 wt.% of iron oxide silica nanofibers was unsuccessful due to blockage in the needle during electrospinning, this might be due to the magnetic properties of the material hence preventing them from dissolving in the spinning solution at high concentrations. Therefore another phase of iron oxide nanoparticles was synthesised.

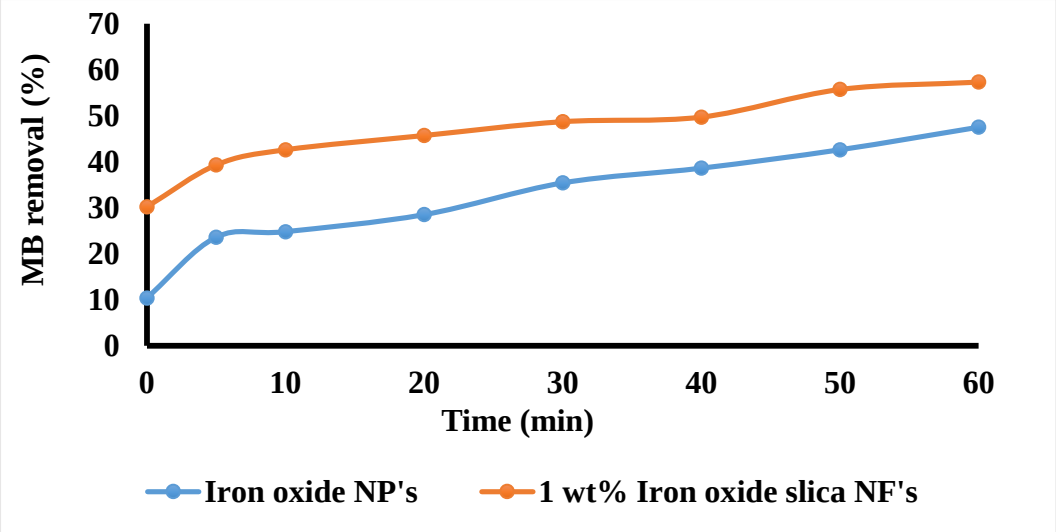

Figure 32: Fenton degradation efficiency of iron oxide and iron oxide-silica nanofibers.

(d) Kinetic studies

Figure 33 and 34 show the kinetic studies of pseudo-first-order and second-order Fenton on Fe_3O_4 and 1 wt.% iron oxide silica NF's. The models described the degradation of Fe_3O_4 to fit Pseudo second-order while 1 wt.% iron oxide silica NF's fit pseudo-first-order due to high regression correlation (R^2), but both materials showed a higher rate (k) on Pseudo second-order suggesting that the reaction is governed by the formation of hydroxyl radicals in the presence of a catalyst. Table 7 gives the summarised results as derived from Figures 33and 34.

Table 7: Pseudo kinetic model for degradation of MB with iron oxide silica nanofibers.

Catalysts	**Pseudo first order**		**Pseudo second order**	
	k (min^{-1})	**R^2**	**k ($ppm^{-1}min^{-1}$)**	**R^2**
Iron oxide NP's	-0.0082	0.9705	0.0116	0.9858
1 wt% iron oxide silica NF's	0.0052	0.9749	0.00162	0.9635

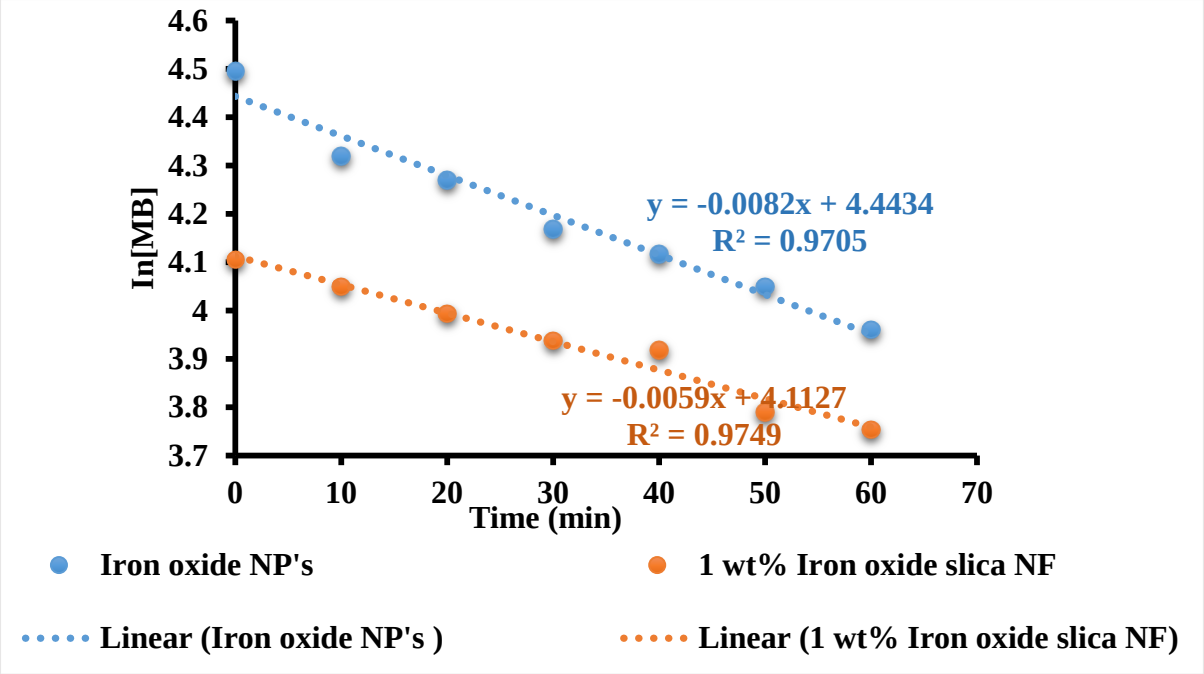

Figure 33: Pseudo first-order kinetics of iron oxide and iron oxide -silica nanofibers.

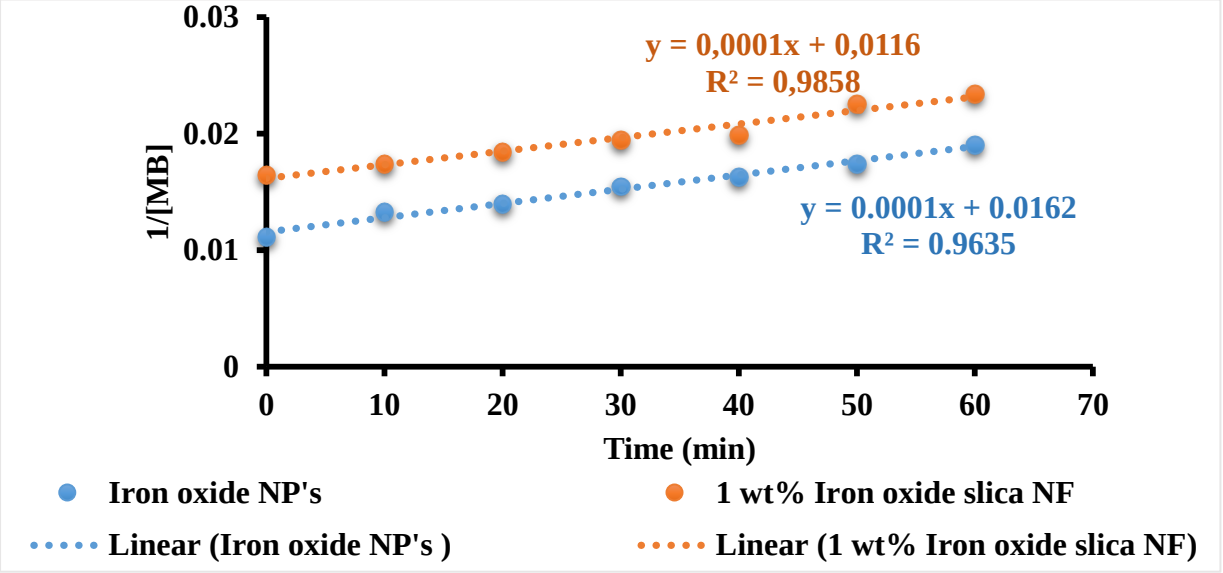

Figure 34: Pseudo second-order kinetics of iron oxide and iron oxide-silica nanofibers.

3.4. Iron oxide silica nanofibers prepared using direct incorporation of prepared iron oxide nanoparticles (Goethite). (Method 3.1)

3.4.1. Distribution and characterization of iron oxide nanoparticles (Goethite) and iron oxide-silica nanofibers using FTIR, UV-vis, Tauc plot, PL, XRD, Raman and TEM.

(a) Ultraviolet-visible and photoluminescence spectroscopy

The Optical properties of iron oxide nanoparticles were determined by the Uv-vis and PL spectroscopy is presented in Figure 35. A prominent adsorption peak for iron oxide nanoparticles appeared at 425 nm with an extrapolated bandgap energy of 1.5 eV from Tauc plot relation that indicated a blue shift from the bulk material (2.5 eV) (Sherman et al., 2016) suggesting a blue shift from bulk material due to decrease in particles that is attributed to the quantum size confinement. Figure 30 c shows the photoluminescence spectra, with an excitation wavelength of 425 nm with an emission peak at 460 nm that red-shifted from the adsorption peak due to excitation of electrons.

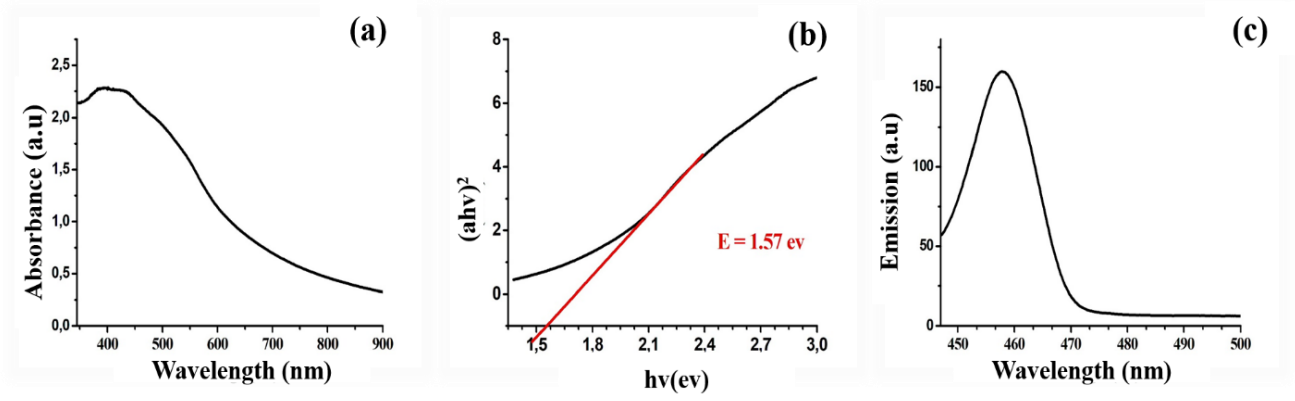

Figure 35: (a) UV-vis spectrum (b) Tauc plot (c) photoluminescence spectrum of iron oxide nanoparticle synthesised by precipitation method (tetraethyl amine).

(b) Fourier-transform infrared spectroscopy of iron oxide nanoparticles

The FTIR spectra of iron oxide in Figure 36 showed functional groups at, 570 cm^{-1}, 788 cm^{-1}, 888 cm^{-1}, 3200 cm^{-1} attributed to Fe-O, N-C, C-H and O-H respectively as presented in Table 8 below. The Fe-O is ascribed to the formation of iron oxide nanoparticles. The observed C-H and N-C bands are due to the reducing agent tetraethylammonium hydroxide (TEOAH) and O-H band due to the water absorbed on the surface of the material.

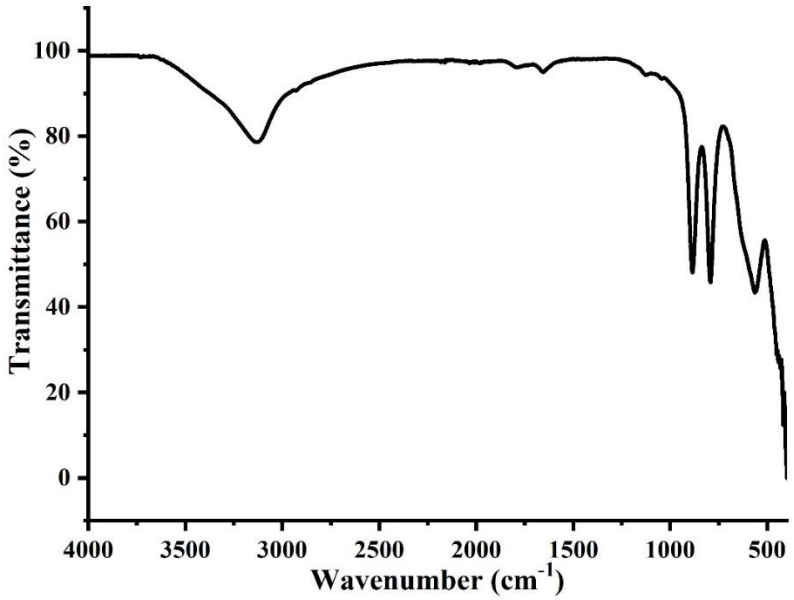

Figure 36: Fourier transforms infrared (FTIR) of iron oxide nanoparticle synthesised by precipitation method (tetraethyl amine).

(c) Transmission electron microscope (TEM) analysis

TEM was used to investigate the morphology of the iron oxide nanoparticles. A mixed shape (rods and hexagonal structure) iron oxide nanoparticles was obtained with particle size distribution ranging from 10 nm – 100 nm as shown in Figure 37. The nanoparticles were well-defined with an average particle size of 35 nm.

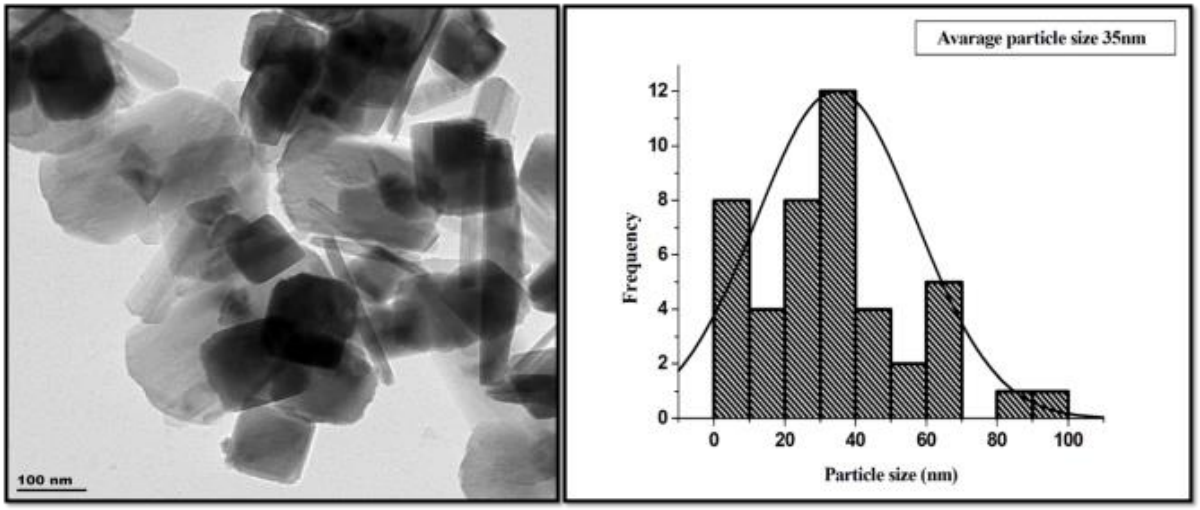

Figure 37: Transmission electron microscope (TEM) of iron nanoparticles synthesized by precipitation method (tetraethyl amine).

(d) X-ray Diffraction (XRD) analysis

The crystalline phase of the synthesized iron oxide nanoparticles was determined by the X-ray diffraction pattern. Figure 38 show XRD micrograph of iron oxide nanoparticles prepared by precipitation method using tetraethylammonium hydroxide as a precipitating agent, the peaks were observed at 2θ = 17. 48°, 21.09°, 26.44°, 33.10°, 35.19°, 36.72°, 40.35°, 41.71°, 53.82°, 57.30° 58.8°, 68.73° and 71.96° relatively indexed to 020, 110, 120, 130, 101, 111, 140, 366, 231,157, 301 and 132 planes assigned to orthorhombic FeOOH according to (JCPDS file No. 01-075-5065) confirming the goethite crystalline phase formation, similar results were obtained by Singh et al., (2015), with the calculated size of 29 nm.

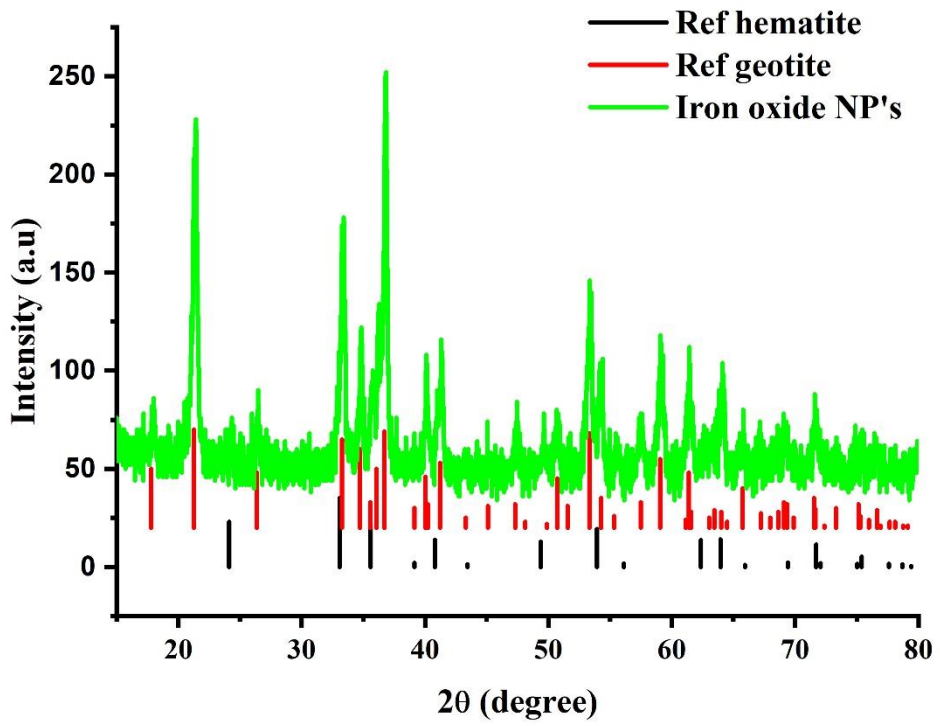

Figure 38: X-ray diffraction Patten of iron oxide nanoparticle synthesised by precipitation method using tetraethylammonium hydroxide.

3.4.2. Characterization of iron oxide-silica nanofibers using FTIR and XRD.

(a) Fourier transform infrared (FTIR) spectral analysis

The functional groups present on the composite were determined by the FTIR. The spectra in Figure 39 showed the presences of both the silica and iron oxide cm^{-1} 1100 cm^{-1} and 3200cm^{-1} attributed to Fe-O, Si-O and O-H that indicate the interaction between the support and the iron oxide. It was observed that as the loading of iron content was increased the Fe-O band becomes more pronounced due to high concentrations of iron species. O-H band attributed to some traces of PVA polymer suggesting incomplete decomposition of PVA during the calcination process.

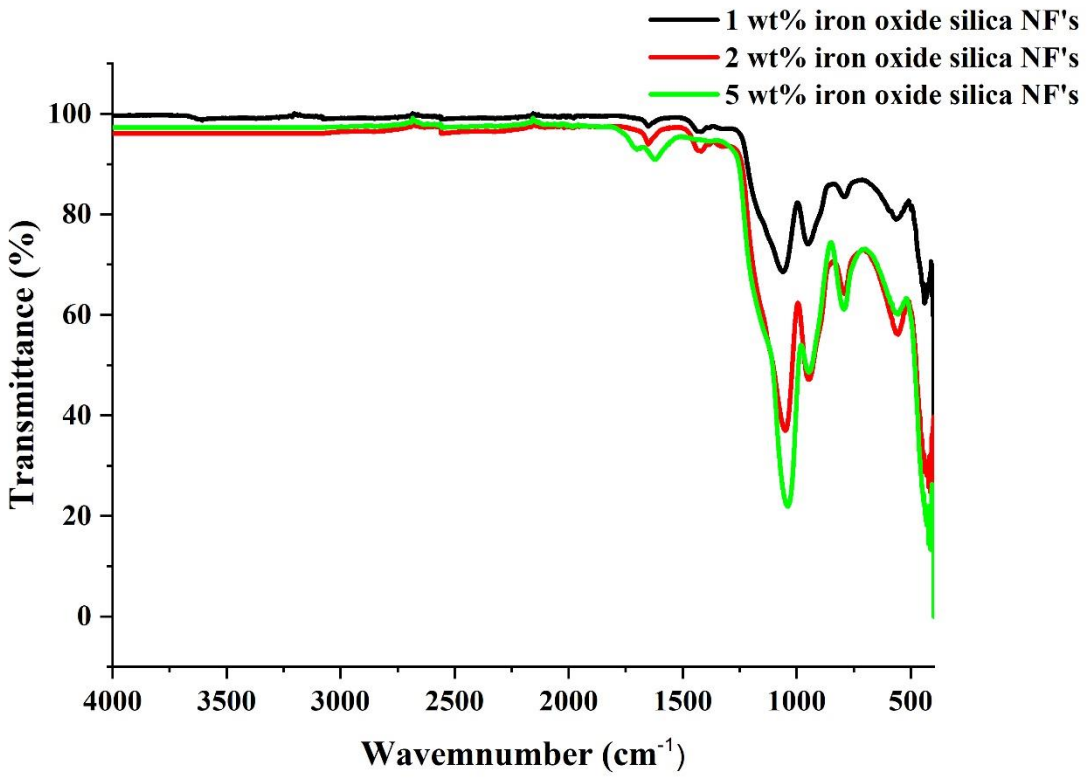

Figure 39: Fourier transform infrared (FTIR) spectra of silica nanofibers incorporated with 1%, 2% and 5% iron oxide nanoparticles.

(b) X-ray Diffraction (XRD) analysis

The incorporated iron oxide - silica nanofibers in Figure 40, showed the peaks at 2θ = 17.48°, 21.09°, 26.44°, 33.10°, 35.19°, 36.72°, 40.35°, 41.71°, 53.82°, 57.30° 58.8°, 68.73° and 71.96° relatively indexed to 020, 110, 120, 130, 101, 111, 140, 366, 231,157, 301 and 132 planes assigned to orthorhombic FeOOH according to (JCPDS file No. 01-075-5065) and an amorphous phase at 25° attributed to silica. This XRD pattern indicates that the synthesized material contains both the silica and the mixed phased iron oxide nanoparticles.

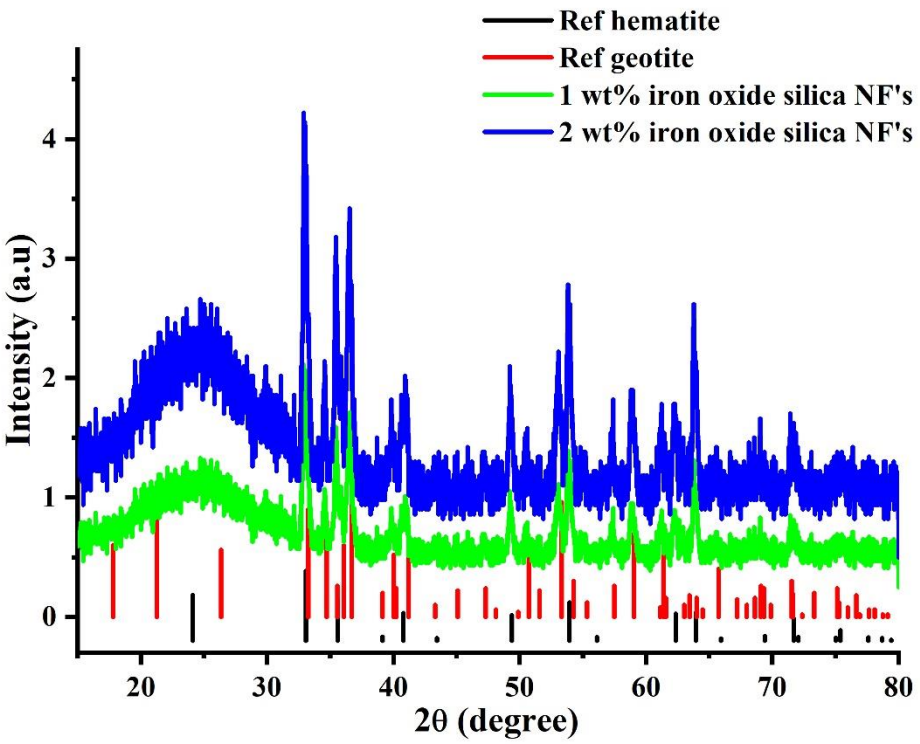

Figure 40: XRD patten of the references goethite, hematite, silica nanofibers incorporated with 1 wt.%,2 wt.% iron oxide nanoparticles.

3.4.3. Effect of loading iron oxide and EDS analysis.

(a) Effect of loading iron oxide.

As the concentration of iron oxide is increased, a significant change was observed as shown in SEM image Figure 41, At 1 wt.% loading iron oxide, the fibres were thin with average diameter spherical particle (90 nm) were observed on the surface of the material. As the concentration of iron oxide nanoparticle is increased to 2% there was an increased fibres diameter (139 nm) and particles on the surface increased (902 nm). At 5% iron oxide loading the surface was covered with agglomerated nanoparticles. This showed that at high concentrations of iron oxide the solution cannot be electrospun, this has be proven when the spinning solution was incorporated with magnetite. Hence the only solution with lower iron oxide loading can electrospun. The SEM-EDX showed the elements present in the composite (O, Si, P and Fe). Table 9 showed an increase in iron percentage as the loading of iron oxide nanoparticles is

increased similar trend was observed in Method 1 (see) this indicates that the SEM-EDS detects the higher percentage of iron when it is sitting on the surface of the material.

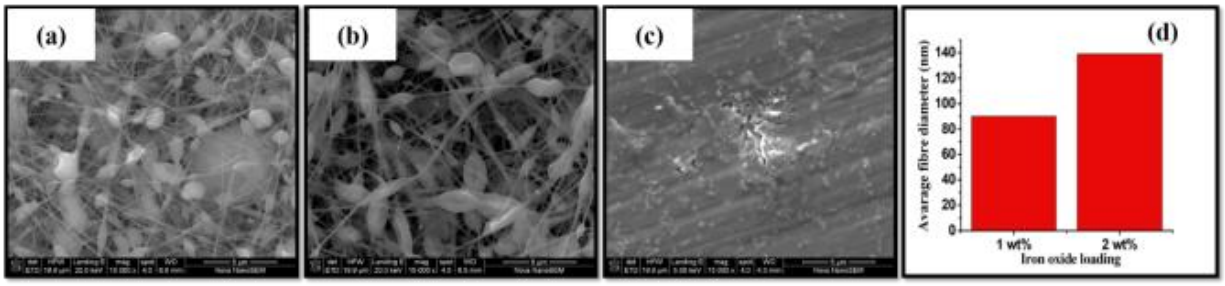

Figure 41: Scanning electron microscope (SEM) silica nanofibers incorporated with (a) 1 wt.%, (b) 2 wt.%, (c) 5 wt.% iron oxide nanoparticles.

(b) Energy-dispersive X-ray spectroscopic (EDS) Analysis

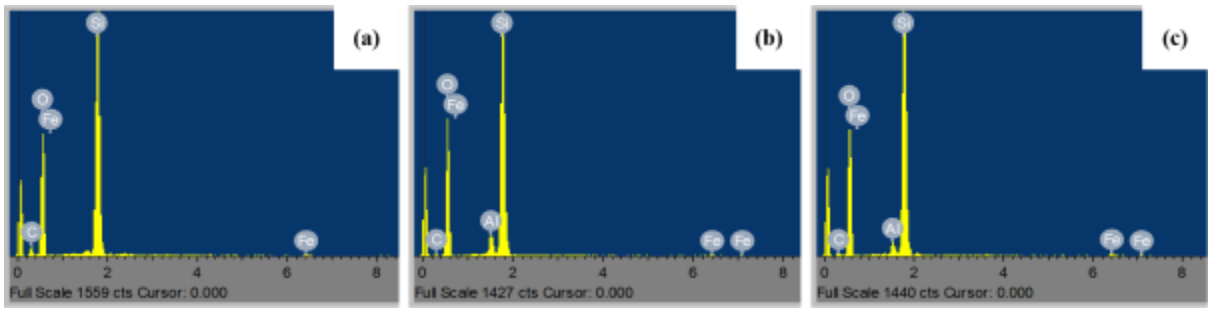

Figure 42: SEM- EDS analysis of silica nanofibers incorporated with (a) 1 wt.%, (b) 2 wt.%, (c) 5 wt.% iron oxide nanoparticles.

Table 8: SEM-EDS atom percentage of the silica nanofibers incorporated with 1 wt %, 2 wt.% and 5 wt.% iron oxide nanoparticles.

Catalysts	Elements percentage (wt. %)						
	C	O	Al	Si	P	Fe	Total
1 wt.% iron oxide silica NF's	18.78	51.87	0,00	27,57	0,65	1,18	100
2 wt.% iron oxide silica NF's	21,24	49,47	0,00	24,89	0,99	3,42	100
5 wt.% iron oxide silica NF's	17,23	48,81	0,65	25,66	0,65	7,02	100

(c) Fenton catalytic activity

The change in the MB percentage removal during the Fenton degradation process presented in Figure 43 showed no significant change in the degradation efficiency between iron oxide nanoparticles and 1 % iron oxide supported on silica nanofibers, although as the concentration of iron oxide was increased to 2 wt% the degradation efficiency improved by 7 %. The catalysts proved to be not so effective due to the large particles formed on the surface of the material, therefore reducing its effectiveness. The large particles might be formed by the small particles clustered together hence covering the active sites that negatively affected the catalytic performance.

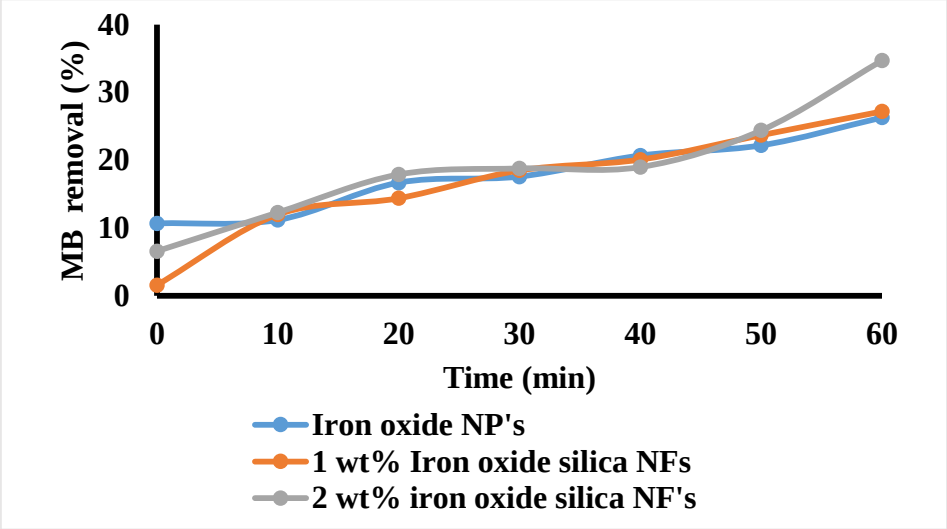

Figure 43: Fenton degradation efficiency of iron oxide and iron oxide-silica nanofibers.

(d) Kinetics studies

Kinetic modelling of MB was carried out by pseudo-first-order ($\ln/C_0$-C) and pseudo-second-order 1/ (C_0-C) to determine degradation reaction. Based on the linear regression coefficient it was observed that the reactions were described by the pseudo-first-order, R^2 = 0.9696, 0.881 and 0.9522 with the highest rate constant k= 0.0318, 0.0049 and 0.0045 respectively for MB adsorption as shown in Table 10. This can be associated with the interaction on the surface between the catalysts and the pollutant.

Table 9: Pseudo kinetic model for degradation of MB with iron oxide silica nanofibers.

Catalysts	Pseudo first order		Pseudo second order	
	k (min^{-1})	R^2	k $ppm^{-1}(min^{-1})$	R^2
Iron oxide nanoparticles	0.0318	0.9696	0.0107	0.9673
1 wt% iron oxide- SiO_2 NF's	0.0049	0.881	0.0006	0.8527
2 wt% iron oxide- SiO_2 NF's	0.0045	0.9522	0.0005	0.9664

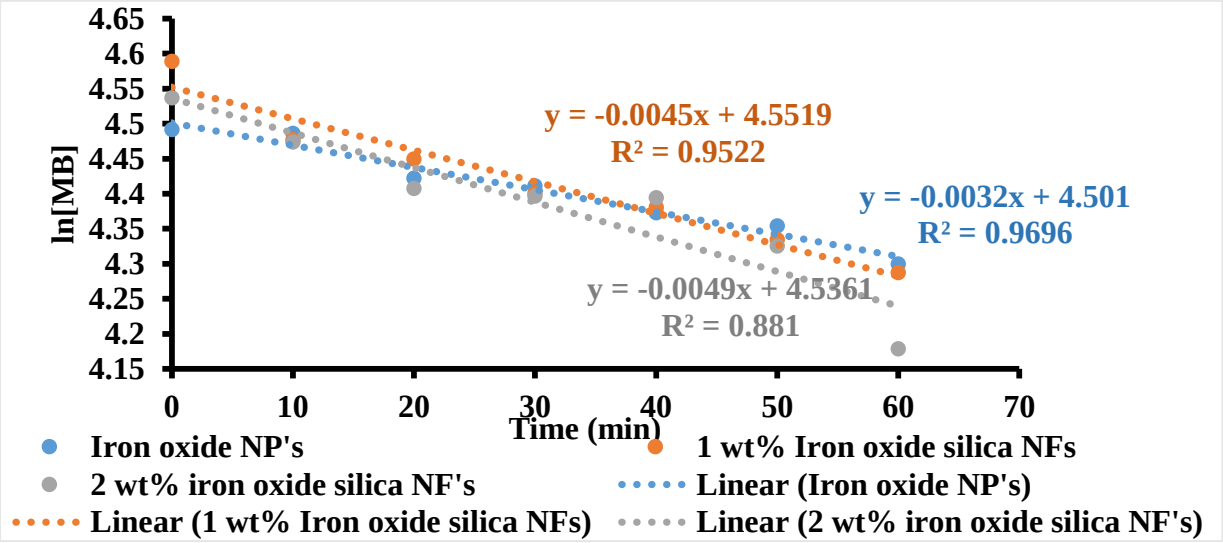

Figure 44: Pseudo first-order kinetics of iron oxide and iron oxide -silica nanofibers.

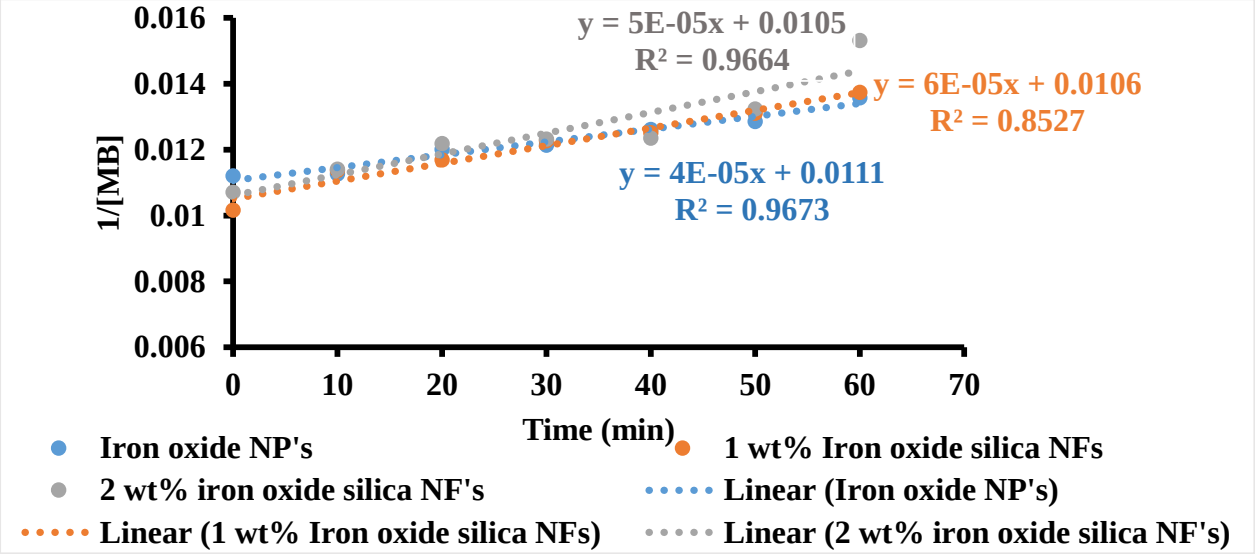

Figure 45: Pseudo second order kinetics of iron oxide and iron oxide-silica nanofibers.

3.6. Leaching test

Leaching in iron oxide-based heterogeneous catalysts. This is known to be a major problem during degradation. The deactivation of the metal irons leads to homogenous catalytic behaviour thus resulting in water pollution, hence leading to another environmental problem. This is mainly caused by the formation of carboxylic acid intermediates during the degradation process such as citrate, tartrate and oxalate (Benhamounda et al., 2018). Thus these intermediates act as ligands and react with Fe ions and form complexes (Ammar et al., 2001). Therefore the degree of leaching test was done to evaluate the iron content after degradation. According to the world health organisation (WHO), the limit of Fe metal required in water is 0.3 ppm (Musa et al., 2013).

Figure 44 and 45 present the concentration of iron leached. The leaching degree test was performed after the Fenton degradation process. The concentration of iron leached for the nanoparticle prepared in method 3 found to be 1.28 ppm for magnetite and 1.68 ppm (goethite) that exceed the WHO limit. On the supported catalysts prepared in method 1 (M1), method 2 (M2) and method 3 (M3) and (M3, 1) the leaching degree in M1 was very high due to iron oxide sitting on the surface of the support, in M2 and M3 the iron was introduced in the spinning solution that might have allowed the iron to interact with the silica hence the iron oxide was both on the surface and also embedded on the fibres, therefore, lowering the leaching degree, but in M4 the nanoparticle was sitting on the surface as shown in the SEM images in Section 4.4.7.1 and resulted in a high degree of leaching. The obtained results were 3.95 ppm, 0.05 ppm, 0.089 and 1.33 ppm for M1, M2, M3 and M3.1 respectively. Their leaching test for the method (M2) and method (M3) catalysts was within the limit of world health organisation (WHO). The degree of leaching for the unsupported nanoparticles was higher than the supported catalysts, this suggests the support reduces the leaching. The low leaching degree in method 2 suggested that there was a good interaction between the iron oxide and the support material.

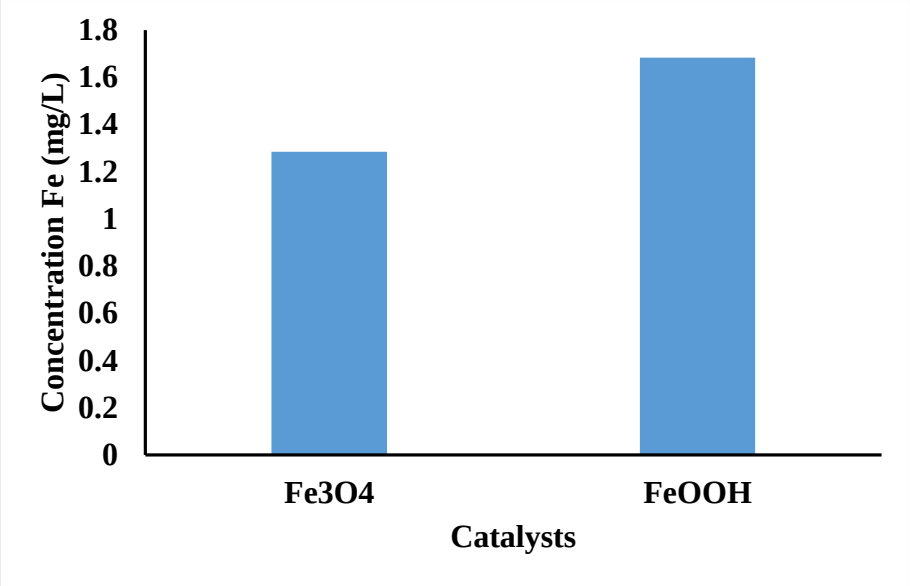

Figure 46: Leaching of Fe in iron oxide nanoparticles catalysts.

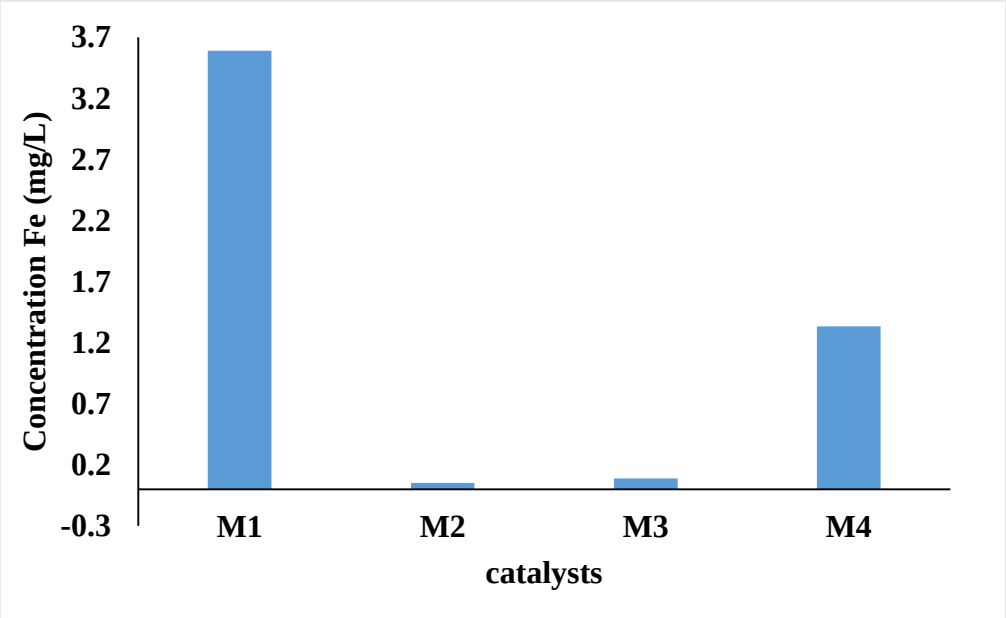

Figure 47: Leaching of Fe in iron oxide-silica nanofibers from M1, M2 M3 and M4 catalysts.

CHAPTER 4

4. CONCLUSIONS AND RECOMMENDATIONS

4.1. Conclusions

The preparation of the catalyst using the three different methods showed different behaviour towards the degradation of methylene blue. The various methods resulted in different interaction of the silica nanofibers with the iron oxide. The FTIR spectra showed the presences of both the silica and iron oxide in the catalyst. While the optimum voltage for all methods was found to be 20 kV. The XRD analysis for iron oxide silica nanofibers using direct incorporation of prepared iron oxide nanoparticles (magnetite) (method 3) direct incorporation of prepared iron oxide nanoparticles (goethite) (method 3.1) also confirmed the presences of iron oxide, but for method 1 and method 2 the crystalline size of the iron oxide may have been less than 5 nm hence couldn't be detected by XRD. Furthermore, the SEM results showed that the loading of the iron oxide on method 1, 2, 3 and 3.1 had an influenced on the surface and size of the nanofibers. The loading showed an increase in fibres diameter with an increase in iron content with the diameter and the surface became rougher.

The catalyst prepared in method showed an increase in catalytic performance with an increase in iron concentration, however, the silica nanofibers alone showed high adsorption capacity. The catalysts prepared in method 2 were more active then catalyst prepared by method 1, method 3 and method 3.1. The catalysts prepared by direct addition of iron precursor into the spinnable sol-gel solution and converted to the iron oxide by calcination process had high catalytic activity, this can be explained by the interaction between the iron oxide and the support material leading to a higher dispersion of the iron oxide that created more active catalytic sites. The support played a role in the methylene blue removal by adsorbing the dye and dispersing the iron oxide. Therefore it can be concluded the catalyst prepared by direct addition of iron precursor into the spinnable solution was more active due to the synergistic effect of both the metal oxide and the support material.

Furthermore, the catalyst prepared by incorporation of iron oxide nanoparticle in method 3 also had similar behaviour in the interaction between iron oxide and silica, the nanoparticles were added in the spinnable solution. The catalytic activity of silica nanofibers incorporated with 1 wt.% of iron oxide nanoparticles (magnetite) had a promising activity of 53.7 %, but due to the non-spinnability when the iron content is increased to 2 wt% and 5 wt%, resulting in blockage

on tip of the needle the catalytic activity couldn't be monitored. Hence the goethite was introduced in method 3.1. The nanoparticles were agglomerated on the surface of the support and affected the catalytic activity negatively.

The leaching tests proved that the nanoparticles leach more when they are not supported whereas when the iron is supported the degree of leaching decreases. This may indicate that metal oxide support interaction is beneficial to decrease leaching. For method 1 and method 3.1, the leaching test was high due to the iron oxide sitting on the support hence being exposed to the intermediates, which deactivate the iron oxide. The leaching degree for Method 2 was low and was within the specification of the world health organization (WHO). The metal oxide support interaction is expected to be the highest for this method, explaining the low leaching observed.

4.2. Recommendations

The amount of the catalyst that was used for the Fenton degradation process was low. It is therefore recommended that the mass of the catalyst be increased to achieve a higher rate of reaction and a higher percentage removal. The degradation Fenton reaction should conduct at least 2 hours to determine if a higher percentage of degradation can be achieved. The silica nanofibers showed higher adoption capacity therefore it can be recommended that the material be applied in adsorption studies. Since the catalytic activity increase with an increase in iron content in the catalysts, it also is recommended that higher iron content in the catalysts should be investigated. Furthermore, the leaching studies can be done using the oxalic acid to compare the leaching degree to test the catalysts at the same conditions since the different catalytic activities leading to different concentrations of acidic intermediates would lead to different leaching.

5. REFERENCES

ALI, A.,ZAFAR, H., ZIA, H., HAQ, I., PHULL, A.R., ALI, J.S & HUSSAIN, A. 2016. The synthesis, characterization application and challenges of iron oxide nanoparticles. Review Nanoparticles, Science and Application, 9, 47-67

ARSALANFAR, M., MIRZAEI, A. A., BOZORGZADEH, H. R., SAMIMI, A., & GHOBADI, R. 2014. Effect of support and promoter on the catalytic performance and structural properties of the Fe – Co – Mn catalysts for Fischer – Tropsch synthesis. Journal of Industrial and Engineering Chemistry, 20(4), 1313–1323. https://doi.org/10.1016/j.jiec.2013.07.011

ATKINS, P. & JONES, L. Chemical principles : The quest insight. 5th edition. Chapter 14. 561

ASGHARZADEH, F., MORADI, M., JONIDI, A., ESRA, A., TAHERGORABI, M., & REZAEI, R. 2019. Data in brief enhanced electro kinetic- pseudo-Fenton degradation of pyrene-contaminated soil using Fe 3 O 4 magnetic nanoparticles : A data set, 24, 4–11. https://doi.org/10.1016/j.dib.2018.11.068

AVETTA, P., PENSATO, A., MINELLA, M., MALANDRINO, M., MAURINO, V., MINERO, C., VIONE, D. 2014. Activation of persulfate by irradiated magnetite : Implications for the degradation of phenol under heterogeneous photo Fenton-like conditions Activation of persulfate by irradiated magnetite : Implications for the degradation of phenol under heterogeneous photo Fenton-like.45, 2-8 https://doi.org/10.1021/es503741d

BEACHLEY, V., & WEN, X. 2009. Effect of electrospinning parameters on the nano fi ber diameter and length. Materials Science & Engineering C, 29(3), 663–668. https://doi.org/10.1016/j.msec.2008.10.037

BHATIA, D., SHARMA, N. R., SINGH, J., & KANWAR, R. S. 2017. Biological methods for textile dye removal from wastewater: A review. Critical Reviews in Environmental Science and Technology, 47(19), 1836–1876. https://doi.org/10.1080/10643389.2017.1393263

CAMPOS, E. A., VILLELA, D., STOCKLER, B., IRINEU, J., OLIVEIRA, S. DE, MATTOS, C., DUTRA, L. 2015. Synthesis , characterization and applications of iron oxide nanoparticles –, 7, 267–276. https://doi.org/10.5028/jatm.v7i3.471

CARRARO, G., GASPAROTTO, A., & MACCATO, C. 2014. Rational synthesis of F-doped iron oxides on Al_2O_3(0001) single crystals, 3, 234-256. https://doi.org/10.1039/C4RA09021G

CHEN, C., TANG, Y., VLAHOVIC, B., & YAN, F. 2017. Electrospun polymer anofibers decorated with noble metal nanoparticles for chemical sensing, 36, 56-66. https://doi.org/10.1186/s11671-017-2216-4

CHEN, D., YU, Z., OCHOA-FERNA, E., RØNNING, M., & HOLMEN, A. 2005. Carbon nanofiber supported Ni catalyst : Effects of nanostructure of supports and catalyst preparation, *103*, 45–49. https://doi.org/10.1016/j.cattod.2005.02.005

CHEN, L., LI, Y., HU, S., SUN, J., DU, Q., YANG, X. & XIA, Y. 2016. Removal of methylene blue from water by cellulose / graphene oxide fibres, 80, 80-87. https://doi.org/10.1080/17458080.2016.1198499

CHEN, W. S., GUO, L. Y., MASROUJEH, A. M., AUGUSTINE, A. M., TSAI, C. K., CHIN, T. Y. & YANG, M. (2016.). A singles-step surface modification of electrospun silica nanofibers using a silica binding protein fused with an RGD motif for enhanced PC12 cell growth and differentiation. 24, 56-64. https://doi.org/10.3390/ma11060927

CHEN, Y., LIU, H., LIU, Y., LEE, T., & LIU, S. 2019. Determination of electrospinning parameters ' strength in poly (D , L) -lactide-co-glycolide micro / nanofiber diameter ailoring, 20, 1-9.

CHOI, S., & LEE, S. G. O. O. 2003. Silica nanofibers from electrospinning / sol-gel process silica nanofibers from electrospinning / sol-gel process, 20(14), 10–13. https://doi.org/10.1023/A

COTTO-MALDONADO, M. C., DUCONGE, J., MORANT, C., & MÁRQUEZ, F. 2017. Fenton process for the degradation of methylene blue using different nanostructured catalysts. 63, 10-18. https://doi.org/10.3844/ajeassp.2017.373.381

Darmawan, A., Smart, S., & Julbe, A. (2011). Iron Oxide Silica Derived from Sol-Gel Synthesis, 448–456. https://doi.org/10.3390/ma4020448

DEVI, S. M., NIVETHA, A., & PRABHA, I. 2019. Superparamagnetic properties and significant applications of iron oxide nanoparticles for astonishing efficacy — a Review, 3, 127–144.

DING, B., WANG, M., WANG, X., YU, J., & SUN, G. 2010. Electrospun nanomaterials for ultrasensitive sensors Increasing demands for ever more sensitive sensors for global. Materials Today, 13(11), 16–27. https://doi.org/10.1016/S1369-7021(10)70200-5

EL-NOUR, K. M. M. A., AL-WARTHAN, A., & AMMAR, R. A. A. 2010. Synthesis and applications of silver nanoparticles, 135–140. https://doi.org/10.1016/j.arabjc.2010.04.008

FATEHI, M. H., SHAYEGAN, J., ZABIHI, M., & GOODARZNIA, I. 2017. Journal of environmental chemical engineering functionalized magnetic nanoparticles supported on activated carbon for adsorption of Pb (II) and Cr (VI) ions from saline solutions. Biochemical Pharmacology, 5(2), 1754–1762. https://doi.org/10.1016/j.jece.2017.03.006

FENG, Z. V., CHEN, W. S., STOICK, M., KAPALA, B., & JOHNSON, E. 2016. Degradation of the electrospun silica nanofiber in a biological medium for primary hippocampal neuron – effect of surface modification, 729–741.

FREYER, A., SAVAGE, N. O., HAVEN, N., ROAD, B. P., HAVEN, W., & STATES, U. 2014. Electrospun Silica Nanofiber Mats Effects of Sol Viscosity and Application to Thin Layer Chromatography.

FRIDRIKH, S. V, YU, J. H., BRENNER, M. P., & RUTLEDGE, G. C. 2003. Controlling the Fiber diameter during electrospinning, 1–4. https://doi.org/10.1103/PhysRevLett.90.144502

GE, S., SHI, X., SUN, K., LI, C., JR, J. R. B., MARK, M. & ORR, B. G. 2010. NIH public access, 113(31), 13593–13599. https://doi.org/10.1021/jp902953t.A

GELTMEYER, J., VAN DER SCHUEREN, L., GOETHALS, F., DE BUYSSER, K., & DE CLERCK, K. 2013. Optimum sol viscosity for stable electrospinning of silica nanofibres. Journal of Sol-Gel Science and Technology, 67(1), 188–195. https://doi.org/10.1007/s10971-013-3066-x

GUAN, H., ZHOU, W., FU, S., Ã, C. S., & LIU, Y. 2009. Solids electrospun nanofibers of NiO / SiO_2 composite. Journal of Physics and Chemistry of, 70, 1374–1377. https://doi.org/10.1016/j.jpcs.2009.08.005

HE, J., WAN, Y., & YU, J. 2008. Effect of concentration on electrospun polyacrylonitrile (PAN) nanofibers, 9(2), 140–142.

HERNÁNDEZ, A. A., GABRIEL, H., ÁLVAREZ, A., & CARIÑO, R. 2020. Iron oxide nanoparticles : synthesis , functionalization , and applications in diagnosis and treatment of cancer. Chemical Papers, *74*(11), 3809–3824. https://doi.org/10.1007/s11696-020-01229-8

HEVELING, J. 2012. Heterogeneous catalytic chemistry by example of industrial applications.

HOBZOV, R., SIRC, J., KOSTINA, N., MUNZAROV, M., JUKL, M., ZAJ, A., & LHOTKA, M. 2012. Morphological characterization of nanofibers : Methods and application in Practice, 20, 12-16. https://doi.org/10.1155/2012/327369

HORZUM, N., MUN, R., GLASSER, G., DEMIR, M. M., LANDFESTER, K., & CRESPY, D. 2012) Hierarchically structured metal oxide/silica nano fibers by colloid electrospinning. https://doi.org/10.1021/am301969w

HUANG, Z., ZHANG, Y., KOTAKI, M., & RAMAKRISHNA, S. 2003. A review on polymer nanofibers by electrospinning and their applications in nanocomposites, 63, 2223–2253. https://doi.org/10.1016/S0266-3538(03)00178-7

JOHNSON, P., LOGANATHAN, C., KRISHNAN, V., SAKAYANATHAN, P., RAJI, V., VIJAYAN, S. & PALVANNAN, T. 2018. Plant extract as environmental-friendly green catalyst for the reduction of hexavalent chromium in tannery effluent. Environmental Technology (United Kingdom), 39(11), 1376–1383. https://doi.org/10.1080/09593330.2017.1329355

KAJBAFVALA, A., BAHMANPOUR, H., MANESHIAN, M. H., & LI, M. 2013. Self-assembly techniques for nanofabrication, 20, 13-18.

KHODAIE, M., GHASEMI, N., MORADI, B., & RAHIMI, M. 2013. Removal of methylene blue from wastewater by adsorption onto

$ZnCl_2$ Activated corn husk carbon equilibrium studies, 26 333-344.

KIM, S. D., PARK, K. S., & GU, M. B. 2002. Toxicity of hexavalent chromium to daphnia magna: Influence of reduction reaction by ferrous iron. Journal of Hazardous Materials, *93*(2), 155–164. https://doi.org/10.1016/S0304-3894(02)00057-2

KOCH, R. 2013. Methylene blue 1., *85*.

KOSA, S. A., AL-SEBAII, N. M., ABD, I. H., MAKSOD, E., & HEGAZY, E. Z. 2016. New method for removal of organic dyes using supported iron oxide as a catalyst, 26,16-23.

KUMAR, A., YADAV, N., BHATT, M., MISHRA, N. K., CHAUDHARY, P., & SINGH, R. 2015. Sol-gel derived nanomaterials and it's applications : A Review, *5*(12), 98–105.

KYSELICA, R., ENIKOV, E. T., POLYVAS, P., & ANTON, R. 2018. Electrostatic focusing of electrospun polymer (PEO) nano fibers, 94, 21–29. https://doi.org/10.1016/j.elstat.2018.05.00

LAI, N., LIOU, S., HUANG, W., SHEN, Y., CHI, C., CHU, M., & YANG, C. 2015. Functional helical silica nano fibers with coaxial mixed mesostructures for the fabrication of PtCo nanowires that display unique geometry-dependent magnetism, *7*(5), 181-8. https://doi.org/10.1038/am.2015.39

Leach, M. K., Feng, Z., Tuck, S. J., & Corey, J. M. 2011. Electrospinning fundamentals : optimizing solution and apparatus parameters electrospinning fundamentals : Optimizing solution and apparatus parameters, . https://doi.org/10.3791/2494

LI, X., ZENG, S., QU, X., DAI, J., LIU, X., & WANG, R. 2018. Synthesis and characterization of Cu decorated zeolite A @ void @ Et-PMO nanocomposites for removal of methylene blue by a heterogeneous Fenton reaction, https://doi.org/10.20944/preprints201810.0606.v1

LIU, K., SHI, Z., & ZHOU, S. 2016. Reduction of hexavalent chromium using epigallocatechin gallate in aqueous solutions: Kinetics and mechanism. RSC Advances, *6*(71), 67196–67203. https://doi.org/10.1039/c6ra02131j

LONG, D. T., THI, H., THU, M., DAT, D. VAN, THUAN, L. VAN, & NGUYEN, H. T. 2019. as photo-Fenton catalyst for degradation of methylene blue. Toxicological & Environmental Chemistry, 0(0), 1–13. https://doi.org/10.1080/02772248.2019.1614588

LUBASOVA, D., & NETRAVALI, A. N. 2020. A novel method for electrospinning nanofibrous 3-D structures, 1–14.

LV, B., XU, Y., WU, D., & SUN, Y. 2008. Preparation and properties of magnetic iron oxide nanotubes, 6, 334–339. https://doi.org/10.1016/j.partic.2008.04.006

MALARA, A., PAONE, E., BONACCORSI, L., MAURIELLO, F., MACARIO, A., & FRONTERA, P. 2019. Pd / Fe_3O_4 Nanofibers for the catalytic conversion of lignin-

derived benzyl phenyl ether under transfer hydrogenolysis conditions, 1–14.

MANIKANDAN, A., VIJAYA, J. J., MARY, J. A., KENNEDY, L. J., & DINESH, A. 2014. Journal of Industrial and Engineering Chemistry Structural , optical and magnetic properties of Fe_3O_4 nanoparticles prepared by a facile microwave combustion method. Journal of Industrial and Engineering Chemistry, 20(4), 2077–2085. https://doi.org/10.1016/j.jiec.2013.09.035

MARIA, F., CHEQUER, D., AUGUSTO, G., OLIVEIRA, R. DE, RAQUEL, E., FERRAZ, A. & OLIVEIRA, D. P. DE. 2013. Textile Dyes : Dyeing process and environmental impact.

MCMURRY, J.E., FAY, R.G & ROBINSON, J.K. CHEMOSTRY 6th edditon. Pearson chapter 13, 491

MISHRA, A. K., & MOHANTY, B. 2008. Acute toxicity impacts of hexavalent chromium on behavior and histopathology of gill, kidney and liver of the freshwater fish, channa punctatus (Bloch). Environmental Toxicology and Pharmacology, 26(2), 136–141. https://doi.org/10.1016/j.etap.2008.02.010

MISHRA, S., & AHRENKIEL, S. P. 2012. Synthesis and characterization of electrospun nanocomposite TiO_2 nanofibers with Ag nanoparticles for photocatalysis applications, *2012*. https://doi.org/10.1155/2012/902491

MOSALLANEJAD, S., DLUGOGORSKI, B. Z., KENNEDY, E. M., & STOCKENHUBER, M. 2018. On the Chemistry of Iron Oxide Supported on γ-Alumina and Silica Catalysts. ACS Omega, 3, 5362–5374. https://doi.org/10.1021/acsomega.8b00201

NAKANE, K., & OGATA, N. 2010. Photocatalyst nanofibers obtained by calcination of organic-inorganic hybrids.

NEYENS, E., & BAEYENS, J. 2003. A review of classic Fenton's peroxidation as an advanced oxidation technique, 98, 33–50.

NIE, G., LI, Z., LU, X., LEI, J., ZHANG, C., & WANG, C. 2013. Applied surface science fabrication of polyacrylonitrile / CuS composite nanofibers and their recycled application in catalysis for dye degradation. Applied Surface Science, 284, 595–600. https://doi.org/10.1016/j.apsusc.2013.07.139

NJERUH, P. F. M. 2010. bsc . fisheries and aquaculture management Introduction :, 1–12.

NOGUEIRA, A. E., CASTRO, I. A., GIROTO, A. S., & MAGRIOTIS, Z. M. 2014. Heterogeneous Fenton-like catalytic removal of methylene blue dye in water using magnetic nanocomposite (MCM-41 / Magnetite), 1-7,

ONG, S., KENG, P., LEE, W., HA, S., & HUNG, Y. 2011. Dye waste treatment, *7*(6), 157–176. https://doi.org/10.3390/w3010157

OSTGARD, D. J., KUSTOV, L., & POEPPELMEIER, K. R. 1992. Comparison of Pt / KL Catalysts prepared by ion exchange oriIncipient wetness impregnation, 357, 342–357.

PATEL, A. C., LI, S., WANG, C., ZHANG, W., WEI, Y., V, D. U. & JANUARY, V. 2007. Electrospinning of porous silica nanofibers containing silver nanoparticles for catalytic applications, 120(11), 12289–12296. https://doi.org/10.1021/cm061331z

PC, P., & CP, B. 2015. Journal of material sciences & engineering raman spectroscopy of iron oxide of nanoparticles (Fe_3O_4), 5(1), 4–6. https://doi.org/10.4172/2169-0022.1000217

PERSANO, L., CAMPOSEO, A., TEKMEN, C., & PISIGNANO, D. 2016. Industrial upscaling of electrospinning and applications of polymer nanofibers : A Review, 504–520. https://doi.org/10.1002/mame.201200290

PIRZADA, T. 2012. Synthesis of polymer silica hybrid xerogels and nanofibers through sol gel processing and electrospinning. 27, 1- 6.

PIRZADA, T., ARVIDSON, S. A., SAQUING, C. D., SHAH, S. S., & KHAN, S. A. 2012. Hybrid silica − PVA nanofibers via sol − gel electrospinning 40, 1-5. https://doi.org/10.1021/la300049j

PIRZADA, T., ARVIDSON, S. A., SAQUING, C. D., SHAH, S. S., & KHAN, S. A. 2014. Hybrid carbon silica nano fibers through sol − gel electrospinning.

POPOV, M. V, ZAZHIGALOV, S. V, LARINA, T. V, CHEREPANOVA, S. V, BANNOV, A. G., LOPATIN, S. A., & ZAGORUIKO, A. N. 2017. Glass fiber supports modified by layers of silica and carbon nanofibers, 1–6. https://doi.org/10.1515/cse-2017-0001

RAMAKRISHNA, S., FUJIHARA, K., TEO, W. E., YONG, T., MA, Z., & RAMASESHAN, R. 2006. Electrospun nanofibers: Solving global issues. Materials Today. Elsevier Ltd. https://doi.org/10.1016/S1369-7021(06)71389-X

RASHEED, R., & MEERA, V. 2016. Synthesis of iron oxide nanoparticles coated sand by biological method and chemical method. Procedia Technology, 24, 210–216. https://doi.org/10.1016/j.protcy.2016.05.029

RAUF, M. A., MEETANI, M. A., KHALEEL, A., & AHMED, A. 2010. Photocatalytic degradation of methylene blue using a mixed catalyst and product analysis by LC / MS, *157*, 373–378. https://doi.org/10.1016/j.cej.2009.11.017

RUPARELIA, J. P., KUMAR, A., & DUTTAGUPTA, S. P. 2008. Strain specificity in antimicrobial activity of silver and copper nanoparticles, 4, 707–716. https://doi.org/10.1016/j.actbio.2007.11.006

SAHA, S., & BHUNIA, A. K. 2013. Synthesis of Fe_2O_3 Nanoparticles and study of its structural ,optical properties, 17, 191–195.

SHAH, H. V, SANDY, J. R., IRELAND, A. J., & SU, B. 2012. Electrospinning of 2D and 3D silica nanofibres from a colloidal solution, 56(2), 112–116.

SHAO, C., KIM, H., GONG, J., & LEE, D. 2002. A novel method for making silica nanofibres by using electrospun fibres of polyvinylalcohol / silica composite as, 2–5.

SHI, F., SHAN, H., LI, D., YIN, X., YU, J., & DING, B. 2019. Journal of Colloid and Interface Science a general strategy to fabricate soft magnetic $CuFe_2O_4$ @ SiO_2 nanofibrous membranes as efficient and recyclable Fenton-like catalysts, 538, 620–629. https://doi.org/10.1016/j.jcis.2018.12.028

SHI, X., ZHOU, W., MA, D., MA, Q., BRIDGES, D., MA, Y., & HU, A. 2015. Electrospinning of nanofibers and their applications for energy devices, 20 15-25.

Shin, S., Yoon, H., & Jang, J. (2008). Polymer-encapsulated iron oxide nanoparticles as highly efficient Fenton catalysts. *Catalysis Communications*, *10*(2), 178–182. https://doi.org/10.1016/j.catcom.2008.08.027

SHOOTO, N. D., DONBEBE, W., SIKHWIVHILU, L., & DIKIO, E. D. 2016. Modified electro-spun polyvinyl alcohol nanofibers used as adsorbant. https://doi.org/10.12783/issn.1544-8053/13/3/7

SINGH, L. P., BHATTACHARYYA, S. K., KUMAR, R., MISHRA, G., SHARMA, U., SINGH, G., & AHALAWAT, S. 2014. 1 . Sol-gel processing of silica nanoparticles and their applications , Advances in colloidal and sol-gel processing of silica nanoparticles

and their applica. Advances in Colloid and Interface Science, 214, 17–37. https://doi.org/10.1016/j.cis.2014.10.007

SMITH, M. 2018. Polymer coated magnetic nanoparticles and modified polymer nanofibers for the effficient capture of mycobacterium tuberculosis(MTB), 21,2-9

SONG, Z., CHIANG, S. W., CHU, X., DU, H., YAO, Y., HE, Y. & XU, C. 2018. Effects of solvent on structures and properties of electrospun poly (ethylene oxide) nanofibers, 45787, 1–10. https://doi.org/10.1002/app.45787

STEPANYAN, R., SUBBOTIN, A., CUPERUS, L., BOONEN, P., DORSCHU, M., OOSTERLINCK, F.& OOSTERLINCK, F. 2014. Fiber diameter control in electrospinning fiber diameter control in electrospinning, 1,73-105. https://doi.org/10.1063/1.4900778

SUTEU, D., BILIUTA, G., RUSU, L., COSERI, S., & NACU, G. 2015. Cellulose cellets as new type of adsorbent for the removal of dyes from aqueous media, 14(3), 525–532.

TARUS, B., FADEL, N., AL-OUFY, A., & EL-MESSIRY, M. 2016. Effect of polymer concentration on the morphology and mechanical characteristics of electrospun cellulose acetate and poly (vinyl chloride) nanofiber mats. Alexandria Engineering Journal, 55(3), 2975–2984. https://doi.org/10.1016/j.aej.2016.04.025

THOMAS, J. A., SCHNELL, F., KAVEH-BAGHBADERANI, Y., BERENSMEIER, S., & SCHWAMINGER, S. P. 2020. Immunomagnetic Separation of Microorganisms with Iron Oxide Nanoparticles, 80, 7-10.

TOSKAS, G., CHERIF, C., HUND, R., LAOURINE, E., FAHMI, A., & MAHLTIG, B. 2011. Inorganic / Organic (SiO 2)/ PEO hybrid electrospun nanofibers produced from a modified sol and their surface modification possibilities, 3673–3681.

TOSKAS, G., CHERIF, C., HUND, R., LAOURINE, E., MAHLTIG, B., FAHMI, A., & HANKE, T. 2013. Chitosan (PEO)/ silica hybrid nanofibers as a potential biomaterial for bone regeneration. Carbohydrate Polymers, 94(2), 713–722. https://doi.org/10.1016/j.carbpol.2013.01.068

TSENG, T. K., LIN, Y. S., CHEN, Y. J., & CHU, H. 2010. A Review of photocatalysts prepared by sol-gel method for VOCs removal, 2336–2361. https://doi.org/10.3390/ijms11062336

UGUR, M. H., OKTAY, B., & GUNGOR, A. 2018. Highly thermally resistant , hydrophobic poly (vinyl alcohol)– silica hybrid nanofibers, 83, 885–897.

VELEIRINHO, B., REI, M. F., & DA, J. A. L. 2007. Solvent and concentration effects on the properties of electrospun poly (ethylene terephthalate) nanofiber mats, 460–471. https://doi.org/10.1002/polb

Wallace, T. H., Novak, J. T., Hoehn, R. C., Randall, C. W., & Wallace, T. H. (2001). Biological Treatment of a Synthetic Dye Water and an Industrial Textile Wastewater Containing Azo Dye Compounds.

WANG, H., HUANG, X., LI, W., GAO, J., XUE, H., & LI, R. K. Y. 2018. TiO_2 nanoparticle decorated carbon nano fi bers for removal of organic dyes, 549, 205–211. https://doi.org/10.1016/j.colsurfa.2018.04.017

WANG, JIANFANG, ZHANG, J., ASOO, B. Y., & STUCKY, G. D. 2017. Structure-Selective Synthesis of Mesostructured / Mesoporous Silica Nanofibers S1 S2, 100, 52–55.

WANG, JING, LIU, C., LI, J., LUO, R., HU, X., SUN, X. & WANG, L. 2017. In-situ incorporation of iron-copper bimetallic particles in electrospun carbon nanofibers as an efficient Fenton catalyst. Applied Catalysis B: Environmental, 207, 316–325. https://doi.org/10.1016/j.apcatb.2017.02.032

WANG, L., ALI, J., ZHANG, C., MAILHOT, G., & PAN, G. 2017. Simultaneously enhanced photocatalytic and antibacterial activities of TiO_2 / Ag composite nanofibers for wastewater purification Journal of Environmental Chemical Engineering Simultaneously enhanced photocatalytic and antibacterial activities of TiO_2 /. Journal of Environmental Chemical Engineering, 12, 0–1. https://doi.org/10.1016/j.jece.2017.12.057

WANG, Q., TIAN, S., & NING, P. 2014. Degradation mechanism of methylene blue in a heterogeneous Fenton-like reaction catalyzed by ferrocene. https://doi.org/10.1021/ie403402q

WANG, X., DOU, L., YANG, L., YU, J., & DING, B. 2017. Hierarchical structured MnO_2@SiO_2 nanofibrous membranes with superb flexibility and enhanced catalytic performance. Journal of Hazardous Materials, 324, 203–212.

https://doi.org/10.1016/j.jhazmat.2016.10.050

WANG, YAN, LI, J., SUN, J., WANG, Y., & ZHAO, X. 2017. Electrospun flexible self-standing Cu–A $_2O_3$ fibrous membranes as Fenton catalysts for bisphenol A degradation. Journal of Materials Chemistry A, 5(36), 19151–19158. https://doi.org/10.1039/C7TA04386D

WANG, YANXIN, HUANG, L., TANG, J., WANG, Y., LI, X., & MA, W. 2016. Luminescent Polyacrylonitrile (PAN) electrospinning nanofibers encapsulating silica nanoparticles carried ternary europium complex, 11, 2058–2065.

WEI, X., WANG, Y., FENG, Y., XIE, X., LI, X., & YANG, S. 2019. Different adsorption-degradation behavior of methylene blue and Congo red in nanoceria / H_2O_2 system under alkaline conditions. Scientific Reports, 3, 2–11. https://doi.org/10.1038/s41598-018-36794-2

WONG, S., BAJI, A., & LENG, S. 2008. Effect of fiber diameter on tensile properties of electrospun, 49, 4713–4722. https://doi.org/10.1016/j.polymer.2008.08.022

XU, P., MING, G., LIAN, D., LING, C., HU, S., & HUA, M. 2012. Science of the total environment use of iron oxide nanomaterials in wastewater treatment : A review. Science of the Total Environment, The, 424, 1–10. https://doi.org/10.1016/j.scitotenv.2012.02.023

YANG, B., TIAN, Z., ZHANG, L., GUO, Y., & YAN, S. 2015. Journal of water process engineering enhanced heterogeneous Fenton degradation of methylene blue by nanoscale zero valent iron (nZVI) assembled on magnetic Fe_3O_4 / reduced graphene oxide. Journal of Water Process Engineering, 5, 101–111. https://doi.org/10.1016/j.jwpe.2015.01.006

YANG, C., MELDON, J. H., LEE, B., & YI, H. 2014. Investigation on the catalytic reduction kinetics of hexavalent chromium by viral-templated palladium nanocatalysts. Catalysis Today, *233*, 108–116. https://doi.org/10.1016/j.cattod.2014.02.043

YANG, H., XU, S., JIANG, L., & DAN, Y. 2012. Thermal decomposition behavior of poly (Vinyl Alcohol) with different hydroxyl content thermal decomposition behavior of poly (vinyl alcohol) with different hydroxyl content, 2348. https://doi.org/10.1080/00222348.2011.597687

YAO, Y., LU, H., LI, J., PENG, Q., WANG, Q., LI, Y.,& LENG, J. 2015. RSC Advances. 5, 89113–89120. https://doi.org/10.1039/C5RA17783A

Yu-li, Y., Yue-zhong, W. E. N., Xiao-ying, L. I., & Si-zhen, L. U. O. 2006. Treatment of wastewater from dye manufacturing industry, 7, 340–344. https://doi.org/10.1631/jzus.2006.AS0340

ZARUBICA, A. R. 2016. Decolorisation of methylene blue over titania – based catalysts : the influence of different ph values used, 5(2), 12–17.

ZHANG, W., HE, Z., HAN, Y., JIANG, Q., ZHAN, C., ZHANG, K. & ZHANG, R. 2020. Structural design and environmental applications of electrospun nano fibers. Composites Part A, 137June, 10-609. https://doi.org/10.1016/j.compositesa.2020.106009

ZHENG, T., PANG, J., TAN, G., HE, J., MCPHERSON, G. L., LU, Y., & ZHAN, J. 2007. Surfactant templating effects on the encapsulation of iron oxide nanoparticles within silica microspheres, (c), 5143–5147.

Zhou, W., Apkarian, R. P., & Wang, Z. L. 2018. Fundamentals of scanning electron microscopy.17,12-18.

Appendix A

The average crystalline size of the iron oxide nanoparticles was calculated using the Scherer equation (Smith et al., 2018)

$$\mathrm{Dp} = \frac{k\lambda}{\beta cos\theta}$$

Whereby the

Dp - the average size of particles domain

K – Scherer constant 0.89

λ- X-ray wavelength of 1.5408nm.

β - peak full width at maximum (FWHM) 1.16

Θ – is broad diffraction angle (35.46)

$$\mathrm{Dp} = \frac{(0.89)(1.5408\ nm)}{1.16\cos(35.46)}$$

$$= 8\ nm$$

Appendix B

Degradation of MB

$$Dilution\ factor\ given\ as = \mathrm{C1xV1} = \mathrm{C2xV2}$$

$$= (0.248\mathrm{mg/L})\mathrm{x}(0.1\mathrm{L}) = \mathrm{C2}(0.001\mathrm{L})$$

$$C2 = 24.8\ mg/L$$

The percentage removal is given as:

$$\%\ \text{removal} = \frac{Ci - Cf}{Ci} * 100$$

Ci = initial degradation concentration

Cf = final degradation concentration

$$= \frac{(100\frac{mg}{L} - 24.8\ mg/L)}{(100\ mg/L)}$$

$$= 75.2\ \%$$

Appendix C

Reaction kinetics Integrated rate laws (McMurry et al., 2015)

If the concentration of a reactant remains constant because it is in great excess with respect to the other reactant, its concentration can be included in the rate constant to simplify the rate equation, obtaining pseudo-first-order or pseudo-second-order rate equation. For example, during the Fenton reaction $[H_2O_2]$ + [MB] → $[H_2O]$ + $[CO_2]$ the rate for this reaction is given by: rate=k[MB]x $[H_2O_2]$ y . The H_2O_2 has a high concentration compared to MB such that its consumption is insignificant. Therefore, it can be assumed that the concentration of the H_2O_2 remains constant throughout the reaction. The rate can be assumed to be rate=kabs [MB]x. The order of the reaction can be determined by performing some experiments (McMurry et al., 2015)

Determination of rate laws

Pseudo-first-order

Given by: Ln[MB]

$$\frac{-d[MB]}{dt} = k[MB]$$

$$\int \frac{-d[MB]}{[A]} = \int k[MB]$$

$$\int \frac{1}{[MB]}.dt[MB] = -k\int dt$$

$$\int_0^t In\,[MB] = -k\int_0^t dt$$

$$In[MB] - In[MB] = -k(t-0)$$

$$In[MB] - In[MB] = -kt$$

$$In[MB] = -kt + -In[MB]$$

Therefore $y = mx + c$

Psuedo Second order

Given by $\frac{1}{MB}$

Rate = k[MB]^2

$$\frac{-d[MB]}{[MB]} = k[MB]^2$$

$$\int \frac{d[MB]}{[MB]^2} = \int -k.dt$$

$$\int \frac{1}{[MB]^2}.d[MB] = -k\int dt$$

$$\int_0^t \frac{-1}{[MB]^2} = -k\int_0^t t$$

$$\frac{-1}{[MB]_t} = -\left(-\frac{1}{[MB]_0}\right) = -k(t-0)$$

$$\frac{1}{[MB]_t} - \frac{1}{[MB]_0} = kt$$

$$\frac{1}{[MB]_t} = kt + \frac{1}{[MB]_0}$$

$$y = mx = c$$

Appendix D

During the first 60 min of degradation, it was observed that the reaction has not reached its equilibrium, therefore, the experiment for the catalyst that had a higher degradation efficiency was extended to 120 min to evaluate the degradation efficiency after the first 60 min. It was observed that with time the catalyst had a complete degradation and the kinetics best-fitted pseudo-first-order.

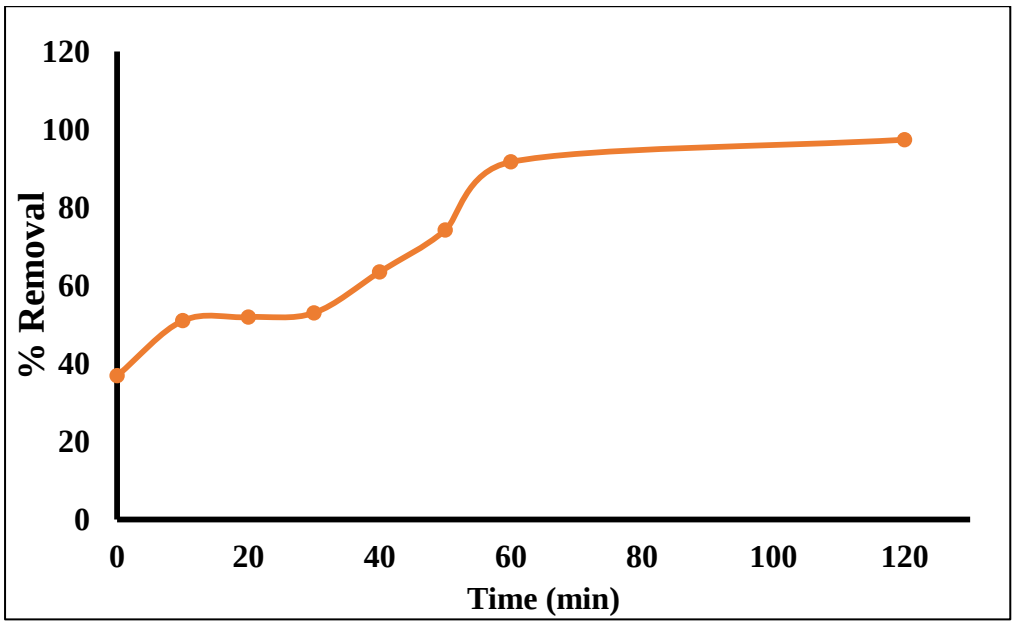

Figure 48: Fenton degradation efficiency of 5 wt.% iron oxide-silica nanofibers (M2) after 120 min.

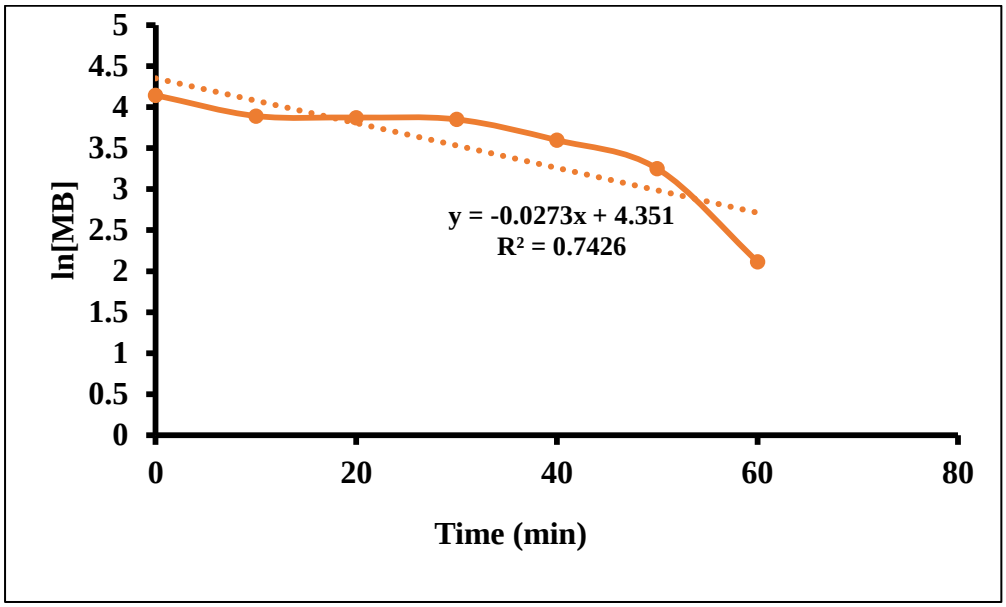

Figure 49: Pseudo first-order kinetics 5 wt.% iron oxide-silica nanofibers (M2) after 120 min.

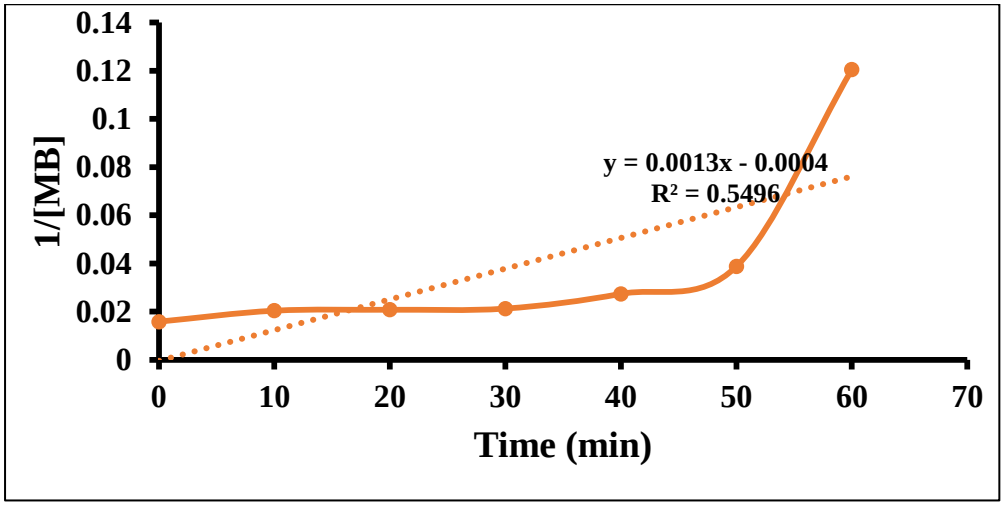

Figure 50: Pseudo second order kinetics 5 wt.% iron oxide-silica nanofibers (M2) after 120 min.